Reactivity and mechanistic studies of small molecules at model metal oxide surfaces: Underpinning PuO_2 safe storage.

Thesis submitted in accordance with the requirements of Cardiff University for the degree of Doctor of Philosophy

Mark Hicks

2015

Table of Contents

1 Introduction

1.1 Nuclear fuel cycle and fuel reprocessing

The nuclear fuel cycle represents the nuclear power generation process, from mining the uranium ore to the treatment of waste. The fuel cycle is divided into two parts, the front end of the process and the back end of the process, with the nuclear power station being in the middle[1].

The processes before reaching the nuclear power station consist of uranium exploration, mining, refining, isotope enriching and fuel element fabrication[1].

Uranium is mined in twenty countries, but 52 % of the world supply of uranium comes from just 6 countries. These countries are Canada, Australia, Russia, Kazakhstan, Namibia and Niger.[2] Uranium is mined in several different types of mine. These include an open pit mine, an underground mine or in-situ leaching mine. In an open pit mine the ore lies close to the surface and the overlying layer of rock is removed creating a large pit where the ore is easily extractable[2]. An underground mine is used when the ore lies deeper under the surface and the construction of access shafts and tunnels under the ground are needed to gain access to the uranium ore[2]. The uranium ore is sometimes contained in ground water or a porous material, such as sand. In this case, a process called *in-situ* leaching is used to extract the uranium ore. Either acid or alkali (depending on the nature of the groundwater) is added to the ground water to dissolve the ore, and the resulting solution is pumped out[2].

The ore then undergoes a milling process to extract the uranium oxides needed for fuel fabrication. Milling is normally carried out close to the mine where the ore has been extracted. The ore is crushed and then leached with sulphuric acid in order to dissolve the uranium oxides.

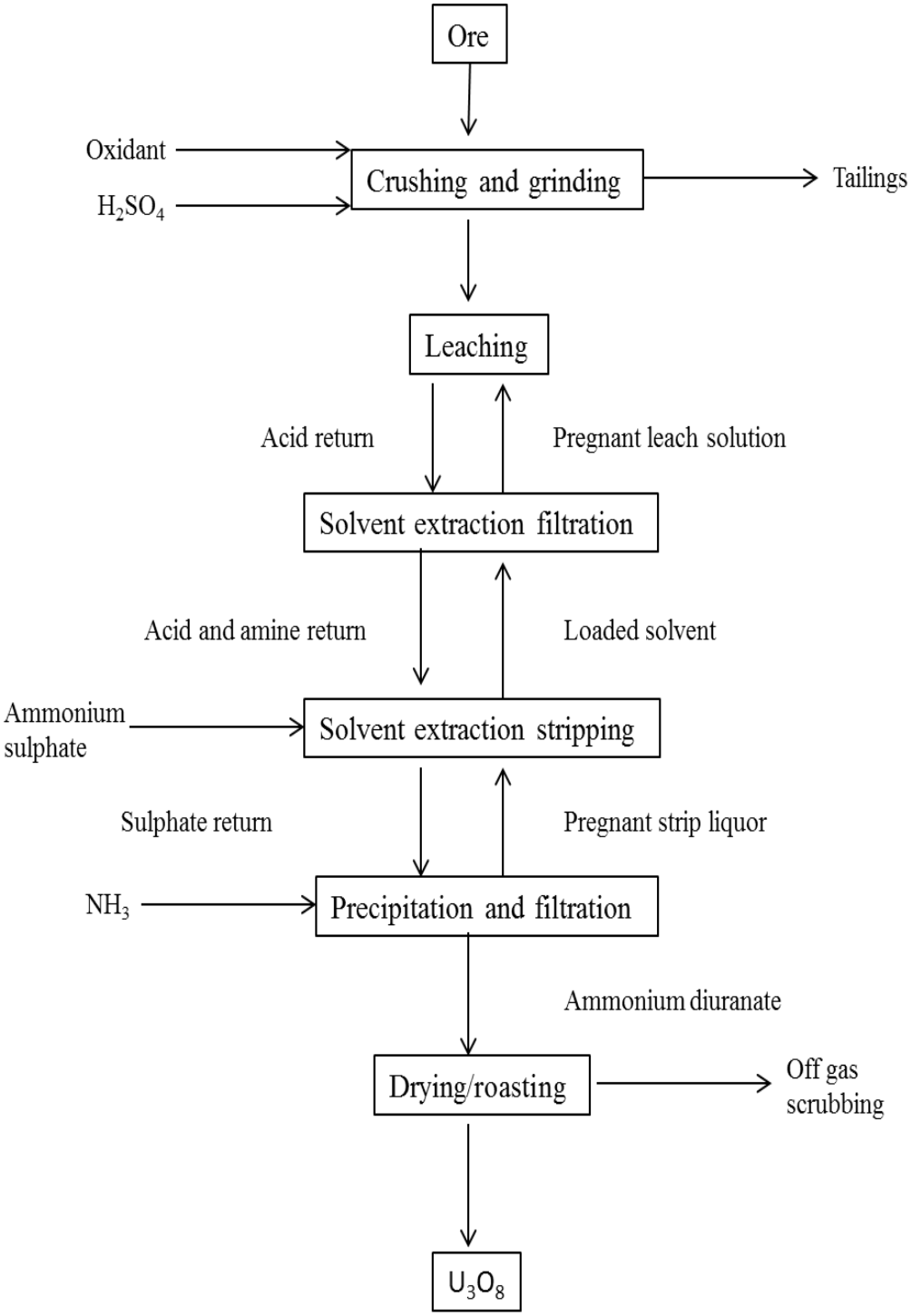

Figure 1-1. Schematic diagram of the milling process of uranium ores[2].

The resulting ore is known as 'yellow cake', this is the form in which the uranium is marketed and exported. Yellow cake typically contains 70 to 90 % U_3O_8, with the presence uranium hydroxide, uranium sulphate, uranium peroxide and various other uranium oxides[2].

The fuel used in most commercial nuclear reactors is based on uranium in the form of uranium dioxide (UO_2) that has been enriched so that percentage of the more readily fissile U^{235} isotope is increased from the natural occurrence of 0.7 % to between 2 and 4 %[1].

Another type of reactor uses a fuel that contains depleted (<0.3 %) U^{235}. Usually this uranium has come from the reprocessing of spent nuclear fuel. An example of this, is when plutonium or plutonium mixed with U^{238} is added as a replacement for the lost U^{235}. This is known as a mixed oxide fuel (MOX)[1].

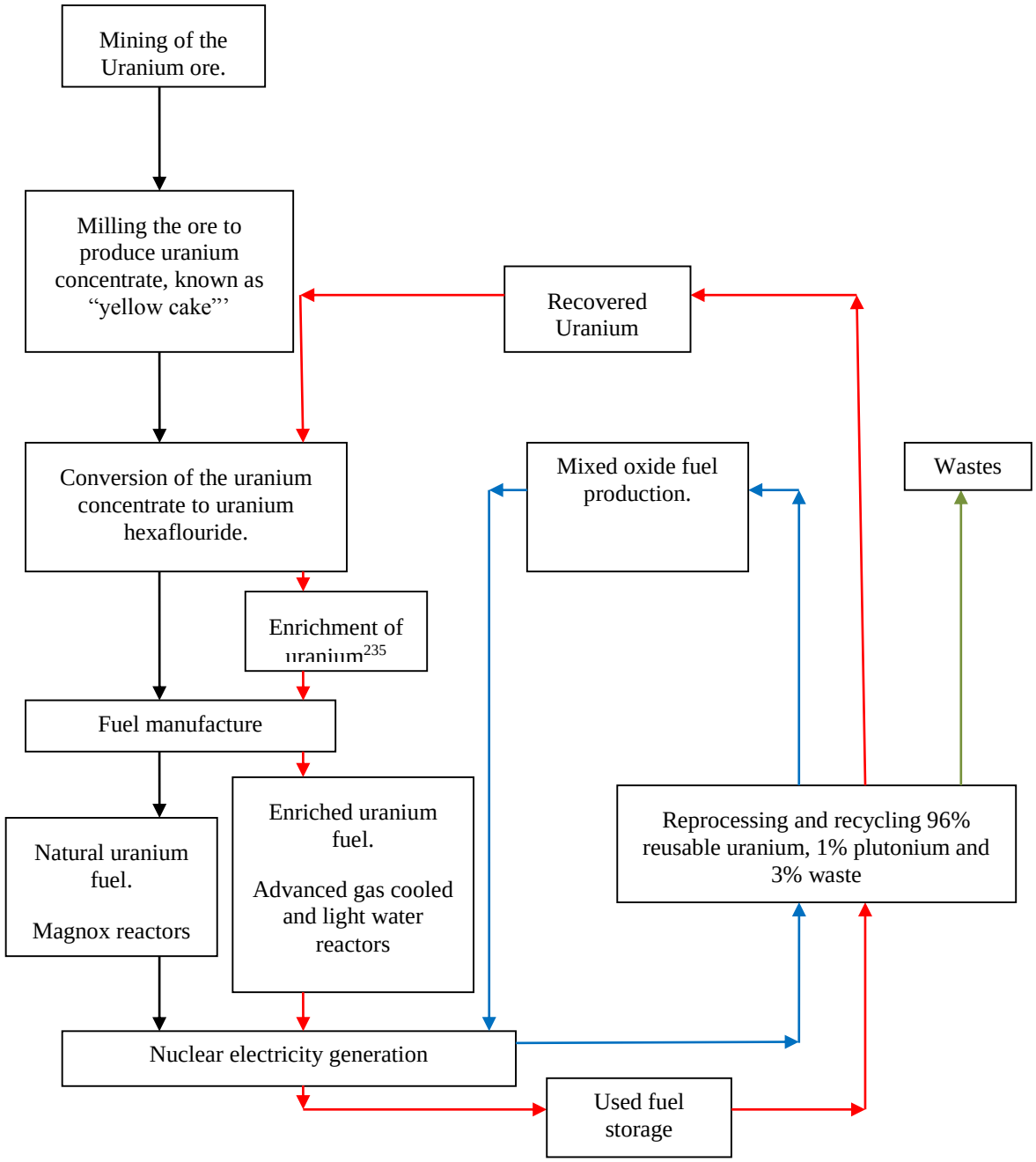

Figure 1-2. Schematic representation of the nuclear fuel cycle[1].

The process after the nuclear power station consists of the reprocessing and handling of radioactive waste[1].This process involves the removal of the spent nuclear fuel, the reprocessing of useful material and the treatment of nuclear waste.

Spent nuclear fuel can contain a large variety of element and will be dependent on the type of reactor used, the conditions used and the type of fuel used[1].

The irradiated fuel elements from the spent nuclear fuel are reprocessed in the UK at the thermal oxide reprocessing plant (THORP) at Sellafield.

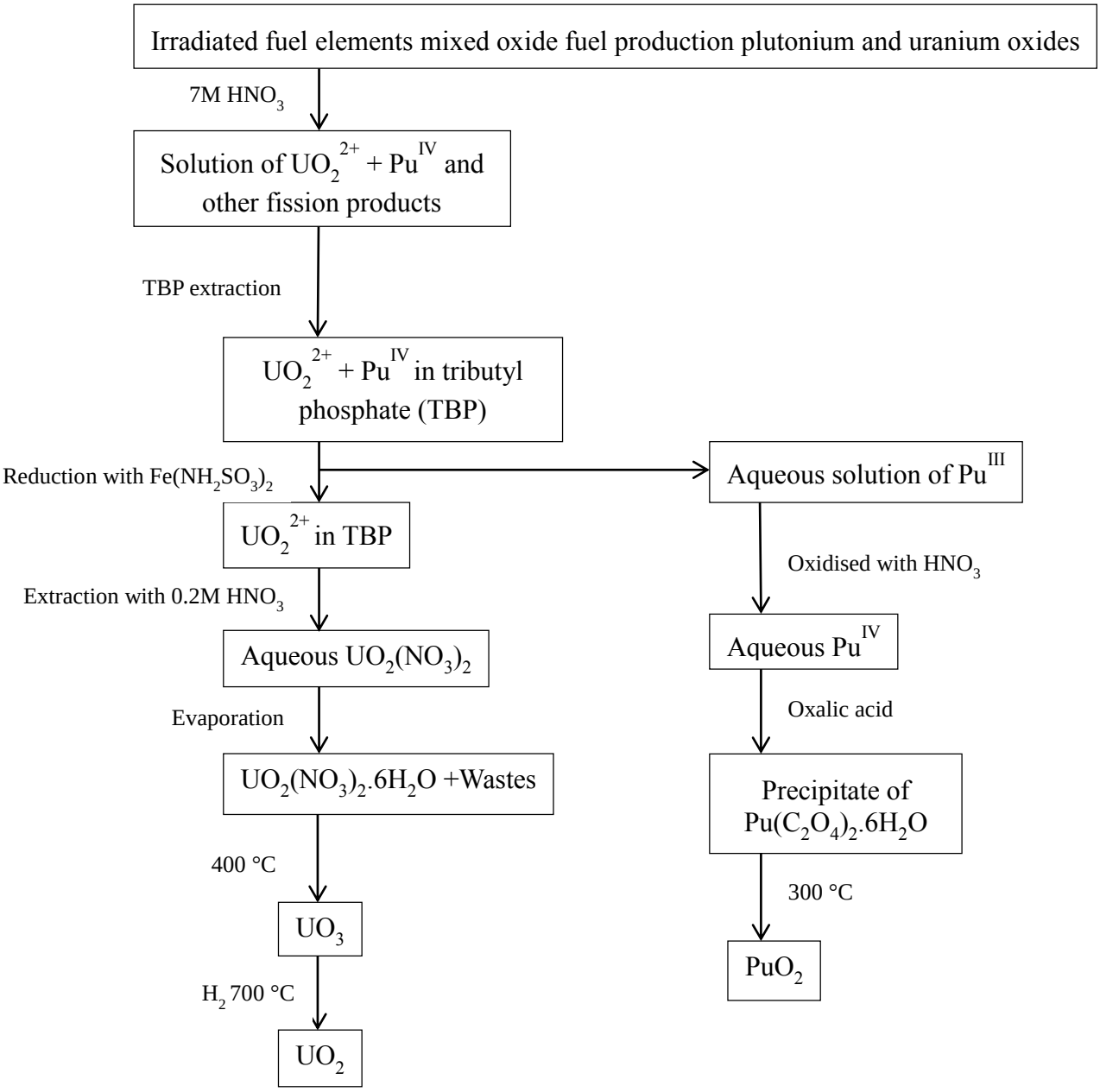

Figure 1-3 Schematic diagram of nuclear fuel reprocessing[3].

The PuO_2 generated at the end of the reprocessing process stored in double walled stainless steel tanks and shielded by concrete of more than a metre in thickness[3].

1.2 Properties of PuO_2 and the recombination of H_2 and O_2 over PuO_2

PuO_2 has a fluorite structure, where Pu^{4+} cations are centred in a face centred cubic arrangement with O^{2-} anions occupying the tetrahedral holes of the structure. Plutonium has a range of non-stoichiometric forms, with the formula PuO_{2-x}, which is dependent on temperature and oxygen partial pressure[4].

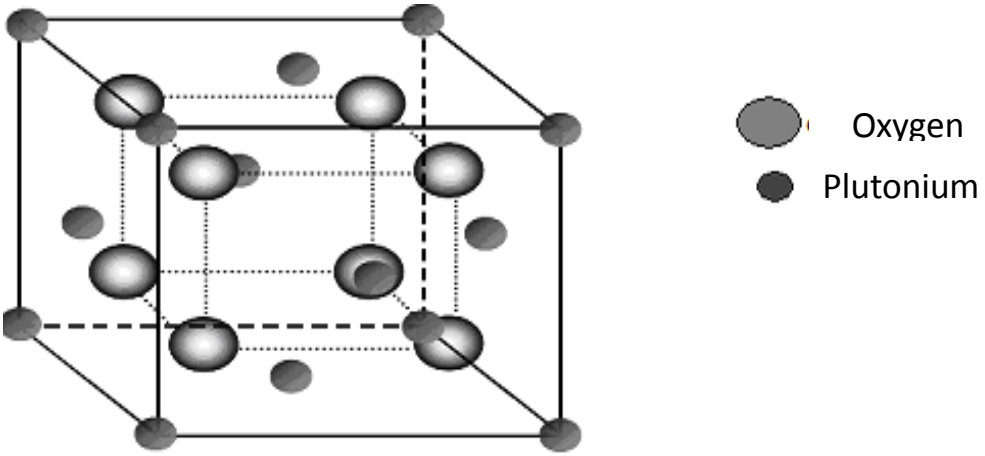

Figure 1-4. The fluorite structure of PuO_2.

The fluorite structure takes its name from the CaF_2 structure, in which Ca^{2+} cations lie in expanded face centred cubic (fcc) conformation with the F^- anions occupying two types of tetrahedral holes.

One of the major concerns with storing PuO_2 is the reaction of water adsorbed and absorbed onto the PuO_2 surface to form gaseous H_2 and O_2. This raises concerns of rises in pressure of the storage vessels and the formation of potentially explosive gas mixtures. As a

result safety standards are in place for the packing and storage of PuO_2 in nuclear storage where only 0.5% wt of residual water is permitted[5,6].

The procedures[5, 6] are effective in limiting the amount of water that is present in the storage canisters. However, these protocols do not remove all water present and over time it has been predicted that the radioactivity of PuO_2 will cause the splitting of this water. This will result in the build-up of H_2 and O_2. It has been reported that H_2 and O_2 will undergo a recombination reaction to form water, which is initiated by alpha radiation[7].

The reactions of H_2 and O_2 over pure and impure PuO_2 have been studied by Morales *et al.*[7] at the Los Alamos nuclear facility in the US. In this work, they study the reaction of a 2 % H_2 in air mixture over PuO_2 in sealed stainless steel vessels by measuring pressure changes and changes in the composition of the reactive gas mixtures at different temperatures over time. Morales *et al.* conclude that temperatures of 100 °C and above are necessary for a reaction to occur indicated by a pressure change taking place in the vessels. They observe that under the conditions of their experiments, the results seen are more consistent with a thermal reaction of H_2 and O_2 over the surface of PuO_2 rather than a radiation induced H_2/O_2 gas phase reaction. They do not suggest a mechanism for the surface reaction of H_2 and O_2 over PuO_2. However, they do acknowledge that knowledge of the mechanism would be fundamental in understanding the thermal reaction taking place in nuclear storage containers[7].

In a literature review[8] of the H_2/O_2 recombination and generation in plutonium storage environments, two mechanisms for the thermal recombination of H_2 and O_2 over PuO_2 are suggested.

The Langmuir Hinshelwood mechanism involves the adsorption of species A and B on the surface of a compound and reacting on the surface to form AB[9]. With regards to the

recombination reaction, this mechanism suggests H_2 and O_2 react over the surface to form OH groups on the surface of PuO_2.

The second mechanism considered is the Eley-Rideal mechanism where species A is adsorbed on the surface, with gas phase species B colliding with A on the surface to form AB[9]. In the review by J.A. Lloyd and P.G Eller[8] this is proposed as a reaction of gas phase ions or radicals generated due to the radioactivity of PuO_2 and their reaction with adsorbed species (H_2 and O_2) on the surface of PuO_2[8].

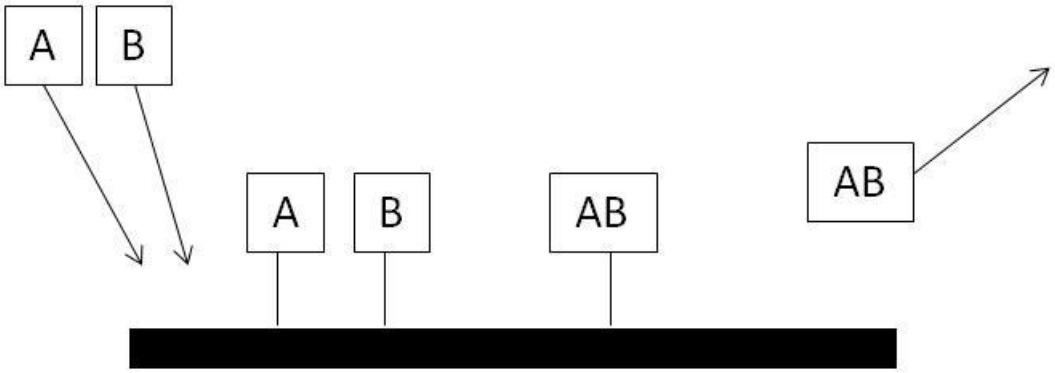

Figure 1-5. Langmuir-Hinshelwood mechanism[8, 9].

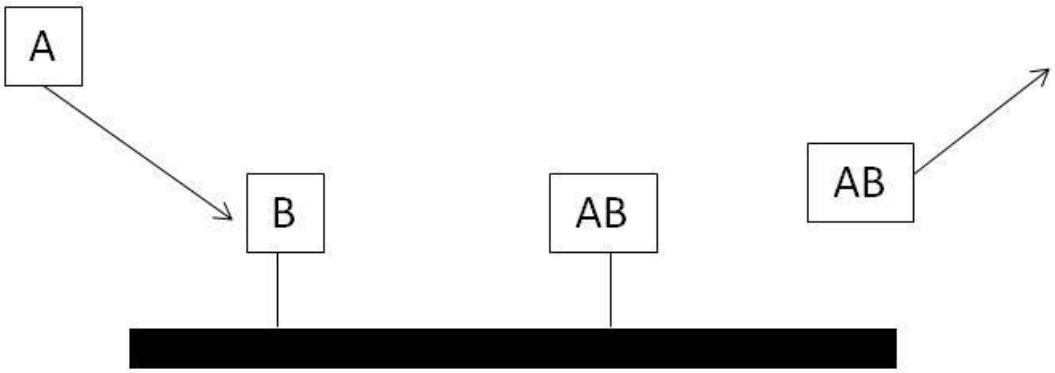

Figure 1-6. Eley-Rideal mechanism[8, 9].

Lloyd and Eller[8] and Morales *et al.*[7] both indicate that surface catalytic reactions can dominate over radiolytic reactions under certain conditions that are comparable with conditions in plutonium storage environments[7, 8].

In both papers it is supported that understanding the mechanism of thermal reactions of H_2 and O_2 is fundamental in predicting the behaviour of H_2 and O_2 over PuO_2 in long term storage. However, PuO_2 presents difficulties in its study since it is a severe radiological poison and strong α-emitter and must be handled with extreme care[10]. CeO_2 is suggested as a model for PuO_2.

1.3 CeO_2 as a model for PuO_2

Both PuO_2 and CeO_2 have a fluorite structure, where Pu^{4+}/Ce^{4+} cations are centred in a face centred cubic arrangement with O^{2-} anions occupying the tetrahedral holes of the structure. Both PuO_2 and CeO_2 have a range of non-stoichiometric forms, with the formula PuO_{2-x} or CeO_{2-x}. PuO_2 also has similar thermodynamic properties to CeO_2, such as Gibbs free energy[11]. In a study looking to identify the products formed by the reaction of water with plutonium metal at 23 °C, the phase diagram of plutonium oxide was indicated to be similar to that of cerium oxide[12]. Marra *et al.*[13] indicated that CeO_2 was a comparable model for PuO_2 for development studies of batching, powder handling, compaction and sintering. Both cerium and plutonium have relatively stable trivalent and tetravalent oxidation states[12]. Plutonium and cerium also have similar ionic radii[14] as shown in table 1-1.

Table 1-1 Ionic radii of Ce^{3+}/Ce^{4+} and Pu^{3+}/Pu^{4+}[14]

Oxidation State	Ionic Radius (Å)
Pu^{3+}	1.00
Pu^{4+}	1.01
Ce^{3+}	0.86
Ce^{4+}	0.87

The similarities in both structure and properties suggest that CeO_2 will provide a good model for the reactivity of PuO_2.

1.4 Properties of CeO_2

CeO_2 is a pale yellow colour solid. It has a wide range of applications, in either its pure form or doped with cations e.g. Mg^{2+}, such as gas sensors, electrode materials for solid oxide fuel cells and catalytic supports for automobile exhaust systems[15]. Cerium metal has an electron configuration of [Xe] $6s^2$ $5d^1$ $4f^1$. In cerium (IV) oxide, cerium exists in the (+4) oxidation state with an electron configuration of [Xe], making it very stable[10]. As a result of this, cerium is the only lanthanide metal to form a stoichiometric oxide in the form of CeO_2, which has a fluorite structure with a lattice constant of 0.541nm[16].

In the fcc structure of ceria, Ce^{4+} cations form a cubic close packing arrangement with all the tetrahedral holes occupied by O^{2-} anions[17].

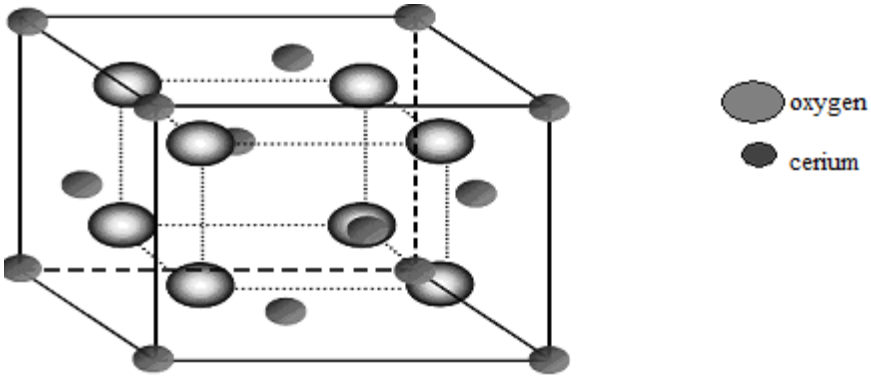

Figure 1-7. The Fluorite structure of CeO_2[17].

The fcc structure of ceria is an octahedral structure with cerium ions centred around oxygen ions. In this structure some of the oxygen ions are mobile and can be removed in a reducing atmosphere. This leads to non-stoichiometric compositions that have the formula CeO_{2-x} where x equals 0 to 0.5. The non-stoichiometric compositions of CeO_2 are easily re-oxidised in the presence of oxygen[18].

This property is of great importance for the use of CeO_2 in automobile catalytic converters[4, 18]. These unique redox properties can be attributed to the retention of the fluorite structure in CeO_2. Surface oxygen mobility allows oxygen ions to be easily removed during reduction when compared with the bulk oxygen ions[17].

Computer investigations into the structure of CeO_2, carried out in 1994[19], indicate via theoretical energy calculations that the (111) index plane is the most stable surface, this surface of CeO_2 is oxygen terminated[19]. Evidence that the (111) index plane of the CeO_2 surface is oxygen-terminated has been provided through non-contact atomic force microscopy (NC-AFM) and scanning tunnelling microscopy (STM) studies undertaken at the University of Tokyo[16]. High-resolution transmission electron microscope (HRTEM) images from a recent study into the structure and chemical changes of ceria irradiated with hydrogen ions showed

untreated CeO_2 to have similar surface defects to the stacking faults present in the fcc structure of pure metals, such as aluminium[15].

The formation of Ce^{3+} on the surface of ceria follows the formation of oxygen vacancies. Oxygen vacancies play a key role in the surface chemistry of oxides and are important in understanding the surface reactions of CeO_2[20]. Defects within the lattice structure of CeO_2 are the cause of its redox ability and subsequently lead to ceria forming non-stoichiometric compositions. These defects can be caused extrinsically, i.e. created by a reaction of the solid with the surrounding atmosphere, or caused intrinsically, caused by impurities in the structure[21]. With regards to extrinsic defects, a large proportion of these defects can be formed by exposure of ceria to a reducing gaseous environment. As a result of reduction, ceria will have excess cation content when compared to its anion content, i.e. some oxygen has been removed, creating an overall positive charge. Recovery of neutrality can be attributed to the donation of two electrons to the resulting oxygen vacancy site after reduction has occurred. This results in two cerium atoms changing charge from +4 to +3[21].

CeO_2 can be classified as a mixed conductor showing both electronic and ionic conduction. Its electrical properties are strongly dependent upon temperature, oxygen partial pressure and the presence of impurities[21]. The electrical conductivity of CeO_2 during reduction in hydrogen increases due to the removal of oxygen and the generation of polaronic electrons.[22]

1.5 Reactivity of CeO_2

One of the biggest uses of CeO_2 is in three way catalysts as part of exhaust systems of vehicles. Its most important function in these systems is the uptake and release of oxygen, known as its oxygen storage capacity. In this application ceria is exposed to varying conditions

between fuel rich (low O_2) and fuel lean (high O_2) conditions. Under fuel rich conditions, the oxygen storage capacity of CeO_2 allows it to donate oxygen for the oxidation of CO and hydrocarbons during fuel rich conditions from automobile exhaust emissions[23]. Under fuel lean conditions, CeO_2 is able to absorb and effectively store oxygen from O_2, NO and water allowing the removal of NO from exhaust emissions[23]. The behaviour of ceria in three way catalysts can be represented by the following equations:

Fuel rich conditions;

- $CeO_2+xCO \rightarrow CeO_{2-x}+xCO_2$
- $CeO_2+HC \rightarrow CeO_{2-x}+(H_2O, CO_2, CO, H_2)$
- $CeO_2+xH_2 \rightarrow CeO_{2-x}+xH_2O$ [23]

Fuel lean conditions;

- $CeO_{2-x}+xNO \rightarrow CeO_2+0.5xN_2$
- $CeO_{2-x}+xH_2O \rightarrow CeO_2+xH_2$
- $CeO_{2-x}+0.5xO_2 \rightarrow CeO_2$ [23]

1.6 Reactivity of CeO_2 with H_2O, H_2, O_2, O_3.

A study[24] of the chemistry of water on the oxidised and reduced surfaces of $CeO_2(111)$ by temperature programmed desorption and x-ray photoelectron spectroscopy was carried out. Results indicate that water does not oxidise Ce^{3+} surface sites on the reduced CeO_2 surfaces, ($CeO_{2-x}(111)$ surface grown on yttria-stabilised $ZrO_2(111)$ under ultra-high vacuum) in the temperature range below 377 °C[24].

However, it has been observed by reflection high energy electron diffraction (RHEED) and low energy electron diffraction (LEED) that water does oxidise Ce^{3+} sites in reduced CeO_2 powders and lattice mismatched films of CeO_{2-x}(111) on Ru(0001)[24]. The exposure of water to a reduced ceria surface has been shown to result in the evolution of H_2 in a temperature-programmed desorption (TPD) experiment[21]. These studies indicate that the reactivity of reduced CeO_2 depends on surface defects, surface termination and morphology.

One of the reactions of great interest with respect to PuO_2 is the radiolysis of water to form H_2 and O_2, as the presence of H_2 and O_2 at certain ratios can lead to a build-up of potentially explosive gas mixture in sealed nuclear waste storage containers[25]. The production of H_2 from radiolysis of water absorbed on CeO_2 was studied as a function of the energy absorbed in the water layer in a study carried out at the University of Notre Dame[25]. It was shown that it requires very high humidity (>85%) for multiple water layers to accumulate on the oxide surface of CeO_{2*}. A study on the adsorption of water on PuO_2 shows the accumulation of multiple water layers also requires very high humidity, above 85%[25]. Only H_2 was observed in the γ-radiolysis over CeO_2 in significant quantities. O_2 was observed but it was at a much lower yield than H_2. The yield of H_2 produced was found to increase with decreasing number of absorbed water layers[25]. However, hydrogen was not produced to the levels one would predict for the radiolysis of H_2O. Surface sensitive studies to elucidate possible recombination mechanisms of H_2 and O_2 were suggested by the authors of this study.

The reduction of cerium oxide and the oxidation of hydrogen by CeO_2 has been shown to follow a Mars van Krevelen type mechanism as proposed by El Fallah et al[26, 27] and others[17, 21]. This is shown in figure 1-8.

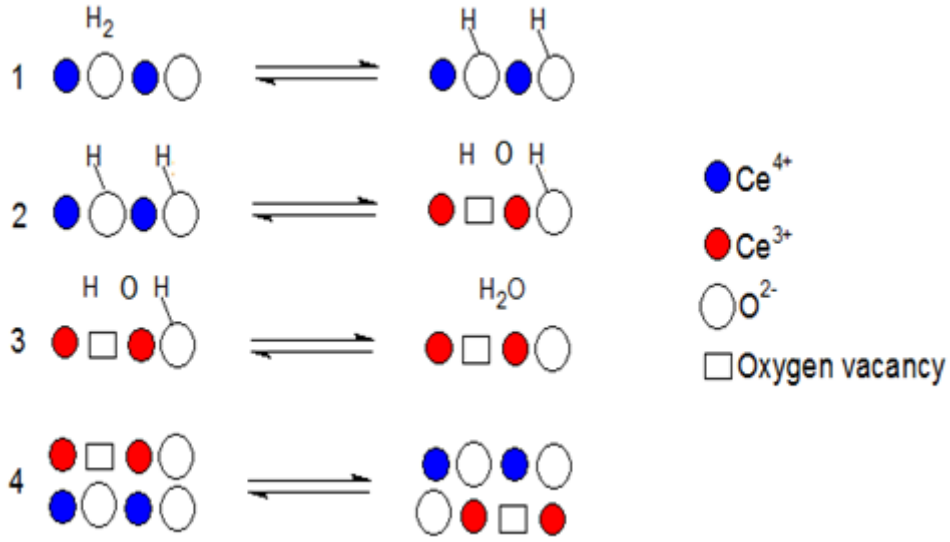

Figure 1-8. Mechanism for the reduction of cerium (IV) oxide by hydrogen[26].

1. Dissociative chemisorption of hydrogen onto the surface to form hydroxyl groups.
2. Anionic vacancy formation with reduction of the neighbouring cations.
3. Water desorption.
4. Diffusion of the surface anionic vacancies into the bulk.

The reduction of CeO_2 is a predominantly a surface process with the reduction of the bulk oxygen being limited by oxygen migration to the surface[28]. It has been shown that surface reduction of CeO_2 by H_2 begins at approximately 200 °C and temperatures greater than 650 °C are required for reduction of the bulk[28]. The re-oxidation of the ceria surface occurs at room temperature[21].

The interaction of hydrogen with CeO_2 samples of differing surface areas was followed by temperature programmed reduction, *in-situ* magnetic susceptibility measurements and x-ray diffraction[18]. This investigation concluded that the formation of one Ce^{3+} ion layer on the surface corresponds to a stable intermediate state[18]

This formation of an intermediate state is supported by an investigation of the reduction of CeO_2 by hydrogen using magnetic susceptibility (a method which utilises the fact that the Ce^{4+} ion is diamagnetic, whereas Ce^{3+} is paramagnetic), UV-Vis, FTIR and XPS[27]. This study showed the interaction of hydrogen with ceria (> 327 °C in temperature) to involve a 3-step process;

(i) Reduction of surface oxygen;

(ii) The formation of a stabilised state with the formal composition of $CeO_{1.83}$; and

(iii) Further reduction at higher temperatures[27].

Re-oxidation of ceria was already complete at room temperature in this investigation, providing further evidence of CeO_2 oxygen storage capacity, the mobile character of O^{2-} species in the fluorite structure of CeO_2 and the redox properties of CeO_2[27]. Structural and chemical changes have been observed on CeO_2 after irradiation with 10 keV H^+ ions[15]. Results from this study indicate oxygen-related defects are produced much more readily than cerium-related defects after hydrogen irradiation[15], providing evidence of surface oxygen mobility on ceria. CeO_2 has been shown to have relatively high reactivity towards H_2 even with high O_2 coverage at room temperature[29].

An investigation into the interaction of ozone with CeO_2 showed that O_3 interacts with electron-excess surface sites (most likely Ce^{3+}) of CeO_2, at between 10 - 65 °C to form two kinds of oxygen species O^{3-} and O^-, both species being capable of taking part in radical chain reactions[30].

In a study to investigate the ability of CeO_2 to act as a photocatalyst for water decomposition to oxygen, it was found that CeO_2 exhibits good photostability[31]. The results from this investigation demonstrate that aqueous CeO_2 suspensions containing Ce^{4+}_{aq} and Fe^{3+}_{aq}, undergoing Ultra-violet/Visible light radiation, are active towards O_2 production and

small amounts of H_2. The amount of O_2 produced was found to be related to illumination time, concentration of CeO_2, initial concentration of electron acceptor (Ce^{4+}) and pH[31].

1.7 Reactivity of cerium (IV) oxide with CO, CO_2 and HCOOH

Investigations of the interaction between carbon monoxide (CO) and CeO_{2-x} have shown that CO readily reacts with polycrystalline CeO_2, even at room temperature[32]. However, it has been reported that CO does not adsorb on clean, single crystal CeO_2(111) or the CeO_2(100) planes under ultra-high vacuum conditions[21]. A lack of CO adsorption implies the inability of CO to reduce CeO_2 crystal surfaces, although CO readily reduces CeO_2 powders; it is suggested that the ultra-high vacuum conditions used for surface studies are responsible for the lack of CO adsorption on CeO_2 crystal surfaces[21]. Prolonged exposure of CeO_2 to CO at 350 °C generates reactive lattice defects and carbon-containing surface species[33]. The results from a report into the effects of surface area and oxygen vacancies on CeO_2 in CO oxidation indicates that the surface area and the surface oxygen vacancies in the ceria can influence the CO oxidation performance together[34]. Both factors play a dominant role in the rate determining step of CO oxidation[34]. In a recent CO/O_2 and CO_2 pulse experiment, it was proven experimentally that Ce^{3+} sites are responsible for CO adsorption on CeO_2 that produce carbonate species which are released as CO_2 by adding oxygen[35]. The reaction of the simplest carboxylic acid (HCOOH) with CeO_2 leads to reduction of the oxide surface producing water and carbon dioxide followed by oxidation of the oxide surface through decomposition of hydrogen and carbon monoxide with formate and $^{-}$OH species present as surface intermediates[36].

1.8 Reactivity of cerium (IV) oxide with NO, N_2O and NO_3

In a literature study carried out at the Los Alamos national laboratory in California[8] on H_2/O_2 generation and recombination in plutonium storage, it is reported that oxidised material such as nitrates, nitrogen oxides and ferric impurities are present in the plutonium storage. This is as a result of calcinations and of irradiation of oxygen and nitrogen in the air present in the storage containers. This irradiation of air has been shown to produce nitrogen oxides, nitric acid and create the possibility of nitric acid reacting with the oxide layer of the metal surface to form solid nitrates[8]. Synchrotron-based x-ray absorption near-edge spectroscopy, high-resolution photoemission, and first-principles density-functional calculations were used to study the interaction of NO_2 with CeO_2[37]. The only product detected from the reaction of NO_2 with CeO_2 at 27 °C was adsorbed nitrate (NO_3), which decomposed between 177 °C and 327 °C[37]. The interaction of NO_2 with CeO_{2-x}, produced a mixture of N, NO and NO_3 adsorbed on the oxide surface at room temperature. The presence of Ce^{3+} surface sites assisted in the transformation of adsorbed NO_3 into the mixture of adsorbates[37].

The chemisorption and reaction of NO and N_2O on CeO_2 surfaces was investigated using soft x-ray photoelectron spectroscopy (SXPS), x-ray absorption spectroscopy, and isothermal and temperature programmed desorption spectroscopy[38]. The interaction of NO with ceria was shown to be dependent upon temperature and the oxidation state of ceria. NO did not adsorb on fully oxidised CeO_2 above 150 °C, but at between 90 °C and 150 °C NO was found to adsorb and react to form N_2O and nitrites on fully oxidised CeO_2. The reduced and sputtered surfaces of CeO_2 were found to be more reactive than the fully oxidised surface, resulting in the dissociation of NO on the reduced surfaces of CeO_2[38].

The adsorption and reaction of NO on CeO_2 was also studied using XPS and TPD[39]. NO was not found to adsorb on fully oxidised ceria in this study. On slightly reduced surfaces

that have exposed Ce^{3+} cations, NO adsorbed at 27 °C. After heating to 123 °C, the adsorbed species were found to dissociate, resulting in oxidation of the surface and the production of gaseous N_2. On more highly reduced CeO_2 surfaces NO was found to dissociate and form surface nitride species that are stable up to 123 °C[39].

At higher temperatures the nitrites were found to decompose to produce gaseous N_2[39]. The results in these studies show that adsorption and subsequent reaction of NO with CeO_2 is influenced by the concentration of Ce^{3+} on the surface of CeO_2 [39].

1.9 Aims

The aims of this project are to establish experimental procedures for the reproducible production of CeO_2 samples.

To study the thermal reactions over CeO_2 as a model for the thermal reactions believed to be occurring over PuO_2 in nuclear storage.

To establish experimental protocols for the detailed characterisation of the surfaces of the CeO_2 samples. To monitor the interaction of small molecules over these surfaces, in particular the interaction of H_2 and O_2.

To determine the viability of UHV mechanistic studies of CeO_2 (111) single crystal as a model for CeO_2 powder samples.

To determine the reactive steps in H_2 and O_2 recombination of cerium oxide to form surface water and to explore the factors that inhibit this reaction.

To study the effects of impurities that are present in PuO_2 storage on the H_2/O_2 recombination reaction over CeO_2. Impurities caused by the radiolysis of HNO_3.

1.10 References

1 T. I. o. E. a. Technology, The Nuclear Fuel Cycle, www.iet.org.uk/factfiles.

2 W. N. Association, Uranium mining overview, http://www.world-nuclear.org/info/Nuclear-Fuel-Cycle/Mining-of-Uranium/Uranium-Mining-Overview/.

3 Greenwood and Earnshaw, *Chemistry of the Elements*, 1997.

4 K. Konashi, H. Matsui, Y. Kawazoe, M. Kato and S. and Minamoto, *J. Phys. Soc. Jpn.*, 2006, **75**, 143.

5 U. S. D. o. Energy, ed. U. S. D. o. Energy, U. S. Department of Energy, 1996.

6 U. S. D. o. E. Standard, ed. U. S. D. o. E. Standard, U. S. Department of Energy Standard, 1999.

7 L. A. Morales, US Department of Energy, Los Alamos National Laboratory, 1998.

8 J. A. Lloyd and G. P. Eller, *Los Alamos National Laboratory*, 1998.

9 M. Bowker, The Basis and Applications of Heterogeneous Catalysis., Issue 53.

10 S. Cotton, *Lanthanide and Actinide Chemistry*, Wiley, 2006.

11 D. G. Kolman, Y. Park, M. Stan, R. J. Hanrahan Jr and D. P. and Butt, ed. U. S. D. o. Energy, Los Alamos National Labratory, University of California, 1999.

12 J. M. Haschke, *Abstracts of Papers of the American Chemical Society*, 1990, **200**, 117.

13 J. Marra, *103rd Annual American Ceramic Society Meeting, Symposium on Waste Management Science and Technology in the Ceramic and Nuclear Industries, Indianapolis,IN (US),*, 2001.

14 R. Shannon, *Acta Crystallographica Section A*, 1976, **32**, 751.

15 M. Song, W. G. Wang, F. M. Chu, X. Y. Yang, K. Mitsuishi, K. Furuya and H. Yasuda, *Nuclear Instruments & Methods in Physics Research Section B-Beam Interactions with Materials and Atoms*, 2002, **191**, 586.

16 Y. Namai, K. I. Fukui and Y. Iwasawa, *Catalysis Today*, 2003, **85**, 79.

17 G. Ranga Rao, a. Mishra and B. G., *Bulletin of the Catalysis Society of India*, 2003, 122.

18 V. Perrichon, A. Laachir, G. Bergeret, R. Frety, L. Tournayan and O. Touret, *Journal of the Chemical Society-Faraday Transactions*, 1994, **90**, 773.

19 J. C. Conesa, *Surface Science*, 1995, **339**, 337.

20 S. Gritschneder and M. Reichling, *Nanotechnology*, 2007, **18**, 6.

21 A. Trovarelli, *Catalysis by Ceria and Related Materials*, 2002.

22 H. A. Al-Madfaa and M. M. Khader, *Materials Chemistry and Physics*, 2004, **86**, 180.

23 A. Trovarelli, M. Boaro, E. Rocchini, C. de Leitenburg and G. Dolcetti, *Journal of Alloys and Compounds*, 2001, **323-324**, 584.

24 M. A. Henderson, C. L. Perkins, M. H. Engelhard, S. Thevuthasan and C. H. F. Peden, *Surface Science*, 2003, **526**, 1.

25 J. A. LaVerne and L. Tandon, *Journal of Physical Chemistry B*, 2003, **107**, 13623.

26 J. Elfallah, S. Boujana, H. Dexpert, A. Kiennemann, J. Majerus, O. Touret, F. Villain and F. Lenormand, *Journal of Physical Chemistry*, 1994, **98**, 5522.

27 A. Laachir, V. Perrichon, A. Badri, J. Lamotte, E. Catherine, J. C. Lavalley, J. Elfallah, L. Hilaire, F. Lenormand, E. Quemere, G. N. Sauvion and O. Touret, *Journal of the Chemical Society-Faraday Transactions*, 1991, **87**, 1601.

28 C. Binet, A. Badri and J. C. Lavalley, *J. Phys. Chem.*, 1994, **98**, 6392.

29 M. Hadano, N. Urushihara, S. Terada, D. Katsuya and H. Uchida, *Journal of Alloys and Compounds*, 2002, **330**, 498.

30 A. Naydenov, R. Stoyanova and D. Mehandjiev, *Journal of Molecular Catalysis a-Chemical*, 1995, **98**, 9.

31 G. R. Bamwenda and H. Arakawa, *Journal of Molecular Catalysis a-Chemical*, 2000, **161**, 105.

32 U. Berner, K. Schierbaum, G. Jones, P. Wincott, S. Haq and G. Thornton, *Surface Science*, 2000, **467**, 201.

33 M. Swanson, V. V. Pushkarev, V. I. Kovalchuk and J. L. d'Itri, *Catalysis Letters*, 2007, **116**, 41.

34 Y. Liu, C. Wen, Y. Guo, G. Lu and Y. Wang, *Journal of Molecular Catalysis A: Chemical*, 2010, **316**, 59.

35 Z. Song, W. Liu and H. Nishiguchi, *Catalysis Communications*, 2007, **8**, 725.

36 S. D. Senanayake and D. R. Mullins, *Journal of Physical Chemistry C*, 2008, **112**, 9744.

37 J. A. Rodriguez, T. Jirsak, S. Sambasivan, D. Fischer and A. Maiti, *Journal of Chemical Physics*, 2000, **112**, 9929.

38 S. H. Overbury, D. R. Mullins, D. R. Huntley and L. Kundakovic, *Journal of Catalysis*, 1999, **186**, 296.

39 R. M. Ferrizz, T. Egami, G. S. Wong and J. M. Vohs, *Surface Science*, 2001, **476**, 9.

2 Chapter 2 - Experimental

2.1 Chemicals used for the preparation of cerium oxide.

- Cerium hydrate oxalate (Sigma Aldrich) stored in 0.9M Nitric acid and provided by the National Nuclear Laboratory in Sellafield.
- Cerium oxide (111) single crystal, sourced from Commercial Crystal Laboratories Incorporated, Florida, USA.

2.2 Cerium (IV) oxide powder

2.2.1 Sample preparation

Cerium oxide was prepared by calcining cerium oxalate hydrate. The cerium oxalate hydrate used was stored in 0.9M nitric acid. The cerium oxalate hydrate used was filtered under vacuum and washed with deionised water until the filtrate was pH 7, using pH paper as an indicator. The washed cerium oxalate hydrate was then calcined under static air for 4 hours with a ramp rate of 20 °C/Min at 400 °C (C400), 500 °C (C500), 600 °C (C600), 650 °C (C650), 700 °C (C700), 800 °C (C800) and 900 °C (C900).

2.3 Sample characterisation

2.3.1 Gas-solid chromatography (GC)

Gas chromatography is a technique commonly used to separate gaseous or chemical mixtures. In chromatography there are two phases, a mobile phase and a stationary phase. In gas-solid chromatography the mobile phase is an inert carrier gas (H_2, He, N_2) and the stationary phase a column packed with a solid support. [1]

The reactive gas mixture is flown into the column and adsorbed directly on the solid particles within the column. The different constituents of the reactive gas mixture are separated here by their different interactions with the stationary phase. The stronger the interaction a molecule has with the column the longer time it will take to pass through the column. Each component of the reactive gas mixture is then carried to a thermal conductivity detector.

In this work argon was the carrier gas, as the aim was detection of changes in the H_2 concentration of the reactive gas mixture.

2.3.1.1 Gas-solid chromatography experimental - Hydrogen consumption of a 5 % H_2, 95 % compressed air mixture over cerium oxide as a result of increasing the temperature.

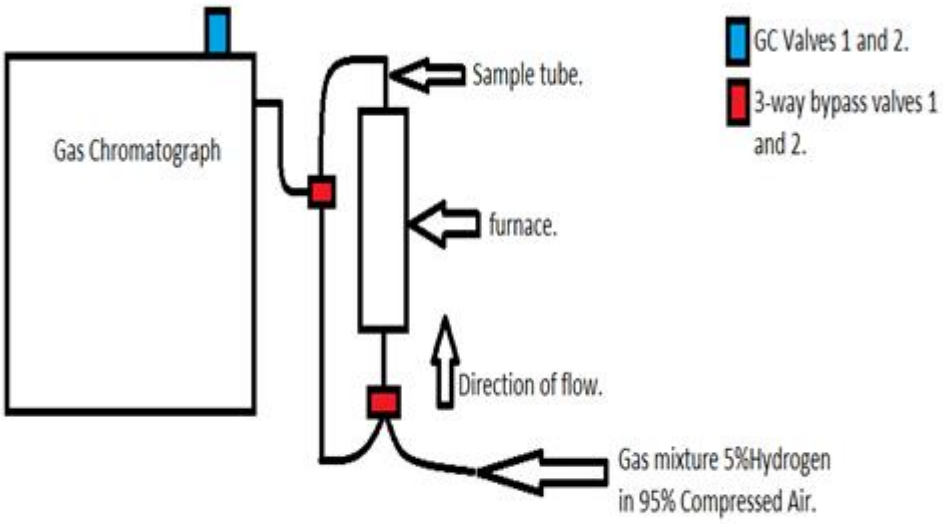

Figure 2-1 Schematic diagram of hydrogen oxidation set up.

Ceria samples were packed into quartz tubes (1 mm thick, 10 mm diameter and 360 mm in length), using quartz wool to hold the sample in place at the centre of the tube. These tubes were then places in stainless steel oven. A gas mixture comprising of 5 % H_2 in 95 % compressed air was flown over these samples at 20 ml/min. Measurements of the hydrogen consumption were taken using a gas chromatograph with a thermal conductivity detector (TCD) at temperatures intervals of 25 – 50 °C ranging from 100 °C to 400 °C.

2.3.2 Thermal gravimetric analysis (TGA)

TGA monitors the mass of a sample as a function of temperature in a controlled atmosphere. The TGA equipment consists of a small crucible that sits on a precision balance and resides in a furnace. TGA can be performed under static air, inert or reaction gases by the use of gas lines connected to the TGA.[2]

2.3.2.1 Thermal gravimetric analysis (TGA) experimental

TGA analysis was performed on cerium oxalate hydrate using a Perkin Elmer TGA 7. Approximately 25 mg of sample was analysed in air. The analysis was run over a temperature range of 30 – 400 °C with a ramp rate of 5 °C min^{-1}.

2.3.3 X-ray diffraction (XRD)

XRD is a technique used to probe the internal structures of solids. It is used to identify crystalline phases of solids by the analysis of the lattice structure of compounds. It is used to

identify bulk phases, to monitor the kinetics of bulk transformations and estimate crystallite size.

XRD operates on elastic scattering of x-ray photons in a periodic lattice. The monochromatic x-rays that are in phase produce constructive interference. The Bragg relationship demonstrates how diffraction of x-rays by crystal planes allows the derivation of lattice spacings;

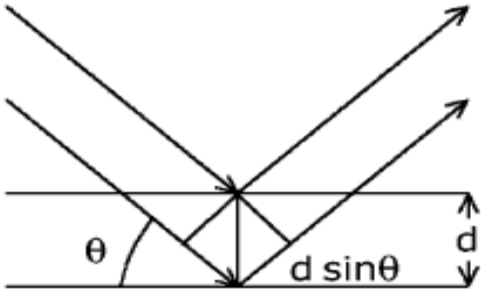

Figure 2-2 Diagram showing the Bragg relationship

$$n\lambda = 2d \sin \theta$$

Equation 2-1. Bragg Equation

Where:

λ = the wavelength of the x-rays;

d = the distance between two lattice planes;

θ = the angle between the incoming x-rays and the normal to the reflecting lattice plane;

n = the order of reflection, n = 1, 2, ….

By measuring the angle 2θ at which constructively interfering x-rays leave the crystal, the Bragg equation gives the corresponding lattice spacings, which are characteristic of a certain compound.

The Scherrer equation is used to estimate the crystallite size of a sample;

$$< L >= \frac{K\lambda}{\beta cos\theta}$$

Equation 2-2. Scherrer Equation

Where:

<L> = is a measure for the dimension of the particle in the dimension in the direction perpendicular to the reflecting plane;

λ = X-ray wavelength;

β = Peak width;

K = Constant (Normally taken as 1)

θ = Angle between the x-ray beam and the reflecting plane.

The Scherrer equation provides a quick estimation of crystallite size using x-ray line broadening.

2.3.3.1 X-ray diffraction (XRD) experimental

X-ray diffraction analysis was carried out on ceria C400 - C900 using a PAN Analytical, XPERT Pro with CuKα radiation. Each sample was placed in a sample holder

(approx. 0.3 g) in order to obtain a flat surface. This analysis lasted around 20 – 30 minutes. The obtained patterns were studied and compared to the JCPDS database.

2.3.3.2 In situ x-ray diffraction experimental

In situ x-ray diffraction was carried out during the calcination of cerium oxalate hydrate to cerium oxide. The cerium oxalate hydrate was calcined at 650 °C in static air, flowing air and an inert (N_2) atmosphere at a flow rate of 20 ml/min. The temperature was raised to 650 °C, taking measurements at 50 °C intervals, whilst at 650 °C measurements were taken every 30 minutes for 4 hours.

2.3.4 Energy-dispersive x-ray spectroscopy (EDX)

Energy-dispersive x-ray spectroscopy is a technique used in conjunction with scanning electron microscopy (SEM). EDX analysis involves the detection of x-rays that are emitted from a sample after bombardment by electrons, which allows the determination of the elemental composition of the sample.

When the sample is bombarded by the electron beam, electrons associated with the sample are ejected. The resulting electron vacancies are then occupied by electrons from a higher energy level. This results in x-ray emission in order to balance the energy difference between the two electron states. The energy of the x-ray emitted is unique to each element.[3] From EDX quantitative data can be determined each element present.

2.3.4.1 Energy-dispersive x-ray spectroscopy (EDX) experimental

Energy dispersive x-ray (EDX) analysis was carried out on ceria samples C400 - C900 using an Oxford instrument with a SiLi detector. The samples were mounted onto aluminium stubs using carbon adhesive discs. EDX analysis was performed using a clean cobalt surface as a reference.

2.3.5 Surface area measurements by the Brunauer Emmett Teller (BET) method.

The determination of surface area by the BET method is based upon gas adsorption. The amount of gas adsorbed at a given pressure allows for the determination of surface area.

The BET theory is an expansion of the Langmuir theory for monolayer adsorption on a surface. It extends the Langmuir theory to incorporate multilayer adsorption.

It works on the following assumptions[4];

i. Adsorption of the first adsorbate layer is assumed to take place on an array of surface sites of uniform energies, based on Langmuir assumptions.

ii. Second layer adsorption can only take place on top of first, third on top of second, etc. In other words there is no interaction between each adsorption layer.

iii. At gas adsorption equilibrium the rate of condensation and evaporation are equal for each individually adsorbed layer.

The resulting BET equation in terms of volume of nitrogen gas adsorbed is as follows;

$$\frac{P}{V(P_0 - P)} = \frac{1}{V_m C} + \frac{(C-1)}{V_m C} \times \frac{P}{P_0}$$

Equation 2-3. BET equation[4]

P = Pressure at equilibrium of adsorbates at adsorption temperature.

P_0 = Saturation pressure of adsorbates at adsorption temperature.

V = Volume of adsorbed gas.

V_m = Volume of adsorbed gas for a monolayer.

C = B.E.T constant.

A plot of $\frac{P}{V(P_0 - P)}$ versus $\frac{P}{P_0}$ should yield a straight line graph, whereby the intercept equals $\frac{1}{V_m C}$ and the slope equals $\frac{(C-1)}{V_m C}$. The BET constant (C) and the volume of gas adsorbed at a monolayer (V_m) can be calculated.

With knowledge of V_m, the surface area of the substrate can be calculated using the following equation;

$$S_A = N \times V_m$$

Equation 2-4. Surface area of the substrate.[4]

S_A = Specific surface area of substrate.

N = Total number of substrate adsorption sites.

V_m = Volume of gas adsorbed at a monolayer.

The total number of substrate adsorption sites can be calculated by equation 2-5;

$$N = \frac{PV_m L}{RT}$$

Equation 2-5. Total number of substrate adsorption sites.[4]

N, P, Vm have their already mentioned meanings.

R= Gas constant.

T = Adsorption temperature.

L = Avogadro's number.[4]

Using the calculated values for S_A and N, one can calculate the specific surface area (SSA) per unit of mass using the following equation;

$$SSA = \frac{S_A}{(mass\ of\ substrate)}$$

Equation 2-6. Specific surface area per unit of mass.

2.3.5.1 Surface area measurements by BET experimental

The BET surface area measurements were carried out using a Micromeretics Gemini 2360 surface analyser. All the ceria samples were degassed for 45 minutes at 120 °C. This was performed to remove any moisture from the surface of the sample. It is estimated that there is a ± 10 % error in the recorded surface area values due to limitations in the technique.

2.3.6 Scanning electron microscopy (SEM)

Electron microscopy is a technique used to determine the size and shape of particles. It can reveal details such as internal structure and in conjunction with EDX it can determine the composition of a selected compound. The interaction of a primary electron beam with a sample can produce information on morphology, crystallography and in conjunction with EDX analysis the chemical composition of the sample.

Scanning electron microscopy (SEM) is performed using a narrow electron beam over a surface. A detector then records the yield of either backscattered or secondary electrons as a function of the primary electron beam to produce an image.

Secondary electrons have low energy and come from the surface of a compound, whereas backscatter electrons originate from below the surface of a compound and carry information regarding the composition of the sample.[3]

2.3.6.1 Scanning electron microscopy (SEM) experimental

Scanning electron microscopy analysis of the ceria samples was carried out using a Carl Zeiss, Evo 40 equipment. Samples were loaded onto an 8-stub carousel using carbon discs to hold the samples in place. The samples were then placed under vacuum before being analysed using the secondary electron detector.

2.3.7 Transmission electron microscopy (TEM)

Transmission electron microscopy utilises an electron beam of high energy and intensity. In TEM transmitted electrons produces a 2D image of the structure of the surface of a sample, this is then magnified to produce a bright field image. Dark field images are produced as result of diffracted electron beams which are off angle from the transmitted beam.[3]

2.3.7.1 Transmission electron microscopy (TEM) experimental

Transmission electron microscopy analysis of the ceria samples was carried out using a JEOL 2100 200 KV electron microscope. Samples were suspended in methanol and deposited by evaporation onto sample discs consisting of holey carbon film on copper.

2.3.8 Raman spectroscopy

Raman spectroscopy is a technique used to study vibrational and rotational modes of a compound. The Raman process involves inelastic or Raman scattering of a monochromatic light from a laser. The laser light interacts with molecular vibrations, phonons or excitations in the compound resulting in the energy of the laser photons being shifted up or down. [5]

Monochromatic light is directed at a sample. The majority of photons from the light experience scattering without any energy exchange with the compound. This is known as Rayleigh scattering. However, some molecules are excited by the monochromatic light source to an unstable state. When the molecule decays, it can either decay to ground state level of the compound in question, this is known as "stokes scattering". Alternatively, the excited state can decay to a level below the ground state level, this is known as "anti-stokes scattering". Both stokes and anti-stokes scattering result in a peak being exhibited in spectra at a certain wavenumbers.[5]

Vibrational energy seen in Raman spectroscopy is specific to chemical bonds and the symmetry of a molecule. Raman spectroscopy can therefore be used for chemical identification and particle size estimation.

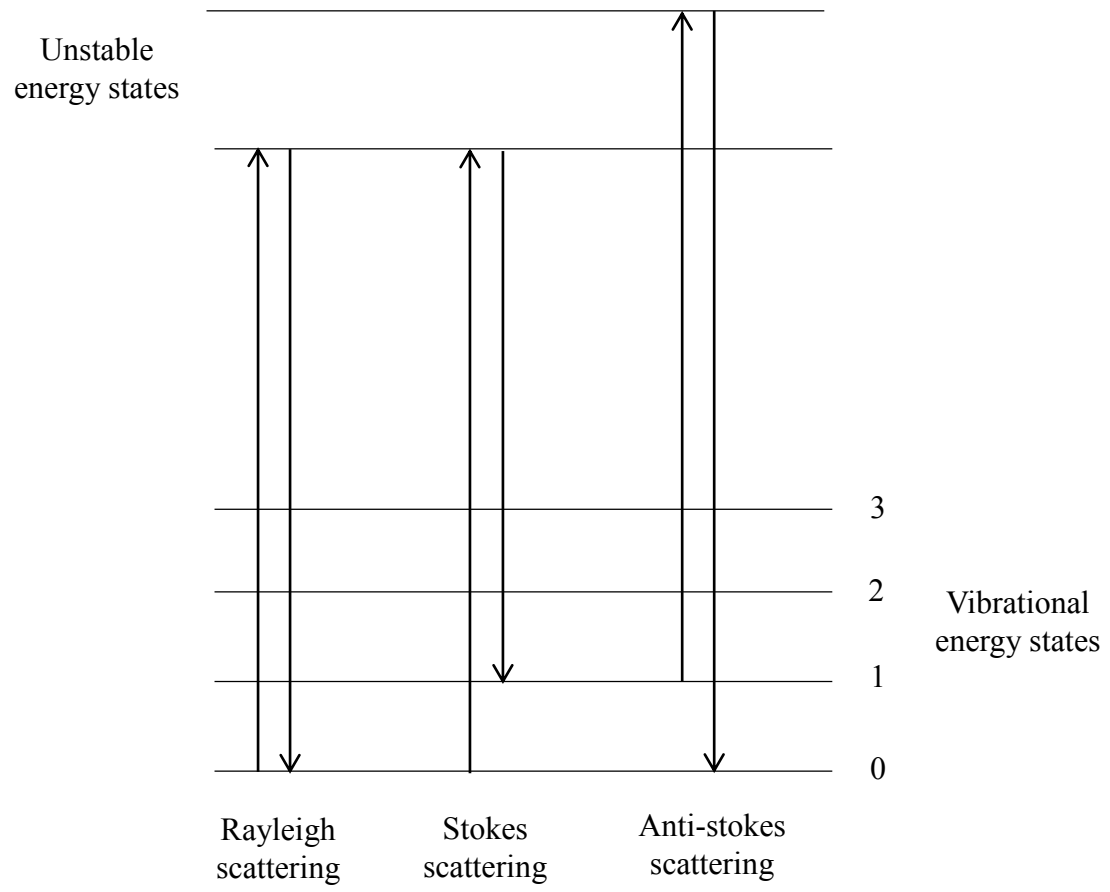

Figure 2-3. Energy level diagram of Rayleigh, Stokes and Anti-stokes scattering in Raman spectroscopy.

2.3.8.1 Raman spectroscopy experimental

The Raman spectroscopy analysis on ceria C400 to C900 was performed using a Renishaw inVia Raman Microscope with a 514 nm and 785 nm Laser source.

This analysis was performed to identify the Ce-O bond vibration that has been reported in the literature[6]. Raman was also used to observe any changes in the spectra as a result of increasing calcination temperatures as changes in the full width half maximum of the Ce-O peak can be related to an increase in defects on the surface of ceria.

2.3.9 Temperature Programmed Reduction (TPR) and Oxidation (TPO).

Temperature programmed reactions monitor a chemical reaction as a function of temperature through thermal conductivity of a gas feed. A gas feed of 10 % hydrogen in argon for TPR and 10 % oxygen in argon for TPO against an argon carrier gas creates a measurable difference in thermal conductivity measurements as a reaction proceeds.

As a reaction proceeds, peaks are seen in the TPR profile. This is as a result of a decrease in the thermal conductivity signal being detected using a thermal conductivity detector (TCD), which is directly related to the amount of reactant gas being consumed. Temperature programmed reactions can be used to identify reaction phases, the amount of reactant gas consumed in each reaction phase and activation energies for surface reactions.

The activation energy of surface reactions can be calculating from TPR data by using the Kissinger equation. In order to use the Kissinger equation, one needs to perform a minimum of 3 different TPR experiments on the same compound using a different ramp rate each time.

$$\frac{ln\beta}{T_{max}^2} = ln\frac{AR}{E_A} - \frac{E_A}{RT_{max}}$$

Equation 2-7. Kissinger equation.

β = Ramp rate.

T_{max} = Temperature at peak maximum.

E_A = Activation energy.

R = Gas constant

A = Pre-exponential factor.

A plot of $\ln(\beta/T_{max}^2)$ versus $1/T_{max}$ can be performed and a straight line fitted to the data, the pre-exponential factor A and the activation energy (E_A) can be calculated from the intercept and slope respectively.[3]

2.3.9.1 Temperature Programmed Reduction (TPR) and Oxidation (TPO) experimental.

Temperature programmed reduction was carried out on each ceria sample using a ChemBET (Quantachrome) chemisorption analyzer. Samples were weighed out and placed in a specially designed U-tube (quartz) where the sample is held in place using two plugs of quartz wool. The system was then purged under an argon atmosphere before undergoing a pre-treatment (110 °C for 1 hour and 5 minutes with a temperature ramp of 5 °C/min). After cooling the temperature programmed reduction takes place using a 10 % H_2 in Ar gas feed which was heated to a maximum of 700 °C – 900 °C at a specific ramp rate of 5 °C/min. A thermal conductivity detector (TCD) was used to measure the amount of H_2 consumed.

Temperature programmed oxidation was carried out on each ceria sample using a ChemBET (Quantachrome) chemisorption analyzer. Samples were weighed out and placed in a specially designed U-tube (quartz) where the sample is held in place using two plugs of quartz wool. The system was then purged under an argon atmosphere before undergoing a pre-treatment (110 °C for 1 hour and 5 minutes with a temperature ramp of 5 °C/min). After cooling the temperature programmed reduction takes place using a 10 % O_2 in Ar gas feed which was heated to a maximum of 200 °C at a specific ramp rate of 5 °C/min. A thermal conductivity detector (TCD) was used to measure the amount of O_2 consumed.

2.3.9.2 Comparison by weight

Temperature programmed reduction reactions were run on all the ceria samples produced (C400 - C900). The samples (0.1g) were pre-treated with argon (20 ml/min) the temperature was increased to 110 °C in order to remove any contaminants on the surface of the sample. The reduction reactions were run under 10 % hydrogen in argon (15 ml/min). The temperature was increased to 900 °C with a ramp rate of 5 °C/min.

2.3.9.3 Comparison by surface area

The samples were run adjusting the weight of the sample in order to obtain the same surface area for each sample. These experiments were carried out in order to determine whether the surface reduction of ceria was surface area dependant.

2.3.9.4 Redox cycles

Temperature programmed reduction reactions were run on ceria samples C400 - C650. The samples were pre-treated with argon at 20 ml/min and raising the temperature to 110 °C to remove any contaminants on the surface of the sample. The reduction reactions were run under 10 % hydrogen in argon at 15 ml/min raising the temperature to 700 °C with a ramp rate of 5 °C/min. This was followed by a temperature programmed oxidation reaction, run under 10 % oxygen in argon at 15 ml/min and raising the temperature to 200 °C. This was then followed by another reduction reaction under the same conditions as mentioned above.

These reactions have been performed in order to determine two things. Firstly, to determine the rate determining step of the redox reaction of ceria. And secondly, to determine if the ceria surface is completely re-oxidised in the presence of oxygen after the surface has been reduced by hydrogen.

2.3.9.5 Temperature programmed reduction of powdered ceria after storage in H_2O_2, HNO_3 and H_2O.

Ceria samples were stored in H_2O_2 (35 % w-w in H_2O), 0.9M HNO_3 and H_2O for 48 hours. The samples were Buchner funnel dried and left at room temperature for 24 hours to dry. Temperature programmed reduction was carried out on each of these ceria samples.

2.3.10 Studying the effect of temperature on hydrogen oxidation on ceria C400, C600 and C900 in an autoclave over time.

Ceria samples C400, C600 and C900 (0.1g) were sealed in a stainless steel autoclave with the air being evacuated using a vacuum pump. The temperature was then raised to 100 °C, 125 °C and 150°C. Once the desired temperature was reached a gas mixture of 2 % hydrogen in synthetic air (1 bar) was released into the autoclave and the pressure monitored over time. These reactions were performed in order to determine the extent of hydrogen uptake on ceria samples C400, C600 and C900 as a result of temperature over time when placed in a sealed vessel.

2.4 Cerium (IV) oxide single crystal

2.4.1 Sample mounting

The ceria single crystal with the (111) plane exposed was mounted using conductive silver epoxy and place onto a molybdenum support disc, which was heated resistively via two tungsten wires running along grooves in the disc. The temperature was controlled and monitored using a K-type thermocouple spot welded to the rear of the Mo-disc.

2.4.2 Sample cleaning

The sample was initially out-gassed in 50 °C increments to a maximum temperature of 550 °C and held at this temperature until the pressure in the UHV system was < $1x10^{-8}$ Torr. The sample was then sputtered using argon ions (4 keV, 10^{-6} Torr argon, 550 °C) for 10 minutes. The sample was then heated in 10^{-5} Torr O_2 (99.999 % purity) for 20 minutes and allowed to cool to < 40 °C in the same pressure of O_2.

2.4.3 X-ray photoelectron spectroscopy (XPS)

X-ray photoelectron spectroscopy (XPS) is a surface sensitive technique that provides information on the oxidation state and elemental composition of a selected compound. The technique is based on the photoelectric effect, which states that if a photon of a specific energy ($h\nu$) is absorbed by an atom then an electron is emitted with a specific kinetic energy (E_K) that is related to the electron binding energy (E_B) which is element specific.

$$E_K = h\upsilon - E_B - \varphi$$

Equation 2-8. Photoelectric equation.[4]

Where:

E_K is the kinetic energy of the emitted electron.

hυ is the energy provided in terms of wavelength.

E_B is the binding energy of the emitted electron.

φ is a work function associated with the spectrometer used.

In XPS, a monochromatic beam of x-rays are targeted at a solid surface, resulting in photoemission from both core and valence levels of surface atoms into the vacuum. A core electron is defined as the inner quantum shells and they play no part in chemical bonding. Core electrons are relatively insensitive to their surroundings when in the solid phase and retain binding energies E_B that are characteristic of an atom type. XPS measures the intensity of a photoelectron as a function of their kinetic energy. However, the XPS spectrum that is often displayed is a plot of the intensity of the photoelectron N(E) versus the kinetic energy E_k or versus the binding energy E_B. Below is a schematic representation of the XPS process[4].

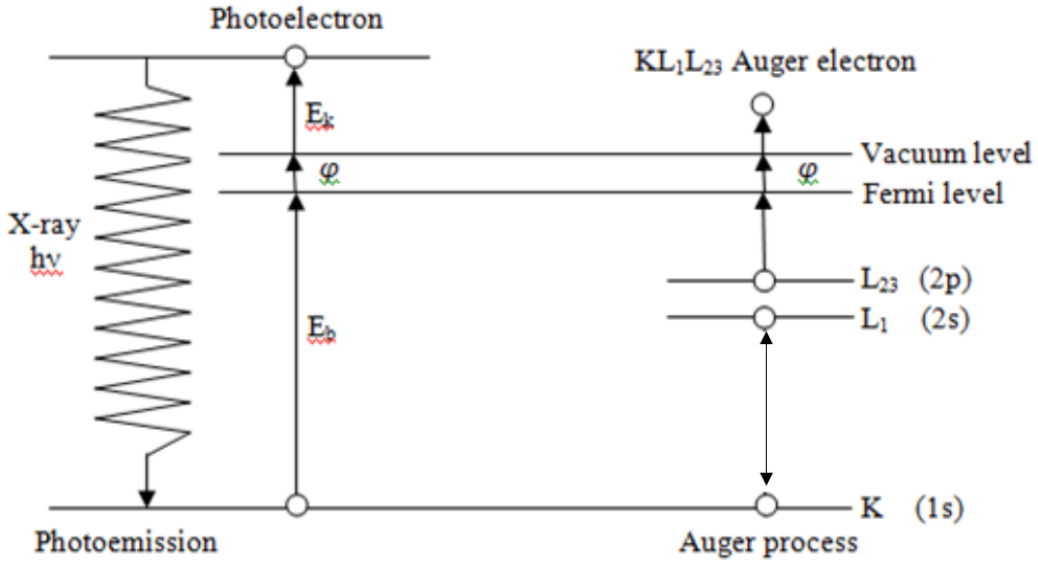

Figure 2-4. Schematic representation of the XPS process.[4]

However, the binding energy is not equal to the orbital energy of the electron as the ionised species relax to shield the newly formed core hole. This results in the observed value of E_B being larger than that that would be predicted by Koopmans' theorem[7].

$$E_B = E_i - E_f$$

Equation 2-9. Electron binding energy equation.

E_B is the binding energy of the emitted atom.

E_i is the total energy of the initial state.

E_f is the total energy of the final state.

Equation 2-9 shows that anything that has an effect on either the initial or final state of the emitting atom will have an effect on the value of the binding energy.

The binding energy of an emitted photoelectron depends upon the localised charge of the emitting atom, this is determined by the ligand that is bound to. The results in a chemical shift, which perturbs electron energies before photo-ionisation has occurred. This effect is referred to as an initial state effect[7].

To minimise the increased energy from the ionisation, electrons in the ionised species undergo a reorganisation resulting in a number of possible of final states, each with their own corresponding energy. This results in extra peaks appearing in the photoelectrons spectrum. These are known as final state effects[7]. Shake-up occurs when an electron within the emitted atom is promoted to a higher level during the photo-ionisation process, this results in a reduction in the kinetic energy required for the transition. Therefore, the main photoelectron peak is accompanied by a satellite peak at a higher binding energy. Cerium also exhibits shake-down peaks where the satellite appears at lower binding energy, in a gain in kinetic energy.

Multiplet splitting arises from the coupling of the remaining unpaired electron spin with unpaired spins in the valence levels of an atom. For all orbitals where the angular momentum number (ι) > 0 (p, d and f levels) spin-orbit splitting is always observed. Here coupling will occur between the fields of spin (s) and the angular momentum given by $j = (\iota + s)$ or $j = (\iota \pm s)$, multiplicities being proportional to $(2j + 1)$[7].

In Ce^{4+} there are three final states $3d^94f^0(5d6s)^5$, $3d^94f^1(5d6s)^4$ and $3d^94f^2(5d6s)^3$ which results in 3 doublets in the photoelectron spectrum. In Ce^{3+} there are two final states $3d^94f^1(5d6s)^4$ and $3d^94f^2(5d6s)^3$ which results in two doublets in the photoelectrons spectrum. These can both be seen in figure 2-5 below.

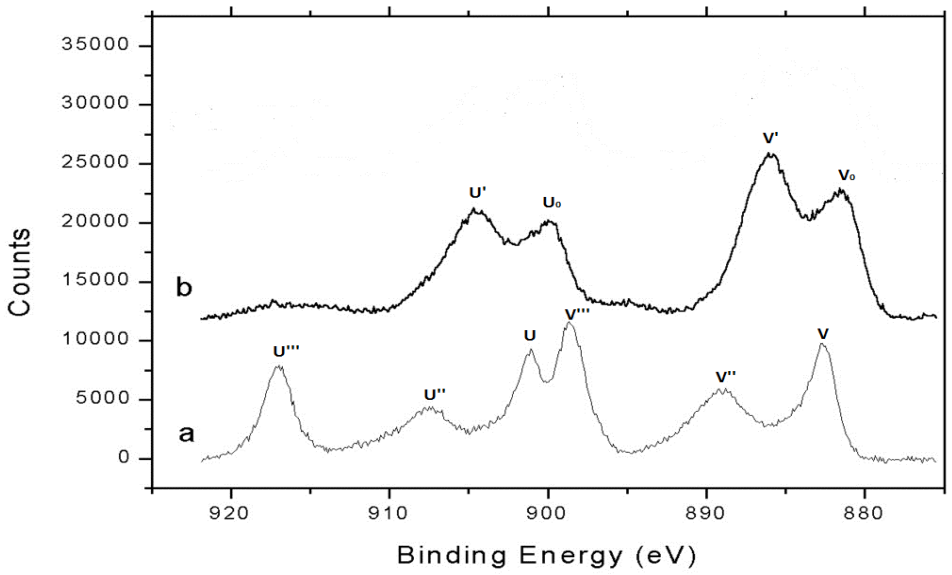

Figure 2-5. Ce 3d spectrum for cerium oxide[8]. a) assumed 100% Ce^{4+} (CeO_2), b) assumed 100% Ce^{3+} (Ce_2O_3).

The x-ray photoelectron Ce 3d spectra of Ce_2O_3 and CeO_2 show uniquely identifiable characteristics of the presence of Ce^{3+} and Ce^{4+}. Figure 2-4 shows the Ce 3d spectrum of CeO_2 and Ce_2O_3, from this it is evident that the U’’’[8] peak is a characteristic of Ce^{4+}. Without the presence of this peak, it would be assumed that the surface has no $4f^0$ states and thus the surface is completely made up of Ce^{3+} which indicates total reduction of the surface.

2.4.3.1 X-ray photoelectron spectroscopy (XPS) experimental

XPS analysis was performed using a Kratos Axis Ultra DLD photoelectron spectrometer equipped with an AlKα x-ray source. Spectra are acquired over an area of 700 x 300 microns at pass energy of 40 eV for high resolution scans. All spectra were calibrated to the C (1s) line of adventitious carbon at a binding energy of 284.7 eV. If no adventitious carbon is present then calibration for CeO_2 was performed against the U''' line at 916.9 eV.

The Ce^{3+}/Ce^{4+} ratios were determined by peak fitting using Casa XPS software using an assumed 100% CeO_2 spectrum and an assumed 100 % Ce_2O_3 spectrum to determine the positions of the peaks.

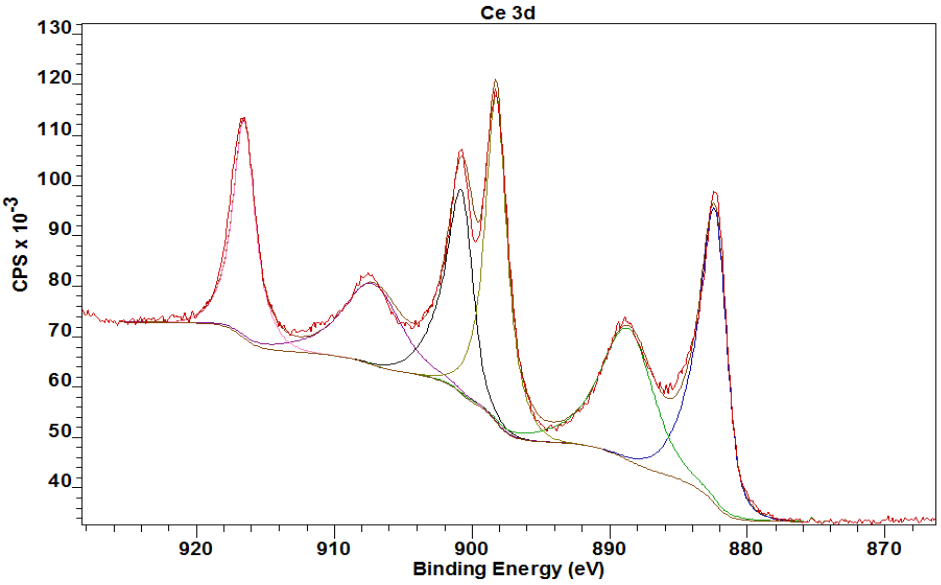

Figure 2-6. XPS Ce 3d Spectrum of an assumed 100 % CeO_2 surface with peak fitting using CASA XPS software.

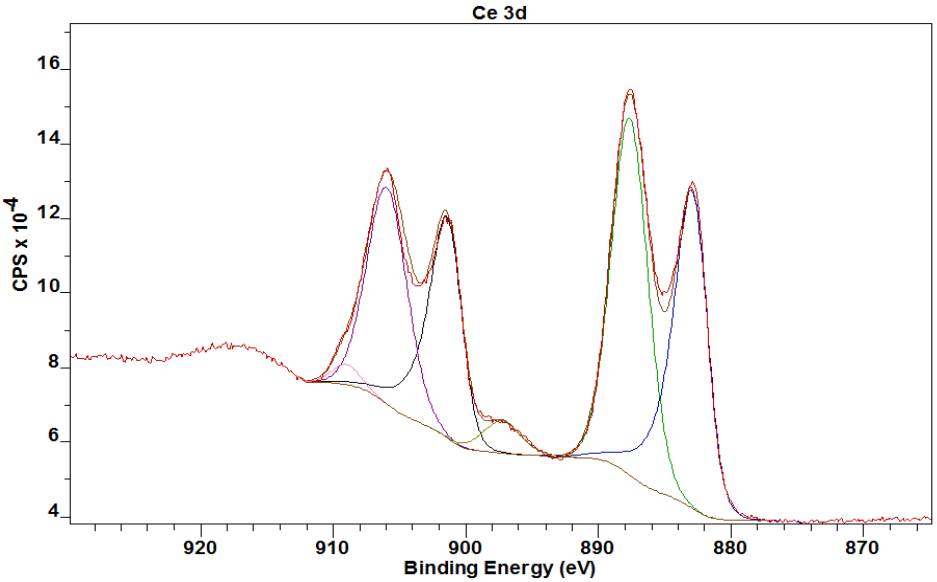

Figure 2-7. XPS Ce 3d spectrum of a sputtered CeO_2 surface, assuming a 100 % Ce_2O_3 surface with peak fitting using CASA XPS software.

2.4.3.2 Reduction of the ceria (111) single crystal under vacuum (10^{-9} Torr), in a hydrogen atmosphere (10^{-7} Torr) and in a hydrogen peroxide atmosphere (10^{-7} Torr).

The ceria (111) single crystal was heated in vacuum to determine if and to what extent reduction occurs upon heating.

The ceria (111) single crystal was heated under vacuum in a hydrogen atmosphere. This was undertaken to determine the extent of reduction upon heating in a hydrogen atmosphere.

The ceria (111) single crystal was heated under a sub ambient (partial pressure of 10^{-7} Torr) hydrogen peroxide atmosphere. This was undertaken in order to determine the effect that hydrogen peroxide has on the reduction profile of ceria. Hydrogen peroxide has the ability to be both reducing and oxidising.

The XPS spectra were taken at room temperature, then in 50 °C intervals up to 400 °C. The XPS spectra were taken coming down in temperature from 400 °C in 50 °C intervals. In the experiment with hydrogen peroxide, XPS spectra were taken from room temperature to 400 °C in 100 °C intervals and coming down in temperature from 400 °C to room temperatures in 100 °C intervals.

2.4.3.3 Oxidation of the reduced ceria (111) single crystal (Under O_2 at 10^{-7} Torr partial pressure).

This experiment was performed in order to identify the oxidation profile of an assumed 100 % Ce_2O_3 surface. The ceria (111) single crystal was reduced by sputtering with argon ions (4keV, 10^{-6} Torr argon, 550 °C) for 10 minutes. The ceria (111) single crystal was then heated to 400 °C under a sub ambient (partial pressure of 1 x 10^{-7} Torr) oxygen atmosphere. Spectra were taken at 100 °C increments.

2.4.3.4 Reduction of the ceria (111) single crystal under vacuum (10^{-9} Torr) and under a hydrogen atmosphere (10^{-7} Torr) at 100 °C, 150 °C and 200 °C for a period greater than 240 minutes.

The ceria (111) single crystal was heated under vacuum (partial pressure of 10^{-9} Torr) and a hydrogen atmosphere (partial pressure of 10^{-7} Torr) at 100 °C, 150 °C and 200 °C and held at those temperatures for a period greater than 240 minutes. These experiments were undertaken to determine the extent of reduction on the ceria single crystal as a result of exposure to the vacuum and a hydrogen atmosphere at different temperatures over an extended time period. XPS spectra were taken at 45 minute intervals.

2.4.3.5 Reduction of the ceria (111) single crystal under an atmosphere of H_2O (partial pressure of 10^{-7} Torr) at 100 °C, 150 °C and 200 °C for a period greater than 240 minutes.

The ceria (111) single crystal was heated under a sub ambient (partial pressure of 10^{-7} Torr) H_2O atmosphere at 100 °C, 150 °C and 200 °C and held at those temperatures for a period greater than 240 minutes. These experiments were undertaken to determine the extent of reduction on the ceria single crystal as a result of exposure to a H_2O atmosphere at different temperatures over an extended time period. XPS spectra were taken at 45 minute intervals.

2.4.3.6 Reduction of the ceria (111) single crystal under an H_2O/H_2 atmosphere (partial pressure of 10^{-7} Torr) at 100 °C, 150 °C and 200 °C for a period greater than 240 minutes.

The ceria (111) single crystal was heated under a sub ambient (partial pressure of 10^{-7} Torr) H_2O/H_2 mixed atmosphere at 100 °C, 150 °C and 200 °C and held at those temperatures for a period greater than 240 minutes. These experiments were undertaken to determine the effect of water on the hydrogen reduction profile of the ceria single crystal at different temperatures over an extended time period. These reactions were run under water rich conditions. XPS spectra were taken at 45 minute intervals.

2.5 References

1 D. C. Harris, *Quantitative Chemical Analysis*, W. H. Freeman, 2010.

2 G. McMahon, *Analytical Instrumentation: A Guide to Laboratory, Portable and Miniaturized Instruments*, John Wiley & Sons, 2007.

3 J. W. Niemantsverdriet, *Spectroscopy in Catalysis: An Introduction*, John Wiley & Sons, 2008.

4 G. Attard and C. Barnes, *Surfaces*, Oxford University Press, 1998.

5 J. W. Niemantsverdriet, *Spectroscopy in Catalysis*, Wiley, 2007.

6 Y. Altaş and H. Tel, *J. Nucl. Mater.*, 2001, **298**, 316; A. Bumajdad, M. I. Zaki, J. Eastoe and L. Pasupulety, *Langmuir*, 2004, **20**, 11223.

7 D. J. Morgan, Cardiff Catalysis Institute, Cardiff University, CF10 3AT.

8 A. Trovarelli, *Catalysis by Ceria and Related Materials*, 2002.

3 The oxidation of hydrogen over cerium oxide.

3.1 Introduction

The aim of this work is to look at the thermal reactions of hydrogen and oxygen over cerium (IV) oxide, for the purpose of mimicking the thermal reactions of hydrogen and oxygen over plutonium (IV) oxide mentioned in chapter 1. In this chapter we attempt to investigate these reactions using a fixed bed flow reactor experimental set up with analysis using a gas chromatography.

As mentioned in chapter 1 the reduction of cerium (IV) oxide and the oxidation of hydrogen by cerium (IV) oxide follows a Mars van Krevelen type mechanism as proposed by El Fallah et al[1, 2] and others[3, 4]

The reduction of cerium oxide is predominantly a surface process with the reduction of the bulk oxygen being limited by oxygen migration to the surface[5]. It has been shown that surface reduction of ceria by H_2 begins at approximately 200 °C and temperatures greater of 650 °C are required for reduction of the bulk[5]. The re-oxidation of the ceria surface $_{occurs}$ at room temperature[3].

It has been suggested that hydrogen dissociation on the surface of ceria is the rate determining step of the surface reduction of ceria and that it is highly dependent on surface area [1]. In this chapter, we look at the reduction of cerium oxide samples with different surface areas by monitoring the oxidation of the hydrogen in the reactive gas mixture.

3.2 Hydrogen oxidation over cerium oxide

3.2.1 Sample preparation

Please refer to section 2.2.1 for sample preparation of Ceria C400 to C900.

3.2.2 Experimental

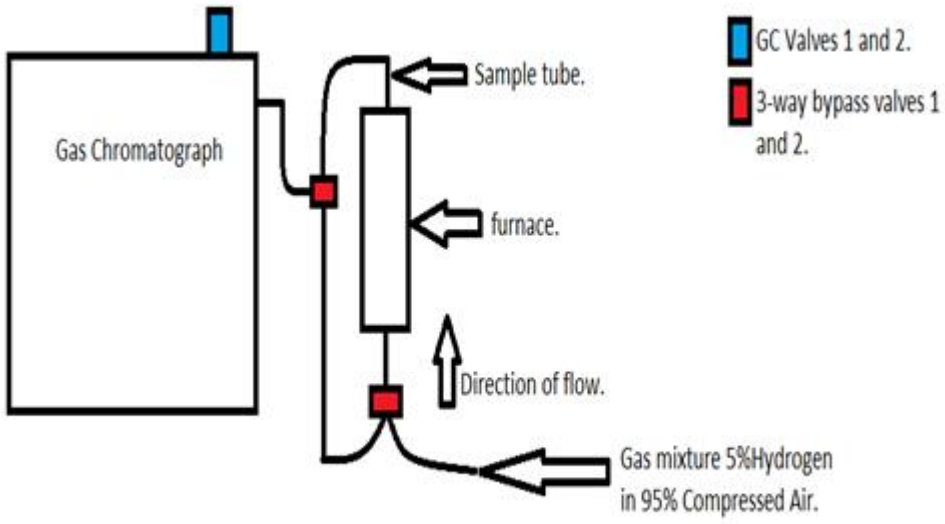

Figure 3-1. Schematic diagram of hydrogen oxidation set up.

0.1 g of ceria C400 was packed into a quartz tube, using quartz wool to hold the sample in place and placed into a furnace. A gas mixture of 5 % H_2 and 95 % air was flowed over the sample at 20 ml/min. The sample was then heated up to 400 °C, taking 3 measurements of hydrogen consumption at 100 °C increments. Measurements of hydrogen consumption were taken by a thermal conductivity detector (TCD) using gas chromatography.

3.2.3 Results and discussion

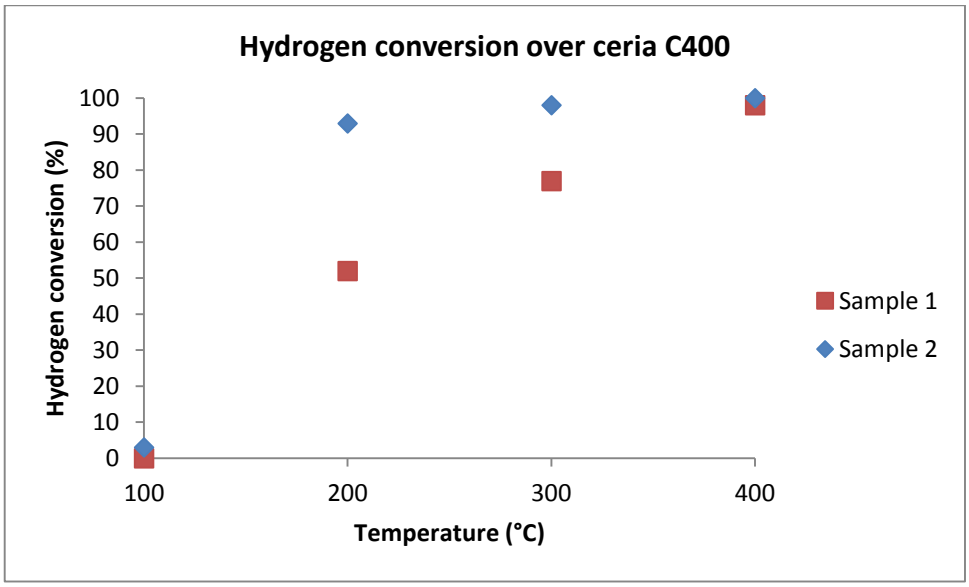

Figure 3-2. Hydrogen consumption of a 5 % H_2, 95 % compressed air mixture over ceria C400 as a result of increasing the temperature.

Table 3-1. Hydrogen consumption of a 5 % H_2, 95 % compressed air mixture over ceria C400 as a result of increasing the temperature data.

Temperature (°C)	Ceria C400 Sample 1	Ceria C400 Sample 2
100	3	0
200	93	52
300	98	77
400	100	98

As can be seen from figure 3-2 and table 3-1 above, the results for hydrogen oxidation of ceria C400 varied significantly between samples. This produced a problem of reproducibility

of results. Samples of the ceria C500 and C600 were run under the same conditions to determine if this problem also occurred on these samples.

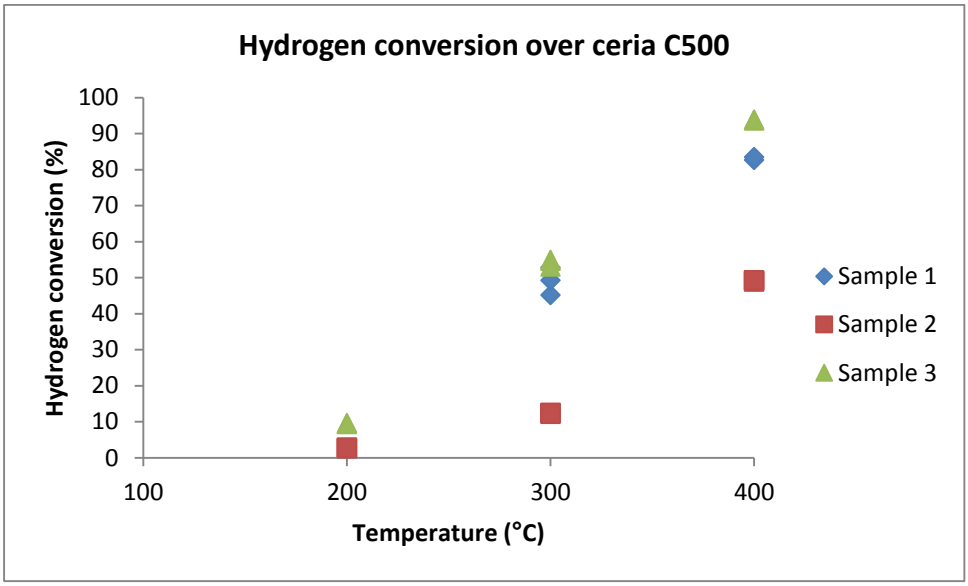

Figure 3-3. Hydrogen consumption of a 5 % H_2, 95 % compressed air mixture over ceria C500 as a result of increasing the temperature.

Table 3-2. Hydrogen consumption of a 5 % H_2, 95 % compressed air mixture over ceria C500 as a result of increasing the temperature data.

Temperature (°C)	Sample 1	Sample 2	Sample 3
200	0	3	10
300	49	12	54
400	83	49	94

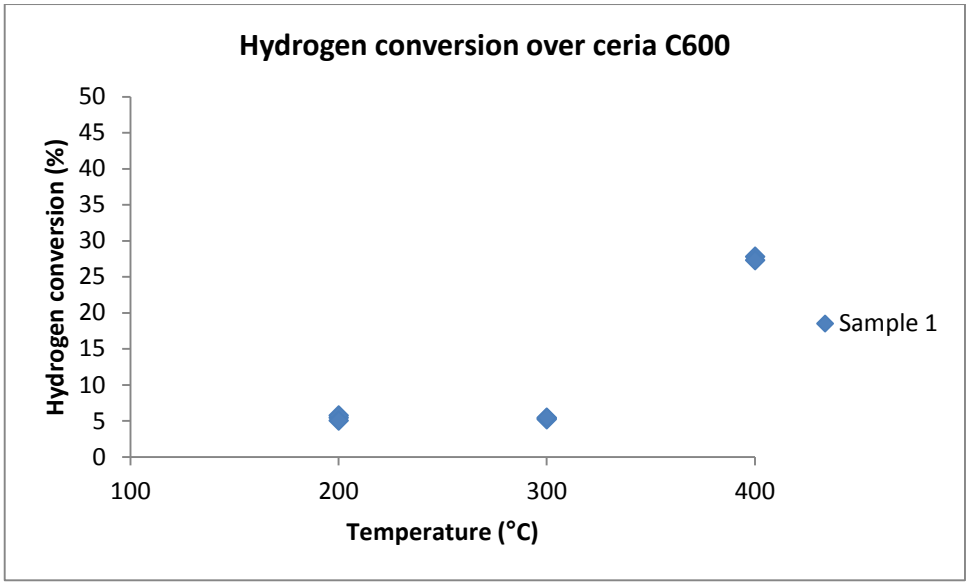

Figure 3-4. Hydrogen consumption of a 5 % H_2, 95 % compressed air mixture over ceria C600 as a result of increasing the temperature.

Table 3-3. Hydrogen consumption of a 5 % H_2, 95 % compressed air mixture over ceria C600 as a result of increasing the temperature data.

Temperature (°C)	Sample 1	Sample 2/3
200	5	0
300	5.	0
400	27	0

Figures 3-2 to 3-4 and tables 3-1 to 3-3 show that reproducibility was a problem with all three samples (C400 – C600). It was believed that the design of the furnace in use may be the reason for the inability to obtain reproducible results. The design of the furnace allowed for a gap of roughly 2 cm from the sample to the inner wall of the furnace and with the top and bottom of the furnace unsealed. It was thought that this was causing a deficiency in the

uniformity of temperature throughout the furnace. This could be cause of the problems that were being witnessed.

In order to solve this problem steel discs were made to be placed at the top and bottom of the furnace, in order to minimise the heat lose through the open parts of the furnace.

Once this work was complete, new samples of ceria C400 were run under the same conditions taking measurements at increments of 50 °C.

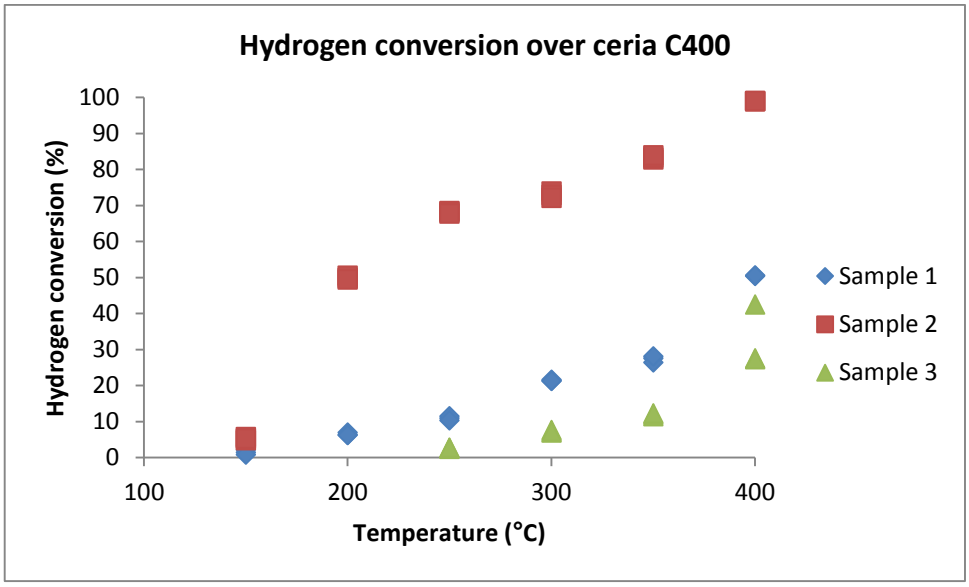

Figure 3-5. Hydrogen consumption of a 5 % H_2, 95 % compressed air mixture over ceria C400 as a result of increasing the temperature (gaps above and below furnace covered with steel discs).

Results from figure 3-5 and table 3-4 indicate that the steel discs did not solve the reproducibility problem. A new sample of ceria C400 was then run under the same conditions, heating to 225 °C and taking measurements at 25 °C increments. However, this time the same sample was run three times, allowed to cool and re-heated in the reactive gas mixture each time. These experiments were done in order to determine whether reproducibility could be obtained internally i.e. on the same sample reduced 3 times.

Table 3-4. Hydrogen consumption of a 5 % H_2, 95 % compressed air mixture over ceria C400 as a result of increasing the temperature (gaps above and below the furnace covered with steel discs) data.

Temperature (°C)	Sample 1	Sample 2	Sample 3
150	1	5	0
200	7	50	0
250	11	68	3
300	21	73	7
350	27	83	12
400	51	99	33

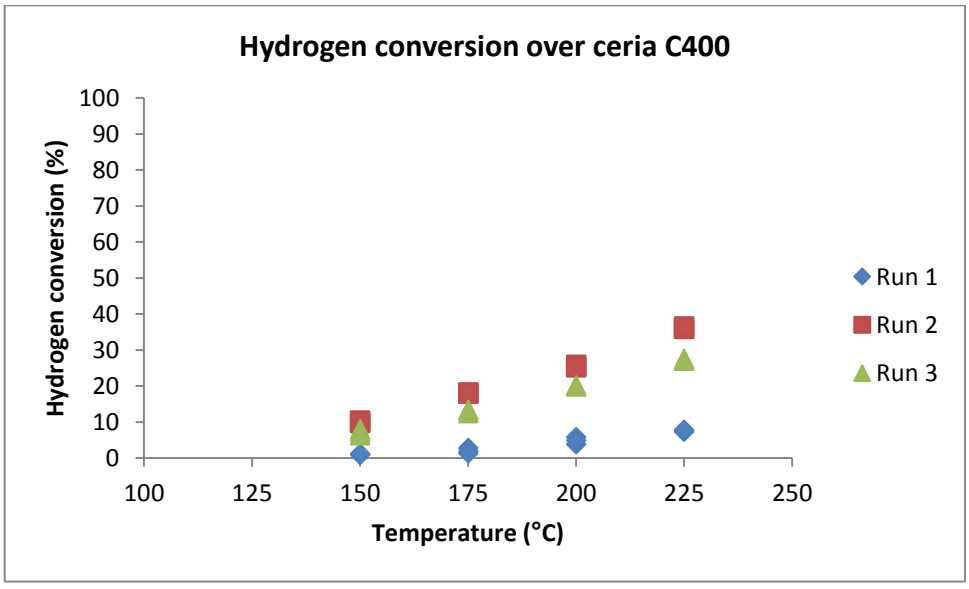

Figure 3-6. Hydrogen consumption of a 5 % H_2, 95 % compressed air mixture over ceria C400 as a result of increasing the temperature (internal runs).

Table 3-5. Hydrogen consumption of a 5 % H_2, 95 % compressed air mixture over ceria C400 as a result of increasing the temperature (internal runs) data.

Temperature (°C)	Sample 1	Sample 2	Sample 3
150	1	10	7
175	2	18	13
200	5	26	20
225	8	36	27

The 2nd and 3rd run of the internal reactions on ceria C400 produced results within 10 % of each other. The results showed hydrogen oxidation over ceria to be reproducible internally but not externally (i.e. between different samples of the same batch of ceria).

Results so far seemed to suggest that reproducibility was obtainable internally but not externally. It was therefore thought that variation in the uniformity of the powdered samples may be the cause of the problem. It was decided to pellet the samples before being packed into the sample tubes. A pellet size of 425 – 600 microns was chosen for the ceria samples.

Reactions were then run under the same conditions on ceria C400 pellets (425 – 600 microns), heating to 200 °C taking measurements at 25 °C increments. However, no reaction was seen. Pelleting the samples decreased the volume of the sample, decreasing the contact time of the sample with the gas mixture and therefore, decreasing the reaction of the H_2 with the ceria. The sample weight was doubled from 0.1g to 0.2g in order to increase the volume of the sample and the contact time with the H_2.

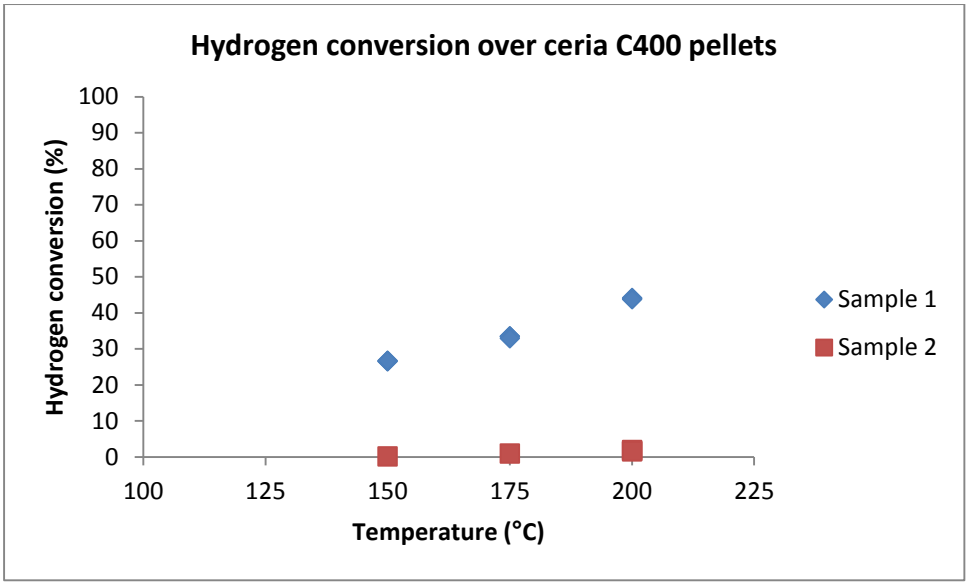

Figure 3-7. Hydrogen consumption of a 5 % H_2, 95 % compressed air mixture over ceria C400 pellets (425 – 650 microns) as a result of increasing the temperature.

Table 3-6. Hydrogen consumption of a 5 % H_2, 95 % compressed air mixture over ceria C400 pellets (425 – 650 microns) as a result of increasing the temperature.

Temperature (°C)	Sample 1	Sample 2
150	27	0
175	33	0
200	44	2

Pelleting the sample did not solve the problem with reproducibility; this is shown in figure 3-7 and table 3-6. This indicates that any variations in the uniformity of the powdered samples were not the cause of the problem. New samples of ceria C400 pellets were run under the same conditions, heating to 275 °C, taking measurements at 25 °C increments. Before any reaction was performed, the flow rate was measured, not only of the gas mixture on its own, but the flow rate of the gas mixture through a blank glass tube and a tube containing the

sample. This was done in order to determine whether the way in which the sample was packed was causing different flow rates through the sample each time. This could be the cause of the failure to gain reproducibility.

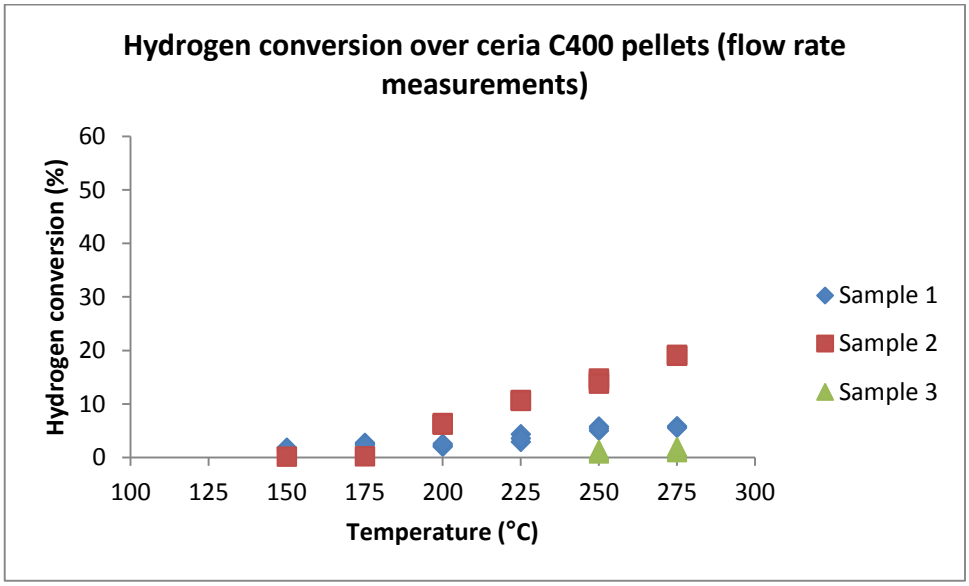

Figure 3-8. Hydrogen consumption of a 5 % H_2, 95 % compressed air mixture over ceria C400 pellets (425 – 650 microns) as a result of increasing the temperature (flow rate measurements).

Table 3-7. Hydrogen consumption of a 5 % H_2, 95 % compressed air mixture over ceria C400 pellets (425 – 650 microns) as a result of increasing the temperature data (flow rate measurements).

Temperature (°C)	Sample 1	Sample 2	Sample 3
150	2	0	0
175	3	0	0
200	2	6	0
225	4	11	0
250	5	14	1
275	6	19	1

Table 3-8. Hydrogen consumption of a 5 % H_2, 95 % compressed air mixture over ceria C400 pellets (425 – 650 microns) as a result of increasing the temperature, flow rate measurements.

Ceria C400 pellets	Weight of sample (g)	Volume of sample (cm^3)	Flow rate of gas mixture (5 % H_2 95 % air) (ml/min)	Flow rate through blank glass tube (ml/min)	Flow rate through sample (ml/min)
Sample 1	0.2	0.2	20.0	20.3	22.1
Sample 2	0.2	0.18	19.7	20.2	20.5
Sample 3	0.2	0.14	19.9	20.8	20.4

Figure 3-8 and tables 3-7 to 3-8 show that samples 2 and 3 had flow rates within 0.1 ml/min of each other and a difference in hydrogen conversion of 18 % at 275 °C, indicating

that the way the samples were packed did not cause a significant change in the flow rate of the gas mixture between samples.

The cerium oxide samples used here were produced by calcining a relatively large amount of cerium oxalate hydrate, which gave approximately 1.5 to 2g of cerium oxide per batch. It was thought that producing the cerium oxide in the larger amounts in a long calcination boat, where the outsides of the boat were away from the centre of the calcination oven was not producing a homogeneous batch of ceria. If this was the case, it could be the cause of the inability to reproduce results. Therefore, a smaller calcination boat was used to produce lower quantities of cerium oxide per batch, approximately 0.5g. By calcining the cerium oxalate hydrate in much small amounts it was hoped that the majority of the sample would be in the centre of the calcination oven and produce a more homogeneous batch of ceria.

Reactions were run on this new batch of cerium oxide produced under the same conditions, heating to 250 °C taking measurements at 25 °C increments; the results are shown in figure 3-9 and table 3-9.

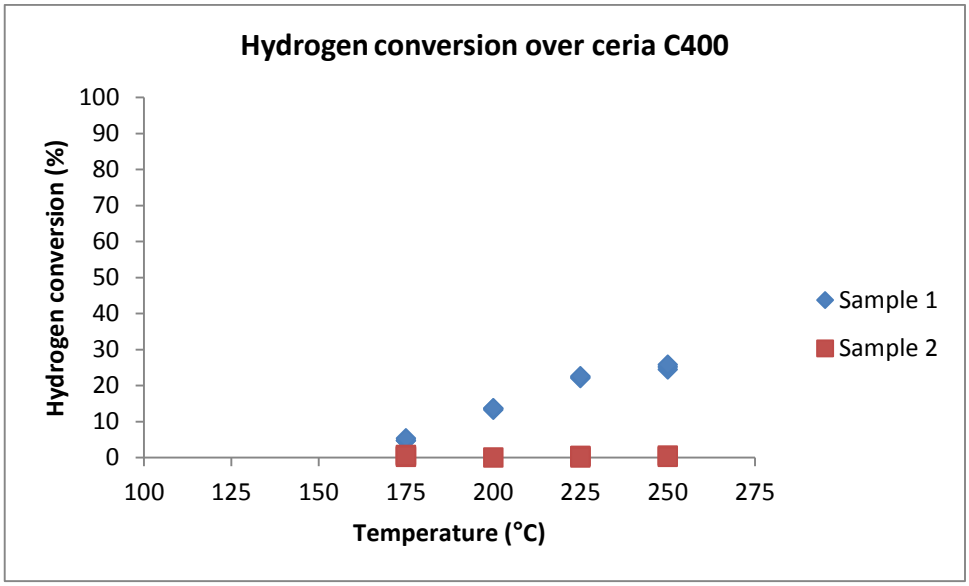

Figure 3-9. Hydrogen consumption of a 5 % H_2, 95 % compressed air mixture over ceria C400 as a result of increasing the temperature.

Table 3-9. Hydrogen consumption of a 5 % H_2, 95 % compressed air mixture over ceria C400 as a result of increasing the temperature data.

Temperature (°C)	Sample 1	Sample 2
175	5	0
200	14	0
225	22	0
250	25	0

Reproducibility of results was still not obtained. Producing ceria in smaller quantities did not solve the problem. In order to determine if the sample preparation used to produce the cerium oxide was the cause of the observed variation in results from samples of the same batch, a commercial ceria (Cerium (IV) oxide, Sigma Aldrich, product code 544841) was tested. As in theory, a commercially available cerium oxide should be uniform throughout the batch and reproducibility should be possible with a commercial cerium oxide.

The first reactions run on the commercial cerium oxide did not produce any results of measurable conversion; it was thought this was because the contact time of the reactive gas with the cerium oxide was insufficient. Therefore, the sample size was doubled and the reactions run under the same conditions as before, heating to 400 °C taking measurements at 100 °C increments.

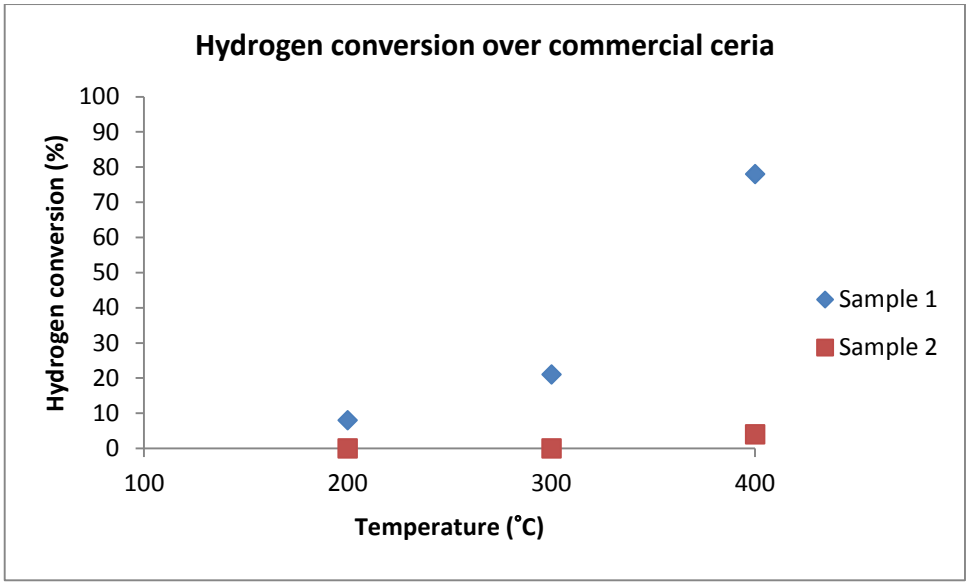

Figure 3-10. Hydrogen consumption of a 5 % H_2, 95 % compressed air mixture over commercial ceria as a result of increasing the temperature.

Table 3-10. Hydrogen consumption of a 5 % H_2, 95 % compressed air mixture over commercial ceria as a result of increasing the temperature data.

Temperature (°C)	Sample 1	Sample 2
200	8	0
300	21	0
400	78	4

Figure 3-10 and table 3-10 show that the problem of reproducibility existed with the commercial cerium oxide as well as those samples produced by calcining cerium oxalate hydrate. As the sample preparation did not seem to be the cause of the inability to obtain reproducibility in the reaction results, a thorough investigation of the experimental set up was undertaken.

As the studies into altering the way the sample were prepared and packed did not provide a solution to the problem, it was believed that the problem lay with the equipment being used. As previously mentioned the design of the furnace being used has a gap of roughly 2 cm between the furnace walls, which may lead to a deficiency in the uniformity of temperature throughout the furnace. The steel discs placed on the top and the bottom of the furnace did not appear to overcome this problem. Therefore, the furnace was replaced with clam-shell steel furnace. As a result of changing the furnace, the sample tubes were also changed from 5 mm diameter quartz tubes to 10 mm diameter quartz tubes.

3.3 Hydrogen oxidation over cerium (IV) oxide (clam-shell steel furnace)

3.3.1 Experimental

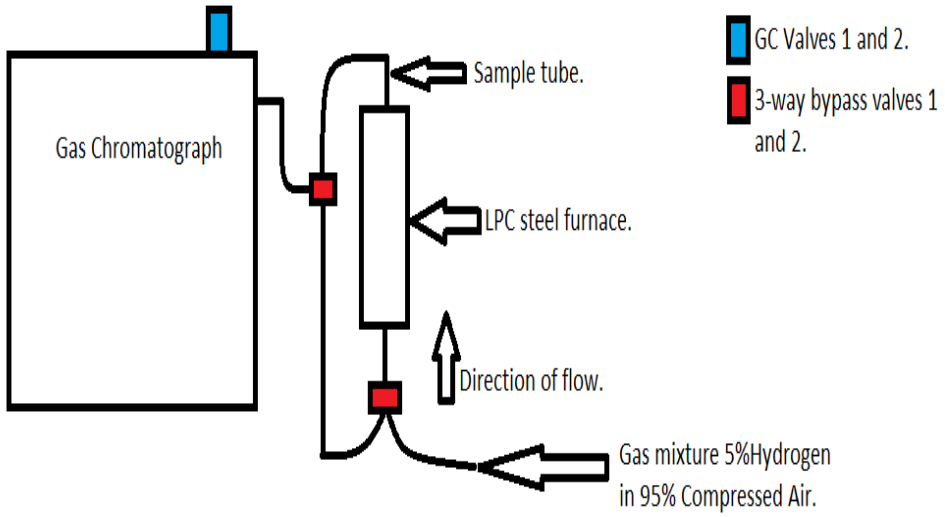

Figure 3-11. Schematic diagram of hydrogen oxidation set up with new steel furnace.

0.5g of pelleted (400 - 625 microns in size) samples of ceria C400 were packed into quartz tubes (1 mm thick, 10 mm diameter and 360 mm in length), using quartz wool to hold

the sample in place at the centre of the tube. A gas mixture comprising of 5 % H_2 in 95 % compressed air was flowed over these samples at 20 ml/min. Measurements of the hydrogen consumption were taken using a gas chromatograph with a thermal conductivity detector (TCD) at temperatures intervals of 25 °C ranging from 100 °C to 200 °C.

3.3.2 Results and discussion

During the initial reactions it was noticed that there was clear fluctuations in the flow rate, not resulting from any reactivity, from run to run. The reactions were stopped and the equipment investigated in order to discover the source of the problem. After detailed inspection of the gas feed tubing, samples tubes, furnace and GC, a hole in the sample loop of valve 1 in the GC was discovered. A new sample loop was sourced and the equipment re-assembled.

The experimental set up was re-assembled and the reactions started again under the same conditions as mentioned above. During the initial stages of these reactions it was noted that the splitting of the peaks was unusual. A number of runs were done altering the parameters of the GC to see if an unknown change from the first time set up had caused the gas mixture to go through the molecular sieve column instead of the standard column. This would explain the unusual peak splitting. Altering the parameters did not provide a solution to the problems encountered with peak splitting. Therefore, the equipment was investigated again and a fault noticed with valve 2 of the GC, which was not turning correctly and as a result the gas mixture was escaping into the atmosphere. This valve was repaired and the experimental set up re-assembled.

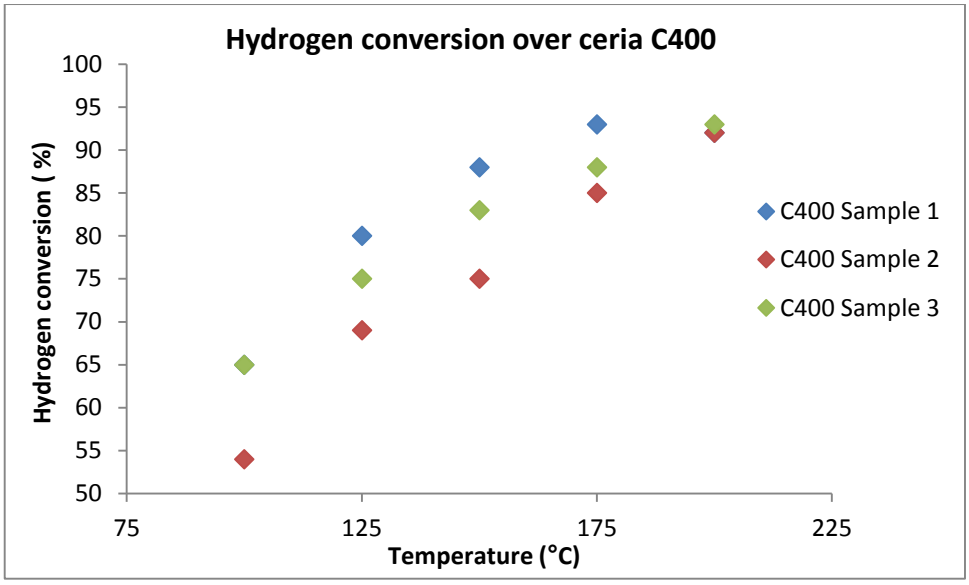

Figure 3-12. Hydrogen consumption of a 5 % H_2, 95 % compressed air mixture over ceria C400 as a result of increasing the temperature.

Table 3-11. Hydrogen consumption of a 5 % H_2, 95 % compressed air mixture over ceria C400 as a result of increasing the temperature data.

Temperature (°C)	Sample 1	Sample 2	Sample 3
100	65	54	65
125	80	69	75
150	88	75	83
175	93	85	88
200	92	92	93

The oxidation of hydrogen over the ceria C400 samples produced results within 10 % of each other, providing reproducible results. The results are shown in figure 3-12 and table 3-

11. These results indicated that increase in temperature caused an expected increase in hydrogen oxidation over ceria C400. The same reactions were repeated with samples of ceria C500 and ceria C600.

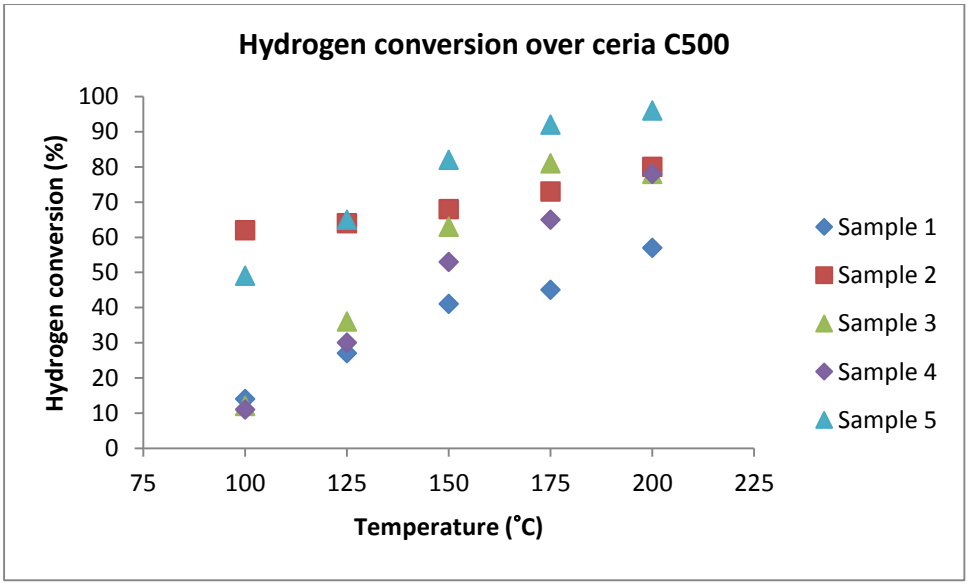

Figure 3-13. Hydrogen consumption of a 5 % H_2, 95 % compressed air mixture over ceria C500 as a result of increasing the temperature.

Table 3-12. Hydrogen consumption of a 5 % H_2, 95 % compressed air mixture over ceria C500 as a result of increasing the temperature data.

Temperature (°C)	Sample 1	Sample 2	Sample 3	Sample 4	Sample 5
100	14	62	12	11	49
125	27	64	36	30	65
150	41	68	63	53	82
175	45	73	81	65	92
200	57	80	78	78	96

The results in figure 3-13 and table 3-12, for individual ceria C500 runs were outside the accepted 10 % error region, so not providing reproducibility. The same was true for samples of ceria C600. This indicated that the problem with reproducibility was still present despite the change of equipment. It was thought the change in sample tube size and resultant change in the volume of the catalyst bed decreased the contact time of the reactant gas mixture with the sample. This could be causing the problems with reproducibility. In order to overcome this problem, the volume of the sample bed was increased. This was done by adding inert silicon carbide to the sample. This increased the volume of the sample bed from 0.5 cm^3 to 2 cm^3.

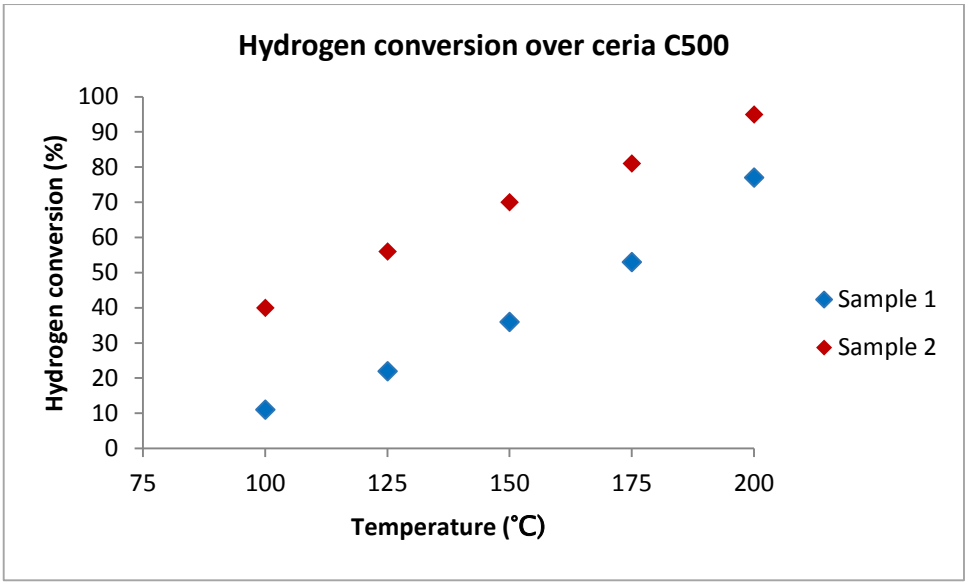

Figure 3-14. Hydrogen consumption of a 5 % H_2, 95 % compressed air mixture over ceria C500 with silicon carbide as a result of increasing the temperature.

Table 3-13. Hydrogen consumption of a 5 % H_2, 95 % compressed air mixture over ceria C500 with silicon carbide as a result of increasing the temperature data.

Temperature (°C)	Sample 1	Sample 2
100	11	40
125	22	56
150	36	70
175	53	81
200	77	95

Figure 3-14 and table 3-13 show that increasing the volume of the sample bed did not solve the problem of reproducibility. As a result, the equipment was again examined to determine if any new problems had occurred. While running sample gas through the system it

was noticed that there was a significant loss of flow rate. During the investigations it was noticed that the 3-way by pass valve was damaged and leaking. This was giving the gas mixture an escape route from the build-up of pressure at the sample loop of the GC. This caused a back pressure down the sample tube. This could have been the cause of the inconsistent results. The decision was made not to replace the 3-way bypass valve but to remove it from the system.

3.4 Hydrogen oxidation over cerium (IV) oxide (without 3-way valve)

3.4.1 Experimental

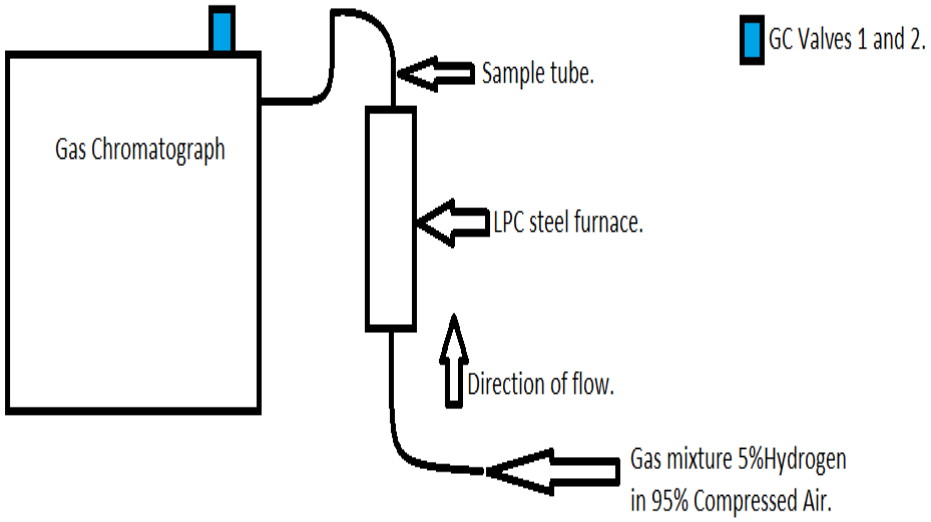

Figure 3-15. Schematic diagram of hydrogen oxidation without bypass valves.

3.4.2 Results and discussion

Reproducibility of results was still not obtained. As a result, it was decided to change the sample tubes from 10 mm diameter quartz tubes to quarter inch steel tubes. It was thought that the volume of the sample tube was too large causing channelling through the sample bed, and insufficient contact time of the reactant gas mixture with the sample.

3.4.3 New Experimental

0.2g of samples of powdered ceria C400 were packed into quarter inch steel tubes, using quartz wool to hold the sample in place at the centre of the tube. A gas mixture comprising of 5 % H_2 in 95 % compressed air was passed over these samples at 20 ml/min. Measurements of the hydrogen consumption were taken using a thermal conductivity detector (TCD) at temperatures ranging from 300 °C to 400 °C.

3.4.4 Results and discussion

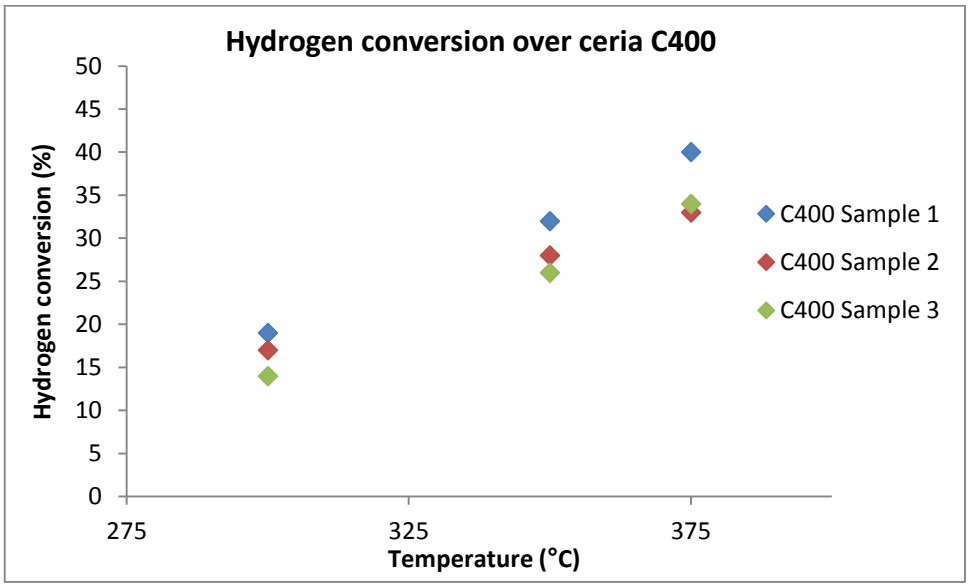

Figure 3-16. Hydrogen consumption of a 5 % H_2, 95 % compressed air mixture over ceria C400, using ¼ inch steel tubes, as a result of increasing the temperature.

Table 3-14. Hydrogen consumption of a 5 % H_2, 95 % compressed air mixture over ceria C400, using ¼ inch steel tubes, as a result of increasing the temperature data.

Temperature (°C)	Sample 1	Sample 2	Sample 3
300	19	17	14
350	32	28	26
375	40	33	34

Results for hydrogen oxidation over 0.2 g samples of ceria C400 in ¼ inch steel tubes, as seen in figure 3-16 and table 3-14, gave results within the accepted 10 % error region. These results indicated that increase in temperature caused an expected increase in hydrogen oxidation over ceria C400. The same reactions were repeated with samples of ceria C500 and ceria C600.

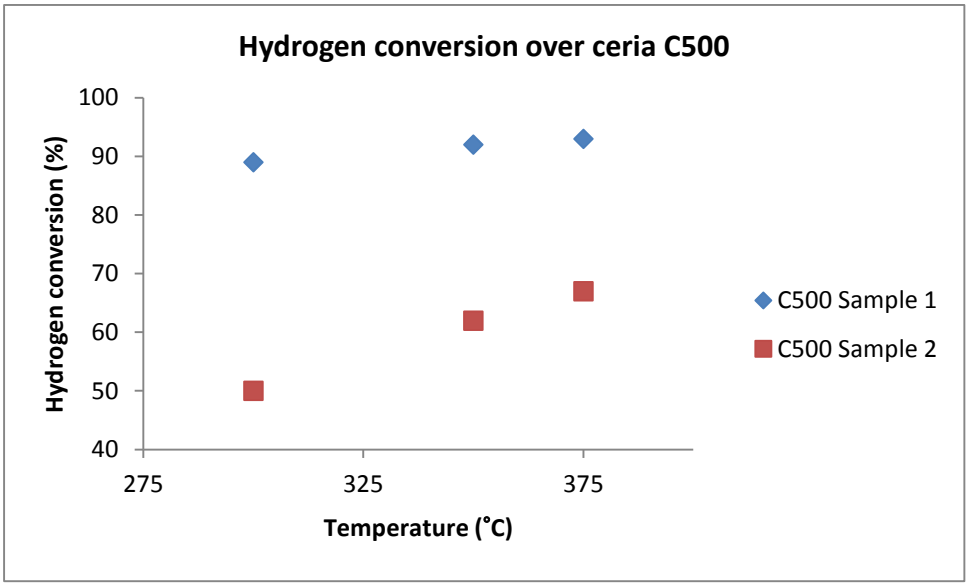

Figure 3-17. Hydrogen consumption of a 5 % H_2, 95 % compressed air mixture over ceria C500, using ¼ inch steel tubes, as a result of increasing the temperature.

Table 3-15. Hydrogen consumption of a 5 % H_2, 95 % compressed air mixture over ceria C500, using ¼ inch steel tubes, as a result of increasing the temperature data.

Temperature (°C)	Sample 1	Sample 2
300	89	50
350	92	62
375	93	67

The results for ceria C500 powder in ¼ inch steel tubes were outside the 10 % error region, and proving non-reproducible. This is shown in figure 3-17 and table 3-15. It was decided to try and run reactions using the lowest surface area sample of ceria C900 to see if reproducibility was obtainable with that batch of ceria.

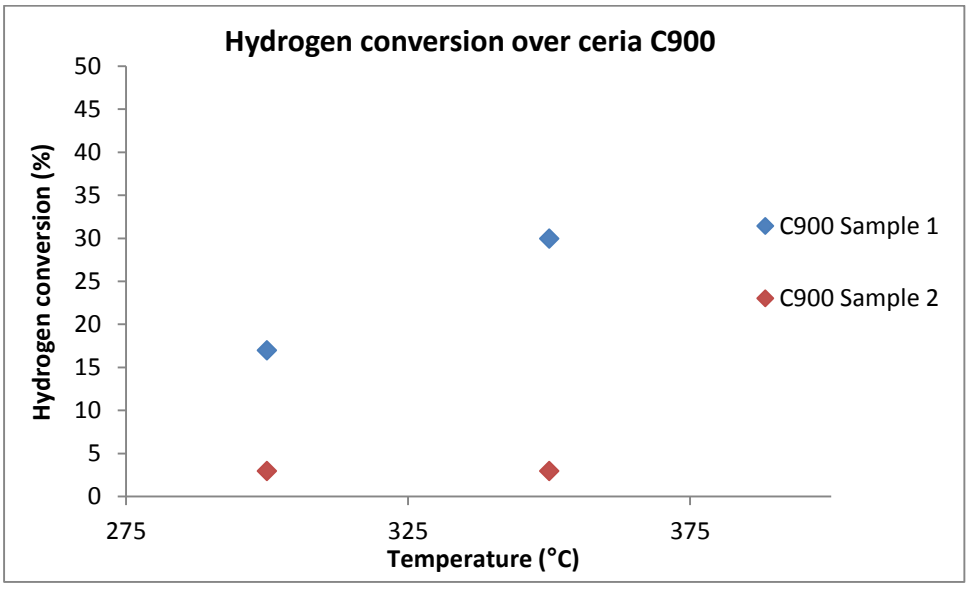

Figure 3-18. Hydrogen consumption of a 5 % H_2, 95 % compressed air mixture over ceria C900, using ¼ inch steel tubes, as a result of increasing the temperature.

Table 3-16. Hydrogen consumption of a 5 % H_2, 95 % compressed air mixture over ceria C900, using ¼ inch steel tubes, as a result of increasing the temperature data.

Temperature (°C)	Sample 1	Sample 2
300	17	3
350	30	3

Figure 3-18 and table 3-16 show that the ceria C900 produced widely varied results, outside the acceptable error region. The problem of reproducibility was not limited to the C500 and C600 batches. It was thought that potential water from the reaction may be condensing in the gas sampling lines to the GC from the sample tube and causing the variation of results. To combat this heating tape was added to the set up and applied to the tubing running from the top of the furnace to the GC. Samples of ceria C900 were run under the same conditions taking measurements at 300 °C and 350 °C.

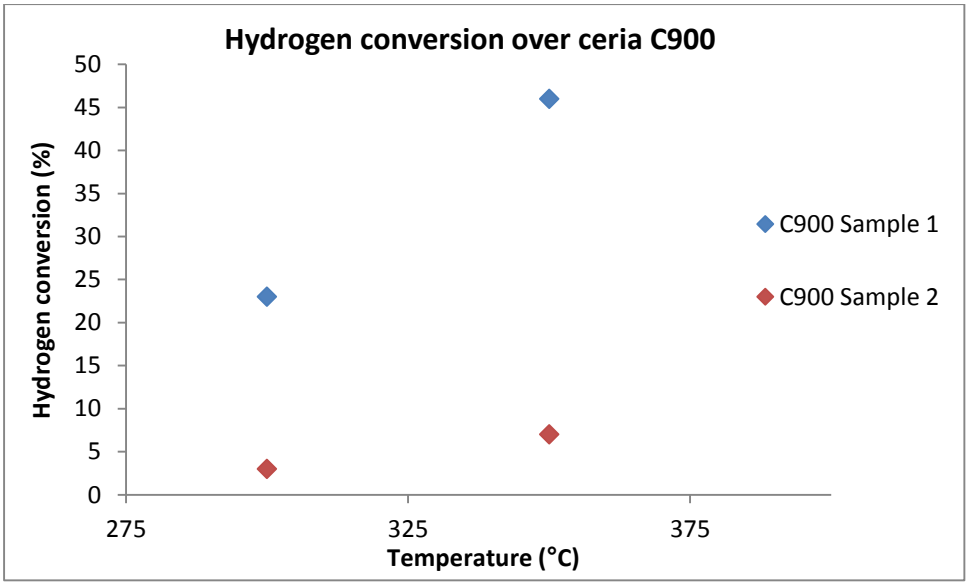

Figure 3-19. Hydrogen consumption of a 5 % H_2, 95 % compressed air mixture over ceria C900, using ¼ inch steel tubes with heating tape, as a result of increasing the temperature.

Table 3-17. Hydrogen consumption of a 5 % H_2, 95 % compressed air mixture over ceria C900, using ¼ inch steel tubes with heating tape, as a result of increasing the temperature data.

Temperature (°C)	Sample 1	Sample 2
300	23	3
350	46	7

Figure 3-19 and table 3-17 show a large variation in hydrogen conversion between sample 1 and sample 2 of ceria C900 with heating tape applied to the system. Applying heating tape did not solve the problem of non-reproducibility. It is assumed that there is a problem with either the experimental set up or the reaction itself. In order to try and determine if the problem is with the experimental system, the experiment was moved to another flow reactor set up. This set up had produced reproducible results for other reactions. However, the system needed to be modified for hydrogen oxidation and also the reactant gas mixture. Due to the nature of the new system, the gas mixture needed to be changed from a mixture of hydrogen and compressed air to a mixture of hydrogen, oxygen and argon. The new gas mixture was 4 % hydrogen in a 96 % mixture of oxygen and argon (21 % oxygen and 79 % argon).

Table 3-18. Calibration data for hydrogen, oxygen and argon on new experimental set up.

Hydrogen		**Oxygen**		**Argon**	
Flow rate (set value) ml/min	**Flow rate (actual flow) ml/min**	**Flow rate (set value) ml/min**	**Flow rate (actual flow) ml/min**	**Flow rate (set value) ml/min**	**Flow rate (actual flow) ml/min**
2.0	1.6	2.0	1.0	5.0	3.1
5.0	4.2	5.0	2.8	10.0	6.2
10.0	9.0	10.0	5.9	30.0	17.1
20.0	18.5	20.0	11.5	60.0	31.2
30.0	27.7	30.0	16.7	90.0	44.3

3.5 Hydrogen oxidation over cerium oxide with new experimental set up

3.5.1 Experimental

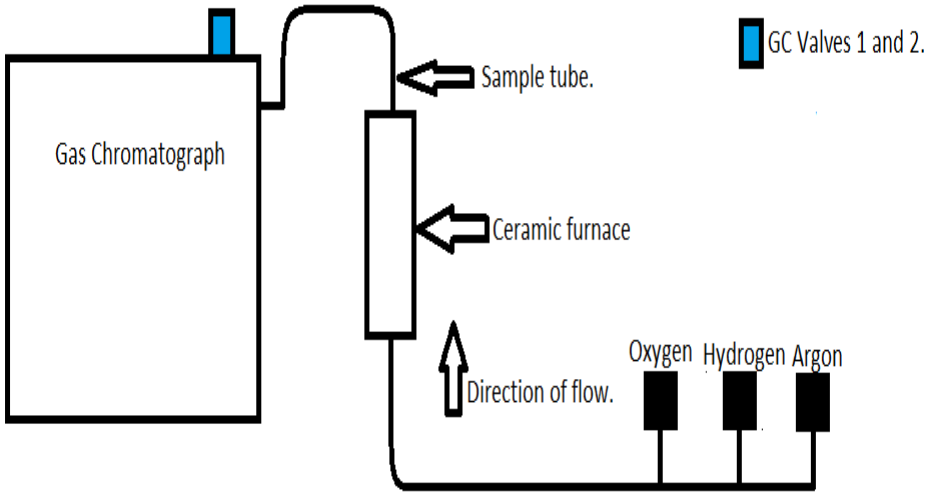

Figure 3-20. Schematic diagram of new hydrogen oxidation set up.

3.5.2 Results and discussion

During the initial calibration of the reactant gas mixture, there was a limitation noticed in the ability of the mass flow controllers to stabilise at low flows. As a result, the lowest flow rate that could be obtained in order to work safely, i.e. working outside the explosion limits of hydrogen in an argon/oxygen mixture, was 100 ml/min.

Initially the equipment was set up with ¼ inch steel tubes. This however, caused fluctuations in the overall flow rate for some unknown reason. The system was changed to ½ inch steel tubes.

During the calcination of cerium oxalate the maximum amount of ceria that can be produced in a single uniform batch is approximately 2g. This is due to the size of the furnaces

available for calcinations. This produces about 1.5g of sample for use after pelleting. This results in the maximum sample weight per run being 0.5g. A pelleted 0.5g sample gives a sample bed of 0.5 cm^3 in volume in 1cm diameter tube.

A flow rate of 100 ml/min over a catalyst bed of 0.5 cm^3 in volume did not produce any reaction. The contact time of the reactant gas mixture with the catalyst was significantly low. Therefore, it is unlikely that there was sufficient contact time with the sample in order to produce a reaction.

3.6 Conclusions

The experiments to determine the extent of hydrogen oxidation over ceria C400 to C900 were unfortunately unsuccessful in producing reproducible results. It can be seen that C400, the CeO_2 with the highest surface area does appear to more reactive towards hydrogen oxidation than the other samples. However, without being able to reproduce results for all the samples this cannot be concluded definitively.

At this point it was decided to stop this work and focus attention on other aspects of the project. At 18 months into a 32 month project, it was decided that the focus should switch away from this work and to commit more time to the temperature programmed studies of cerium oxide powders and the ultra-high vacuum studies of the cerium oxide single crystal to study the thermal reactions involving H_2 and O_2 over ceria.

3.7 References

1 J. Elfallah, S. Boujana, H. Dexpert, A. Kiennemann, J. Majerus, O. Touret, F. Villain and F. Lenormand, *Journal of Physical Chemistry*, 1994, **98**, 5522.

2 A. Laachir, V. Perrichon, A. Badri, J. Lamotte, E. Catherine, J. C. Lavalley, J. Elfallah, L. Hilaire, F. Lenormand, E. Quemere, G. N. Sauvion and O. Touret, *Journal of the Chemical Society-Faraday Transactions*, 1991, **87**, 1601.

3 A. Trovarelli, *Catalysis by Ceria and Related Materials*, Imperial College Press, 2002.

4 G. Ranga Rao, a. Mishra and B. G., *Bulletin of the Catalysis Society of India*, 2003, 122.

5 C. Binet, A. Badri and J. C. Lavalley, *J. Phys. Chem.*, 1994, **98**, 6392.

4 Reduction of cerium oxide powder

4.1 Introduction

The aim of this work is to investigate the thermal reactions of hydrogen and oxygen over cerium (IV) oxide, for the purpose of mimicking the thermal reactions of hydrogen and oxygen over plutonium (IV) oxide referred to in chapter 1. In this chapter we follow these reactions over a cerium oxide powders using temperature programmed reduction (TPR).

The reduction of cerium oxide and the oxidation of hydrogen by cerium oxide follows a Mars van Krevelen type mechanism. This mechanism is as follows;

1. Dissociative chemisorption of hydrogen onto the surface to form hydroxyl groups.
2. Anionic vacancy formation with reduction of the neighbouring cations.
3. Water desorption.
4. Diffusion of the surface anionic vacancies into the bulk.

The reduction of cerium oxide is a predominantly a surface process with the reduction of the bulk oxygen being limited by oxygen migration to the surface[1]. It has been shown that surface reduction of ceria by H_2 begins at approximately 200 °C and temperatures greater than 650 °C are required for reduction of the bulk[1]. The re-oxidation of ceria surface occurs at room temperature[2].

In this chapter, we look at the reduction and oxidation of a range of cerium oxide powders produced by calcination of cerium oxalate hydrate at different temperatures. These reactions are monitored by thermal conductivity measurements using temperature programmed techniques and by examining pressure changes in sealed reactor vessels.

4.2 Results and discussion

4.2.1 Thermal gravimetric analysis (TGA) of cerium oxalate hydrate.

A washed sample of cerium oxalate hydrate was analysed by TGA in order to determine the temperature at which decomposition occurs and to also determine the extent of hydration. This is shown in figure 4-1.

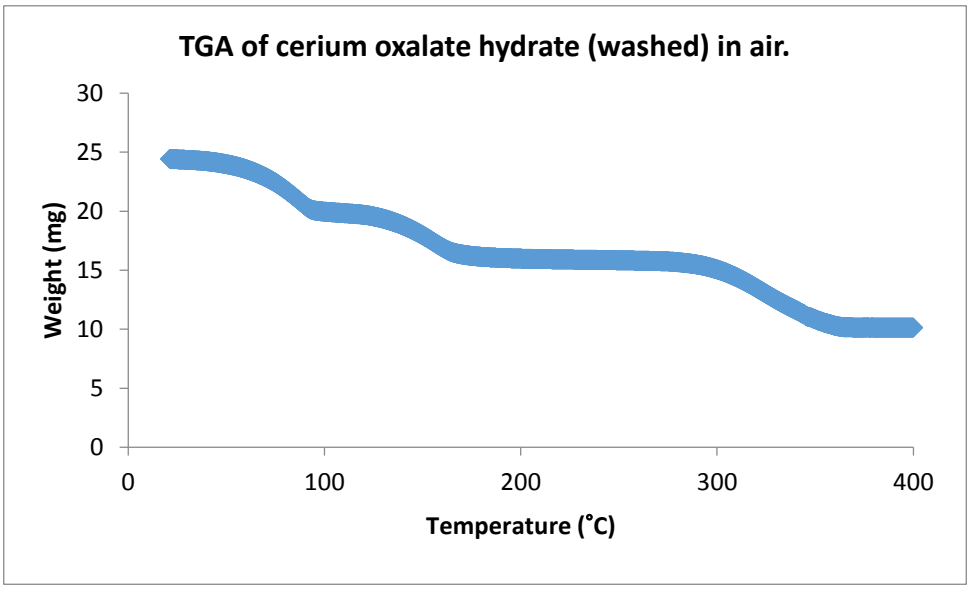

Figure 4-1. TGA analysis of the calcination of cerium oxalate hydrate to cerium oxide.

The decomposition of cerium oxalate hydrate involves three steps. The first step is the loss of physisorbed water, which occurs at approximately 25 °C and is complete by 92 °C. The second step is the loss of water of hydration, which begins at approximately 100 °C and is complete by 170 °C. The third step is the full decomposition of the oxalate to the oxide, which begins at 270 °C and is complete by 370 °C. The amount of water of hydration was calculated from the above data and the molecular formula of the cerium oxalate hydrate found to be $Ce_2(C_2O_4)_3.8H_2O$.

Table 4-1. Data from TGA analysis of the calcination of cerium oxalate hydrate to cerium oxide, showing the temperatures at which weight loss occurs and the respective weight loss in mg.

Step	Temperature Range (°C)	Weight Loss (mg)
Step 1 – Loss of physisorbed water.	25 - 92	4.2
Step 2 – Loss of water of hydration.	100 - 170	3.6
Step 3 – Full decomposition of cerium oxalate to cerium oxide.	270 - 370	5.6

It has been reported that the thermal decomposition of cerium oxalate hydrate involves two steps. The first step is due to loss of water of hydration at a temperature range from 100 °C to 170 °C. The second step in the range of 270 °C to 370 °C is a result of decomposition of the cerium oxalate to cerium oxide.[3, 4]

Figure 4-1 above supports the reported literature[3, 4] in presenting the two steps mentioned. However, Figure 4-1 showed an earlier step which is not mentioned in the literature; this step shows weight loss in the temperature range 25 °C to 92 °C. It is believed that this is as a result of the loss of physisorbed water on the surface of the oxalate.

4.2.2 *In situ* x-ray diffraction (XRD) of cerium oxalate hydrate.

Washed samples of cerium oxalate hydrate were calcined at 650 °C for 4 hours under flowing air, static air and a nitrogen atmosphere. These reactions were monitored by taking XRD measurements at 50 °C intervals and taking XRD measurements at 15 minute intervals whilst holding at 650 °C for 4 hours. These experiments were performed in order to monitor the formation of cerium oxide by decomposition of cerium oxalate hydrate and to note the effect of different atmospheres on this process.

4.2.2.1 Flow of air

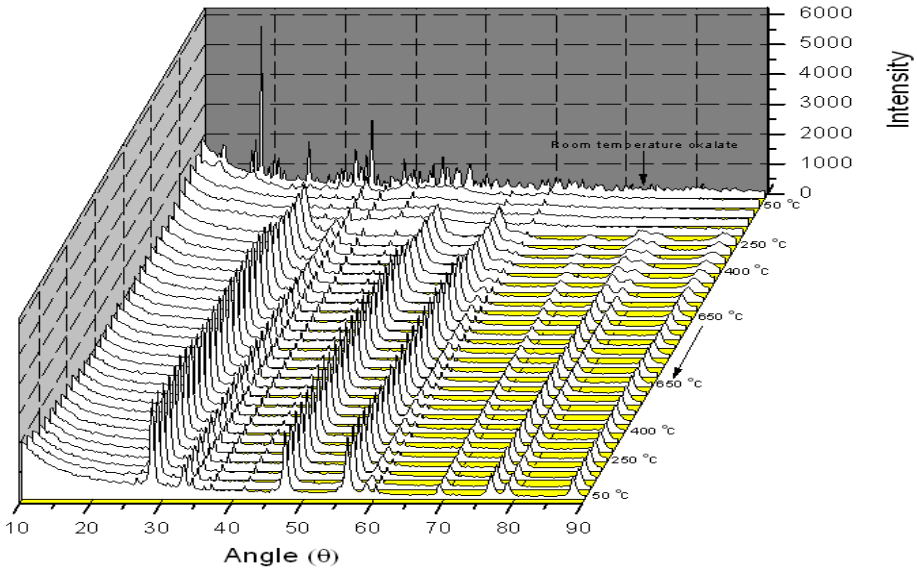

Figure 4-2. *In situ* XRD patterns of the calcination of cerium oxalate hydrate at 650 °C under a flow of air.

4.2.2.2 Static air

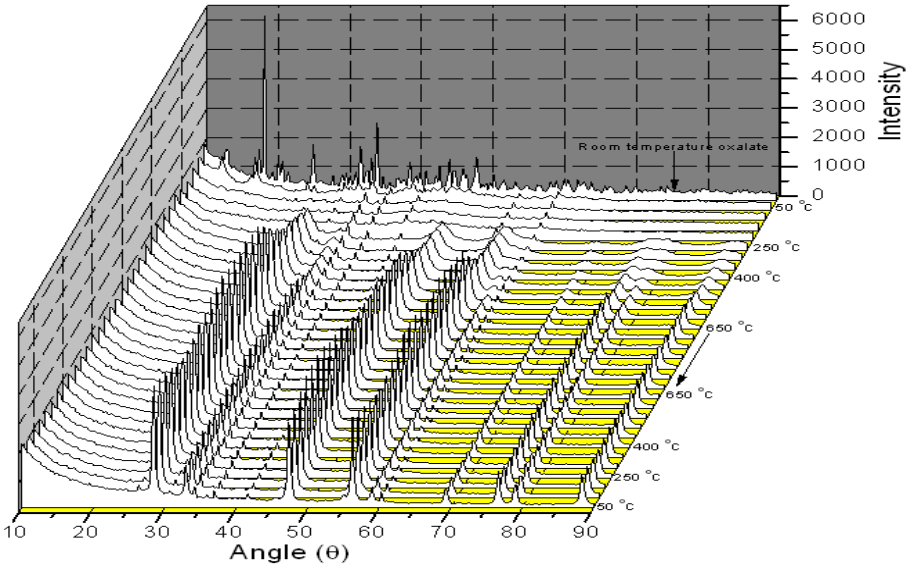

Figure 4-3. *In situ* XRD patterns of the calcination of cerium oxalate hydrate at 650 °C under static air.

4.2.2.3 Flow of nitrogen

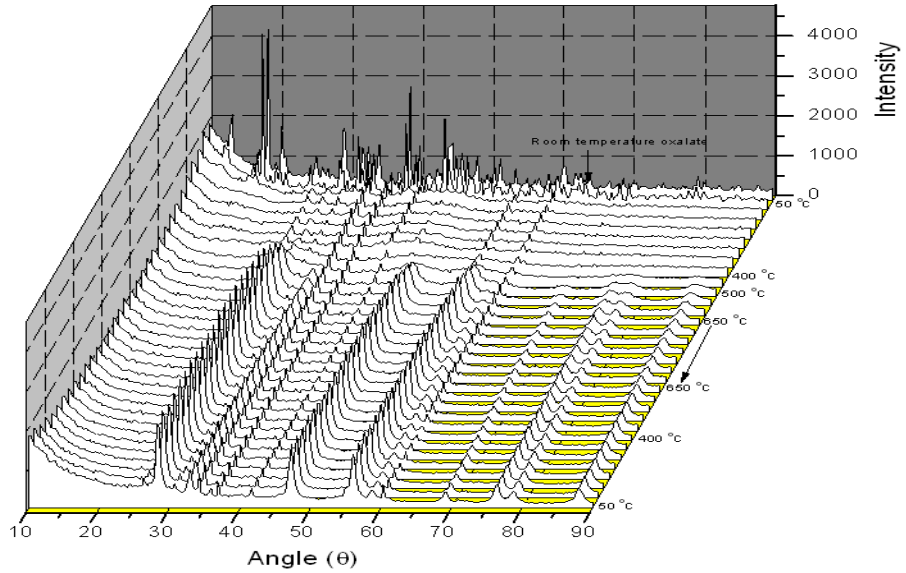

Figure 4-4. *In situ* XRD patterns of the calcination of cerium oxalate hydrate at 650 °C under a flow of nitrogen.

Table 4-2. Crystallite size estimation using the Scherrer equation of ceria C650 produced during in-situ XRD calcination under static air, flowing air and nitrogen atmospheres.

Calcination atmosphere	Crystallite size (nm)
Static air	25
Flowing air	15
Nitrogen	13

The *in-situ* XRD reactions under static air (figure 4-3) and a flow of air (figure 4-2) showed changes in the crystal structure of cerium oxalate hydrate at 50 °C; this corresponds to the loss of physisorbed water and supports the TGA data in table 4-1. The first time patterns representing the crystal structure of CeO_2 were seen was at 250 °C, this is the first sign of decomposition of the oxalate to cerium oxide and is consistent with the findings from the TGA analysis. As expected the reflection peaks become narrower as the temperature is increased which represents a growth in crystallite size of the CeO_2 forming. Calcination under the inert nitrogen atmosphere result in very broad reflection peaks and requires temperatures above 400 °C for significant reflections resulting from CeO_2 to be seen. The *in situ* XRD results show that inert atmospheres, such as nitrogen (figure 4-4) inhibit the decomposition of cerium oxalate hydrate to cerium oxide.

4.2.3 Powder x-ray diffraction

X-ray diffraction analysis was carried out on ceria C400 - C900 to identify the formed product of the calcination of cerium oxalate hydrate. It was also undertaken to observe any

differences in crystallite structure of the cerium oxide formed that is caused by changes in calcination temperature. The obtained patterns were studied and compared to the JCPDS database for confirmation of cerium oxide formation.

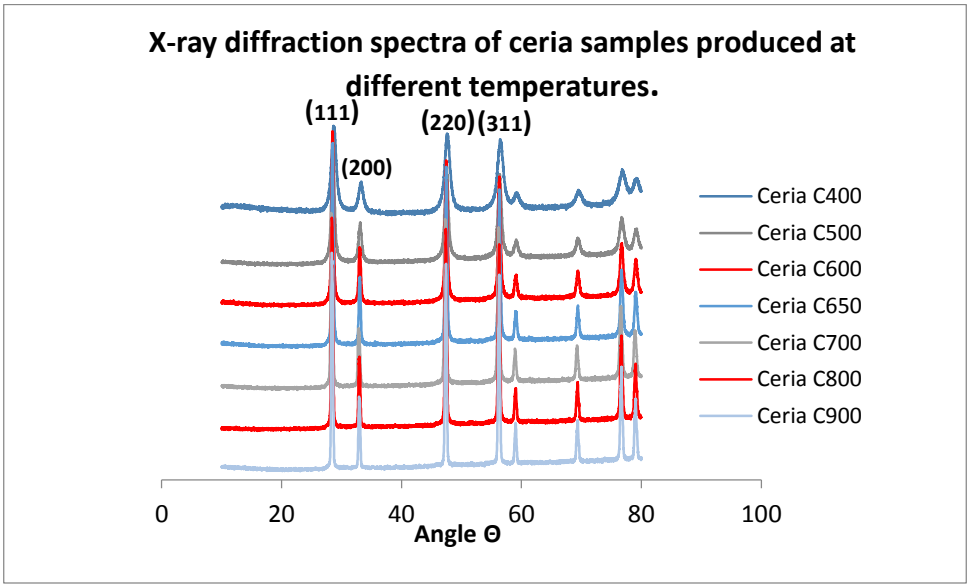

Figure 4-5. X-ray diffraction spectra of ceria produced at temperature 400 °C to 900 °C.

Table 4-3. Lattice parameters and estimated crystallite sizes from XRD data of ceria C400 to C650.

Calcination temperature (°C)	400	500	600	650
Crystal system	Cubic	Cubic	Cubic	Cubic
Space group	Fm-3m	Fm-3m	Fm-3m	Fm-3m
Unit cell volume (cm^3)	157.79	158.45	158.55	158.45
d-spacing (A) (Reflection)	3.1 (111) 2.7 (200) 1.9 (220) 1.6 (311)	3.1 (111) 2.7 (200) 1.9 (220) 1.6 (311)	3.1 (111) 2.7 (200) 1.9 (220) 1.6 (311)	3.1 (111) 2.7 (200) 1.9 (220) 1.6 (311)
Estimated crystallite size (nm)	10.2	16.4	27.3	58.6
XRD reference code	03-065-5923	01-089-8436	01-081-0792	01-089-8436

Table 4-4. Lattice parameters and estimated crystallite sizes from XRD data of ceria C700 to C900.

Calcination temperature (°C)	700	800	900
Crystal system	Cubic	Cubic	Cubic
Space group	Fm-3m	Fm-3m	Fm-3m
Unit cell volume (cm^3)	158.45	158.55	158.46
d-spacing (A) (Reflection)	3.1 (111) 2.7 (200) 1.9 (220) 1.6 (311)	3.1 (111) 2.7 (200) 1.9 (220) 1.6 (311)	3.1 (111) 2.7 (200) 1.9 (220) 1.6 (311)
Estimated crystallite size (nm)	65.8	82.0	92.9
XRD reference code	01-089-8436	01-081-0792	00-034-0394

The XRD data presented in figure 4-5 and tables 4-3 and 4-4 show that the ceria samples produced belong to a cubic crystal system with an Fm-3m space group. The data shows that

ceria C400 to C900 have the same lattice parameters. The differences seen between the different calcination temperatures are when the crystallite sizes were estimated from the (111) reflection. The crystallite size was estimated using the Scherrer equation, using the (111) reflection. The crystallite size is shown to decrease with increasing calcination temperature. All the XRD patterns obtained are consistent with other cerium oxide patterns reported in the literature[5].

.

4.2.4 Energy-dispersive x-ray spectroscopy (EDX) of ceria C400 to C900

EDX analysis was performed on each of the ceria samples produced to determine the approximate elemental composition of the ceria samples. This analysis was also used to identify any high concentration impurities that may be present on the ceria produced.

Table 4-5. EDX approximate elemental compositions of cerium oxide produced by calcination of cerium oxalate at 400 °C to 900 °C.

Ceria Sample	Percentage of oxygen present.	Percentage of cerium present.
C400	25	75
C500	27	73
C600	34	66
C650	26	74
C700	30	70
C800	34	66
C900	33	67

The results in table 4-5 show that the samples of ceria produced at calcination temperatures from 400 °C to 900 °C have an approximately 2:1 ratio of cerium to oxygen by percentage molar weight, this can only be taken an approximation, however, as EDX has limitations when the detection of lower atomic weight elements are concerned[6]. However, what can be concluded from the results is that the ceria is predominantly cerium and oxygen and that any impurities, such as sodium, are not there in high concentrations. There may still be small quantities of impurities present on the ceria, but they are in too small quantity to be picked up by EDX analysis.

4.2.5 Surface area measurements of ceria C400 to C900 by the BET adsorption method.

The B.E.T. surface area of the different ceria samples was determined using nitrogen adsorption. These experiments were performed in order to identify changes in surface area as a result of changing calcination temperatures. These are shown in table 4-6.

Table 4-6. B.E.T Surface area and crystallite size data of ceria samples produced by calcining cerium oxalate at different temperatures.

Calcination Temperature (°C)	Surface Area (m^2g^{-1})
400	42
500	34
600	9
650	5
700	3
800	3
900	1

The surface area of ceria decreases with increasing calcination temperature. This is consistent with the crystallite size date from XRD analysis seen in tables 4-3 and 4-4. It shows an expected decrease in surface area as the crystallite size increases.

4.2.6 Scanning electron microscopy (SEM)

Scanning electron microscopy was used to identify whether the morphology of the ceria is affected by increasing the calcination temperature.

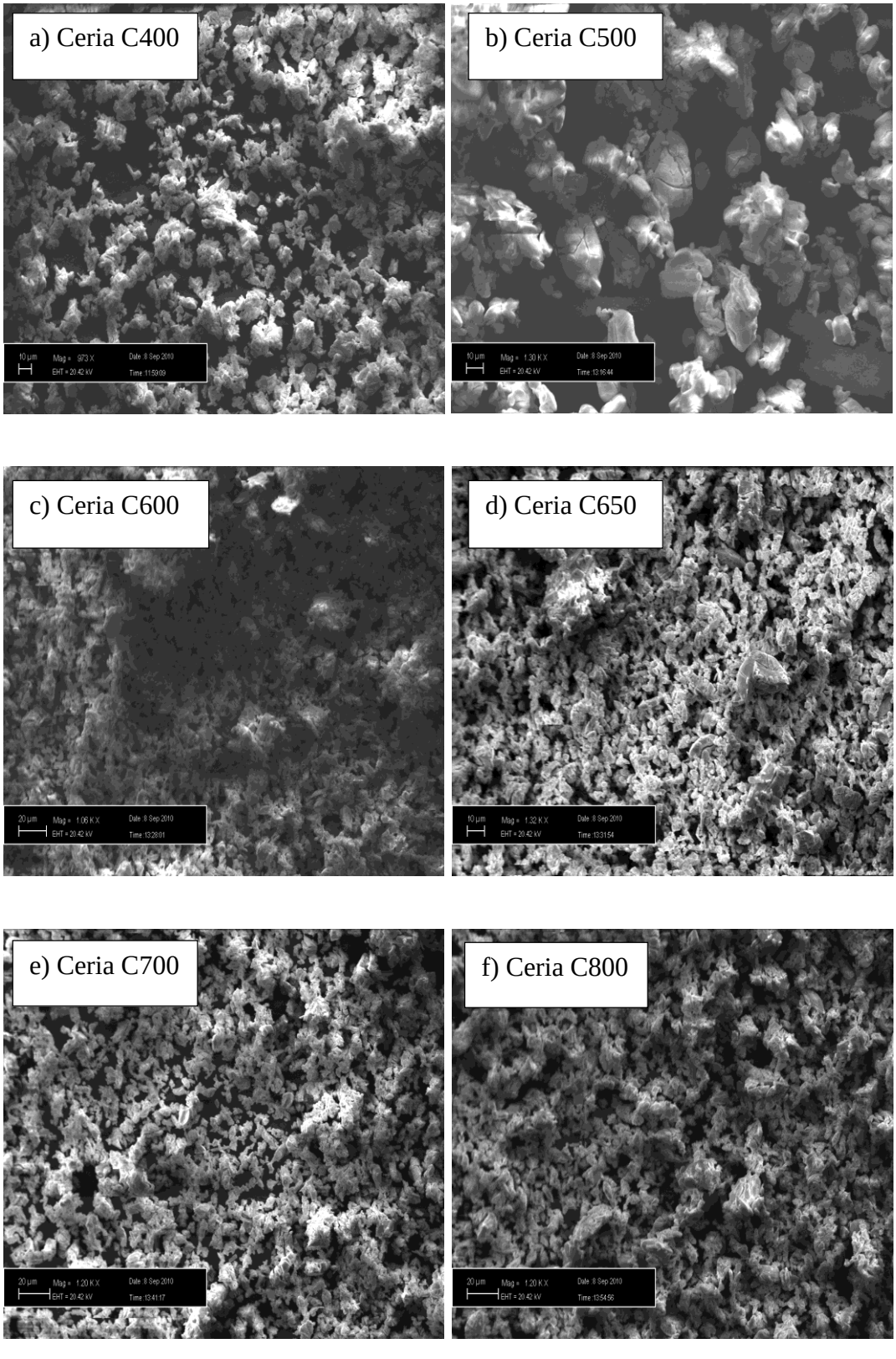

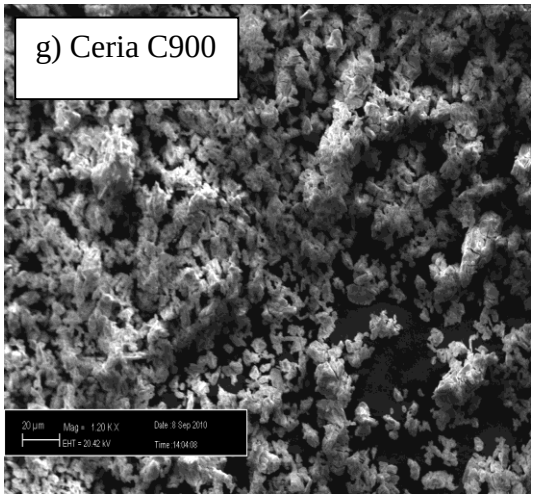

Figure 4-6. SEM images of ceria produced by calcination of cerium oxalate at a) 400 °C, b) 500 °C, c) 600 °C, d) 650 °C, e) 700 °C, f) 800 °C g) 900 °C.

The images in figure 4-6 show scanning electron microscope images of cerium oxide produced by calcining cerium oxalate at 400 °C to 900 °C. At this magnification, no differences are seen in the images a) to g) of figure 4-6. Imaging at higher magnifications was attempted but unfortunately, focussed images were not attainable at higher magnifications.

There may still be differences and morphology caused by increasing the calcination temperature in the production of cerium oxide. Unfortunately, images at high enough magnification to prove or disprove could not be obtained.

4.2.7 Transmission electron microscopy (TEM)

Transmission electron microscopy was used to identify whether the morphology of the ceria is affected by increasing the calcination temperature.

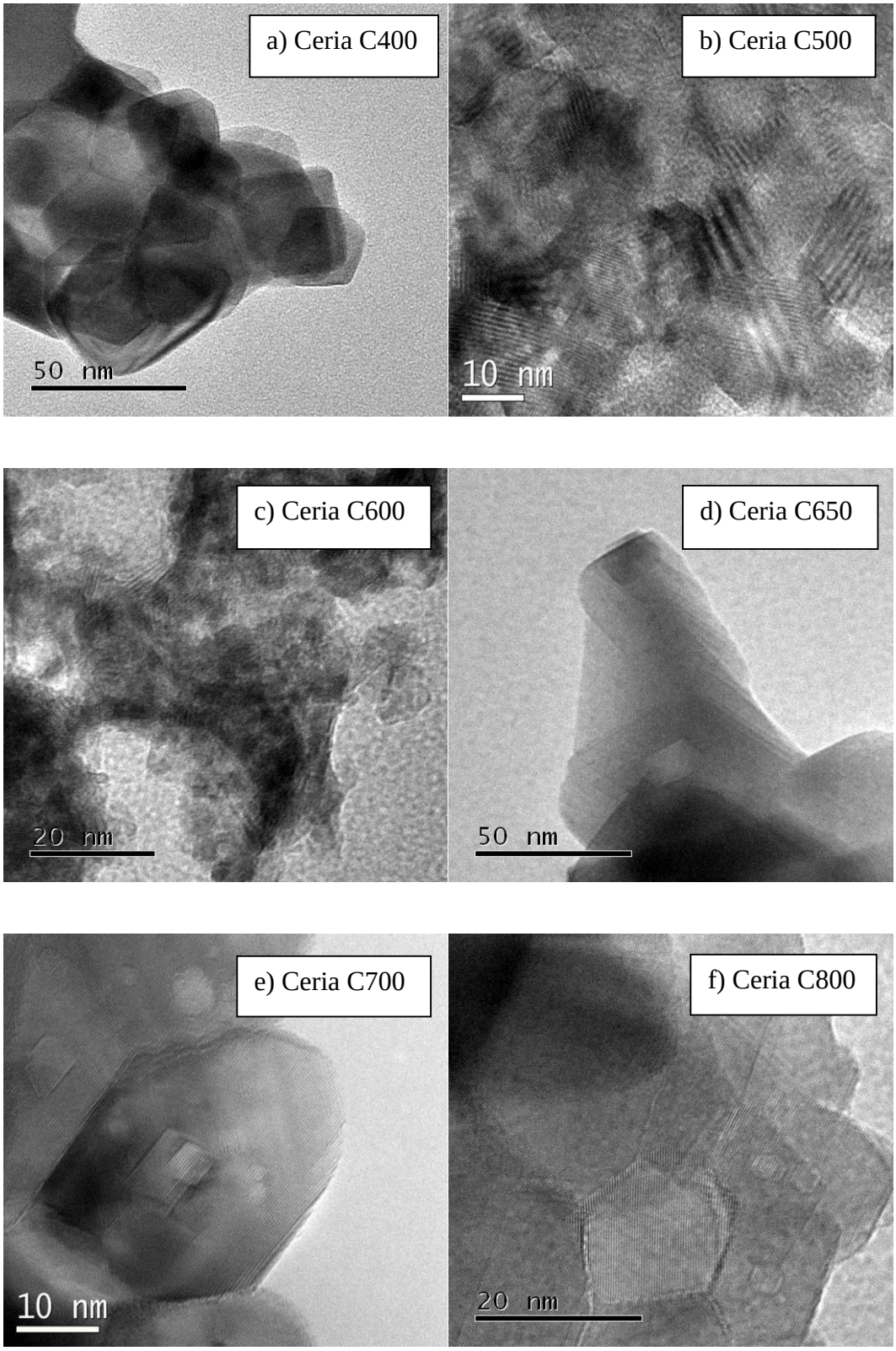
a) Ceria C400
50 nm
b) Ceria C500
10 nm
c) Ceria C600
20 nm
d) Ceria C650
50 nm
e) Ceria C700
10 nm
f) Ceria C800
20 nm

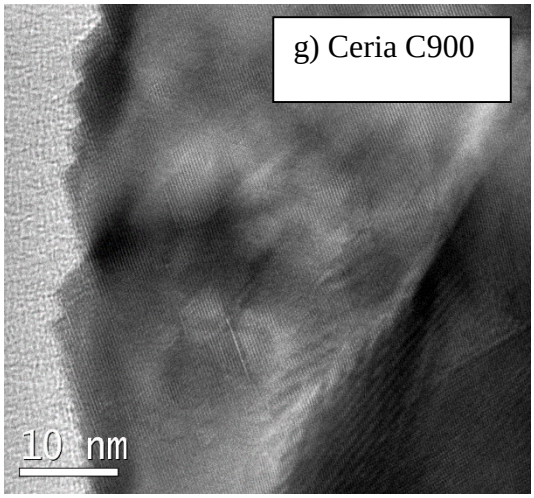

Figure 4-7. TEM images of ceria produced by calcination of cerium oxalate at a) 400 °C, b) 500 °C, c) 600 °C, d) 650 °C, e) 700 °C, f) 800 °C g) 900 °C.

The images in figure 4-7 show transmission electron microscope images of cerium oxide produced by calcining cerium oxalate at 400 °C to 900 °C. There are no differences in the crystal structure of the cerium oxide produced at different calcination temperatures as seen in images a) to g).

4.2.8 Raman spectroscopy of ceria C400 – C900

Raman spectroscopy analysis was performed on ceria C400 to C900 to identify the Ce-O bond vibration that has been reported in the literature[3]. Raman was also used to observe any changes in the spectra as a result of increasing calcination temperatures as changes in the full width half maximum of the Ce-O peak can be related to an increase in defects on the surface of ceria.

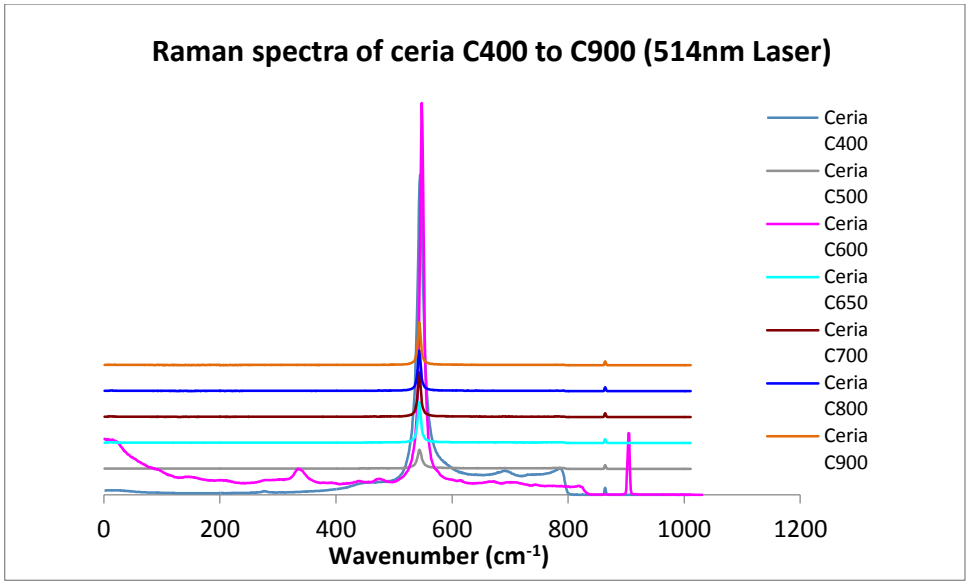

Figure 4-8. Raman spectra of ceria C400 to C900 using a 514 nm laser source.

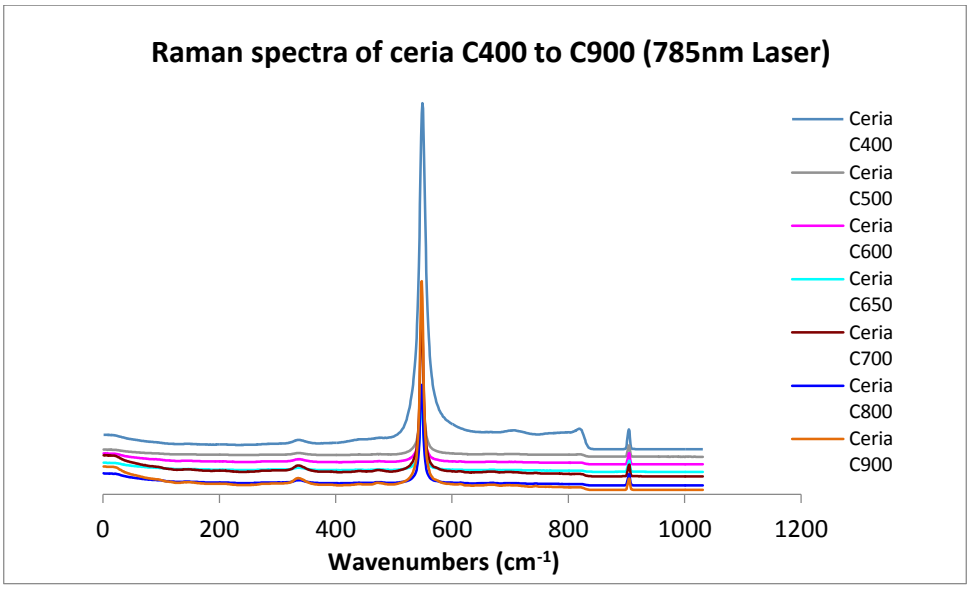

Figure 4-9. Raman spectra of ceria C400 to C900 using a 785 nm laser source.

Table 4-7. Full width half maximum and peak data from Raman spectroscopy.

Calcination Temperature (°C)	FWHM 514nm Laser	Peak Position (Wavenumber cm^{-1})	Bond	FWHM 785nm Laser	Peak Position (Wavenumber cm^{-1})	Bond
400	17.9	461	Ce-O	16.2	463	Ce-O
500	12.3	463	Ce-O	12.8	463	Ce-O
600	10.1	464	Ce-O	10	464	Ce-O
650	9.1	464	Ce-O	9.4	464	Ce-O
700	8.8	463	Ce-O	9.3	464	Ce-O
800	8.7	464	Ce-O	8.6	464	Ce-O
900	8.6	464	Ce-O	8.9	464	Ce-O

All the ceria samples produced a strong peak at between 461 and 464 wavenumbers cm^{-1}, which is consistent with the Ce-O band reported in the literature[3]. This can be seen in figure 4-8 and figure 4-9. There was a decrease seen in the full width half maximum (FWHM) as the calcination temperature increased. It is reported that a decrease in the FWHM indicates an increase in surface defects[7, 8]. Another explanation of this decrease is as a result of a lowering of the stoichiometric amount of oxygen on the surface, which indicates that oxygen vacancies are present[7]. The results in table 4-7 suggest that an increase in calcination temperature in the production of cerium oxide results in an increase in the amount of oxygen vacancies on the surface.

4.2.9 X-ray photoelectron spectroscopy (XPS)

XPS was performed on the ceria samples C400 - C900 to determine the presence of Ce^{3+} on the surface before reduction. It was also used to identify oxygen vacancies on the surface of the ceria samples before reduction.

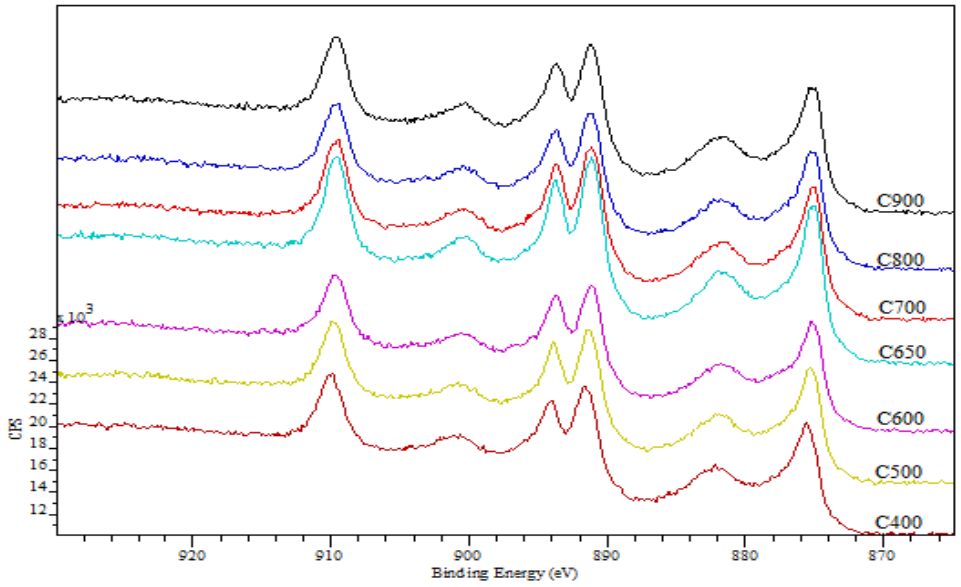

Figure 4-10. Ce 3d XPS spectra of cerium oxide produced by calcining cerium oxalate hydrate at 400 to 900 °C.

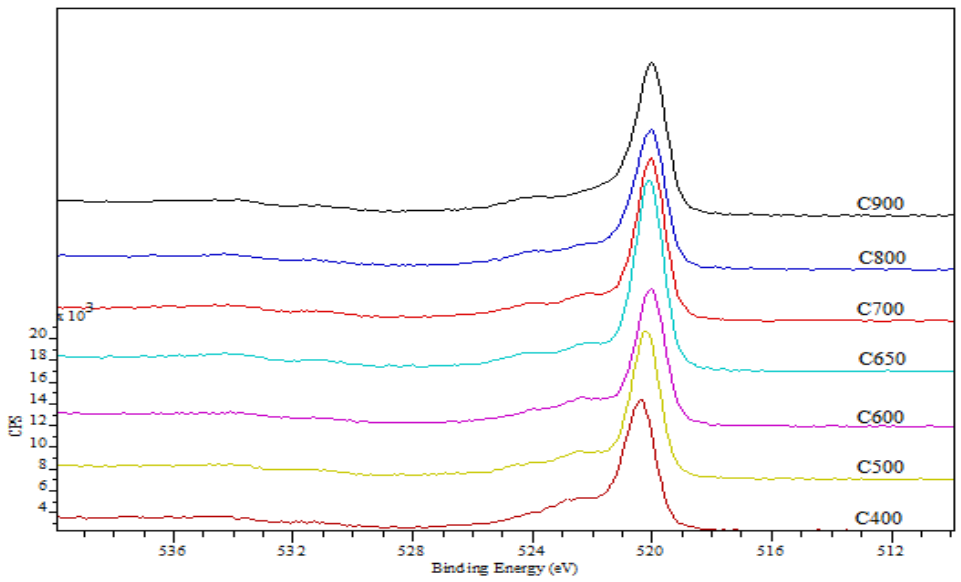

Figure 4-11. O 1s XPS spectra of cerium oxide produced by calcining cerium oxalate hydrate at 400 to 900 °C.

The Ce 3d XPS data in figure 4-10 shows all the characteristic peaks of a fully oxidised CeO_2 surface and is consistent with the reported literature[9, 10]. It can be concluded that increasing the calcination temperature does not cause any increase in the amount of Ce^{3+} present on the surface of the powders.

For a clean surface, one would expect to see a single peak at 520 eV in the O 1s XPS spectra of cerium oxide, which is consistent with the reported literature with that of a fully oxidised surface[10].

However, the O 1s XPS data in figure 4-11 shows the presence a peak at higher binding energy. This can be attributed to the presence of OH groups or oxygen vacancies on the surface of the CeO_2.

4.2.10 Temperature Programmed Reduction (TPR).

4.2.10.1 Comparative weight measurements

Temperature programmed reduction reactions were run under 10 % H_2 in argon on all the ceria samples produced (C400 - C900). These experiments were performed in order to map the hydrogen reduction profiles of the different ceria samples and to determine the effect different surface areas, as well crystallite size has on the reduction profile of ceria.

4.2.10.1.1 Surface and bulk reduction

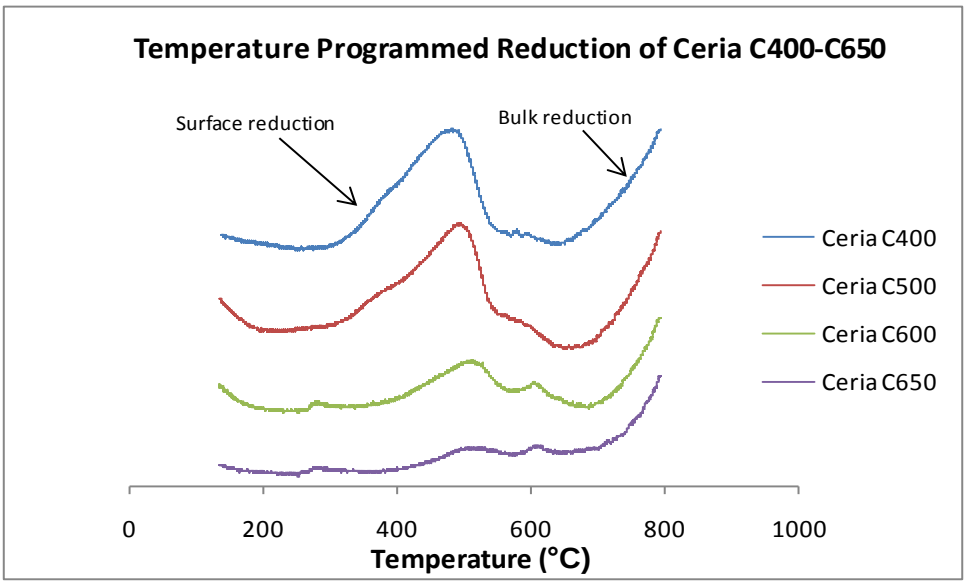

Figure 4-12. Temperature programmed reduction of ceria C400, C500, C600 and C650

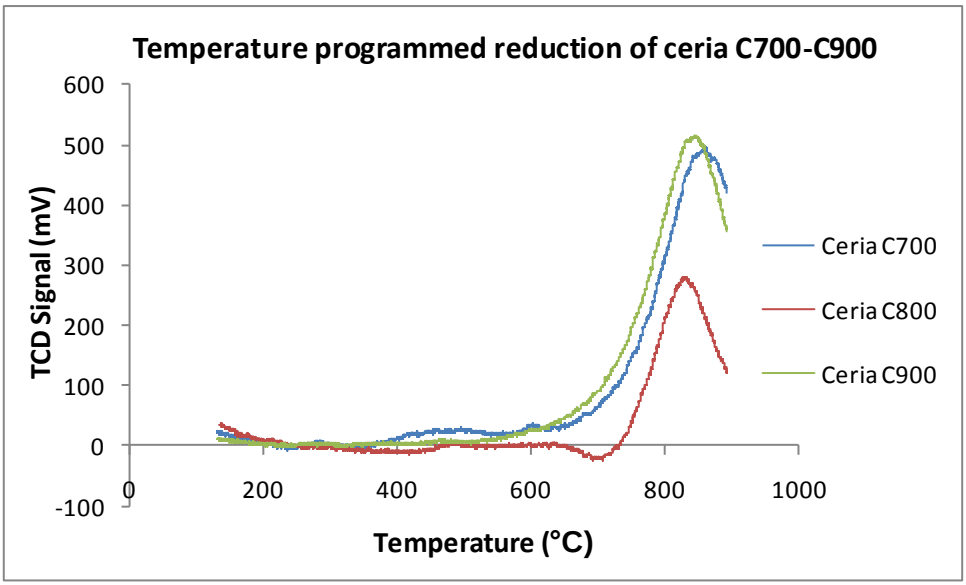

Figure 4-13. Temperature programmed reduction of ceria C700, C800 and C900.

The reduction profile of ceria, seen in figure 4-12 is characterised by two peaks, the first peak being attributed to the reduction of the uppermost layers of Ce^{4+} in ceria or the ceria surface and the second peak originates from the reduction of the bulk.[11] The reduction profiles measures consistent with the literature[12] for temperature programmed reduction profiles of

ceria. From figure 4-12, it can be seen that surface reduction begins at approximately 300 °C, with the temperature at which maximum reduction occurs increasing with increasing calcinations temperature and decreasing surface area. Bulk reduction of the ceria is seen to begin at temperatures in excess of 650 °C

There is no evidence of surface reduction for ceria samples produced by calcination at 700 °C and above. These samples have a surface area of less than 5 m^2g^{-1}. Surface reduction may be occurring on the samples with a surface area less than 5 m^2g^{-1} but the amount of hydrogen being consumed is below the detection limits of the equipment being used.

The number of moles of hydrogen consumed was calculated using the reduction of copper (II) oxide as a standard.

Table 4-8. No. of moles of hydrogen consumed during surface reduction of ceria C400, C500, C600 and C650

Calcination Temperature (°C)	Hydrogen consumed (moles)
400	$1.9e^{-04}$
500	$1.6e^{-04}$
600	$5.9e^{-05}$
650	$1.8e^{-05}$

The reduction profiles (Figures 4-12 and 4-13) show that the amount of hydrogen consumed during surface reduction decreases with decreasing surface area of the ceria sample.

4.2.10.2 X-ray photoelectron spectroscopy after TPR.

XPS was performed on the ceria samples C400 - C900 to determine the presence of Ce^{3+} on the surface after reduction. It was also used to identify oxygen vacancies on the surface of the ceria samples after reduction.

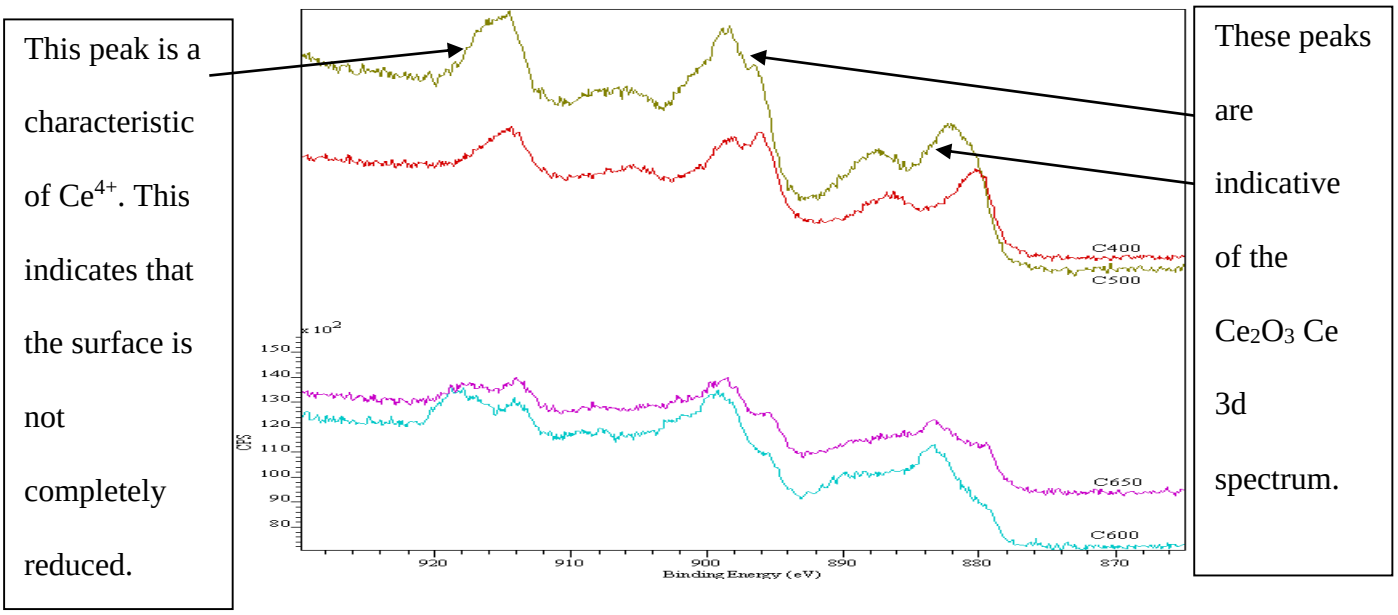

Figure 4-14. Ce 3d XPS spectra of cerium oxide produced by calcining cerium oxalate hydrate at 400 to 650 °C after reduction.

The presence of a peak here indicates an increase in the concentration of Ce^{3+} on the surface.

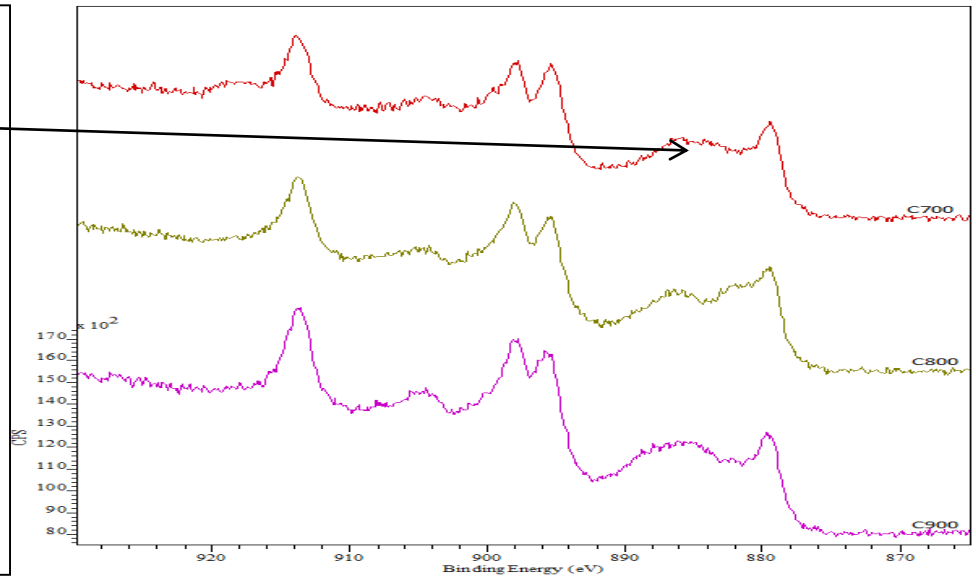

Figure 4-15. Ce 3d XPS spectra of cerium oxide produced by calcining cerium oxalate hydrate at 700 to 900 °C after reduction.

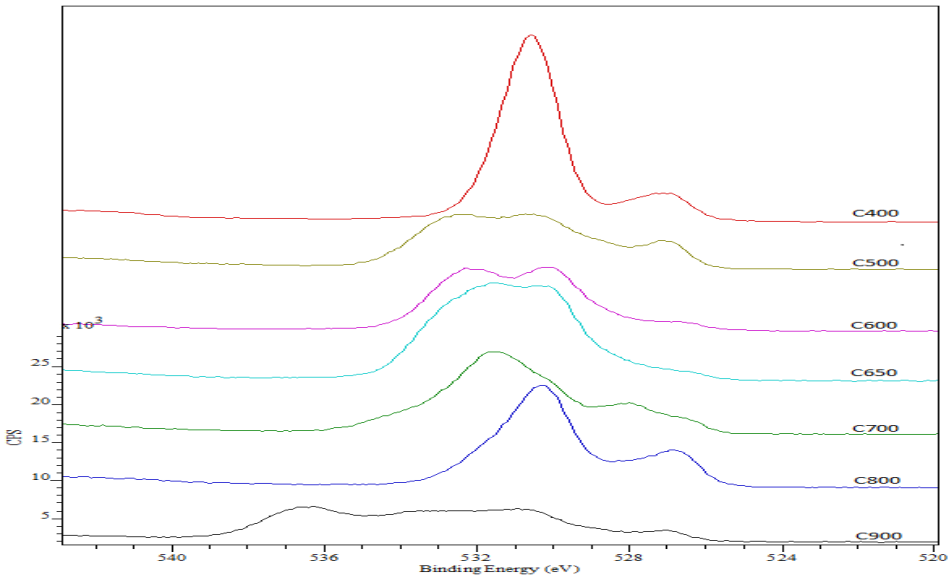

Figure 4-16. O 1s XPS spectra of cerium oxide produced by calcining cerium oxalate hydrate at 400 to 900 °C after reduction.

The Ce 3d XPS spectra after reduction confirm that surface reduction has taken place during TPR reactions on ceria C400 to C900. Figure 4-14 and 4-15 show the characteristic

peaks of a Ce_2O_3 surface emerging through the CeO_2 spectra. This is evidence of an increase in Ce^{3+} on the surface.

In figures 4-12 and 4-13, it is shown that surface reduction is not observed for samples with a surface area <5 m^2g^{-1} during temperature programmed reduction. In contrast, XPS spectra (figure 4-15) show that surface reduction has occurred on the samples with a surface area of 5 m^2g^{-1} or lower as shown in figure 4-15. This suggests that the amount of hydrogen required for surface reduction to be completed on ceria with a surface of 5 m^2g^{-1} or lower is too small for detection by thermal conductivity.

The O 1s spectra of ceria C400 to C900, figure 4-16, shows multiple peaks from 520 eV to 532 eV, this suggests the formation of oxygen vacancies on the surface as has been previously reported.[2, 10]

4.2.10.3 Activation energy (E_A) determination

The activation energy for surface reduction was calculated using the Kissinger equation. This was achieved by running the reduction reaction 3 times for each sample of ceria, with a different ramp rate each time.

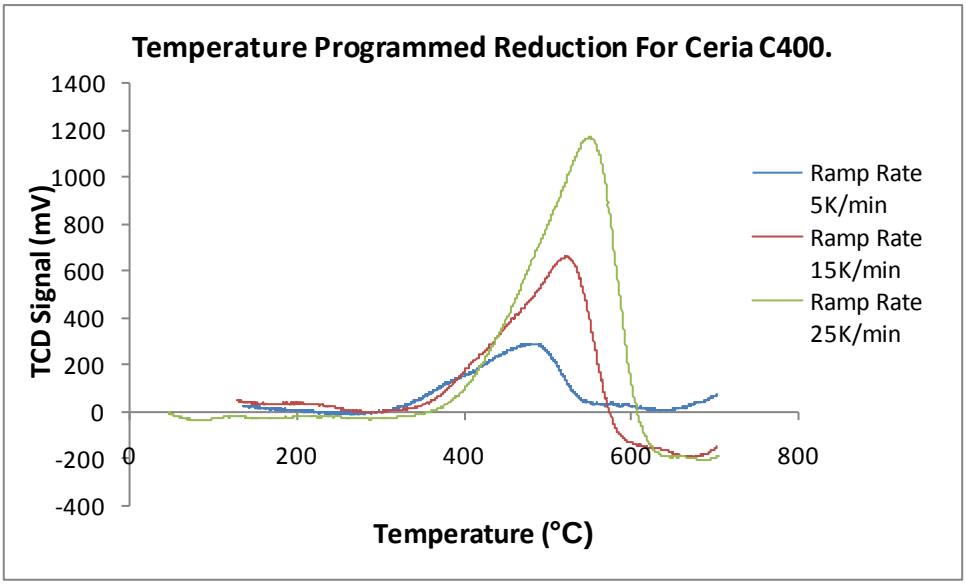

Figure 4-17. Temperature programmed reduction for ceria C400 at 3 different ramp rates.

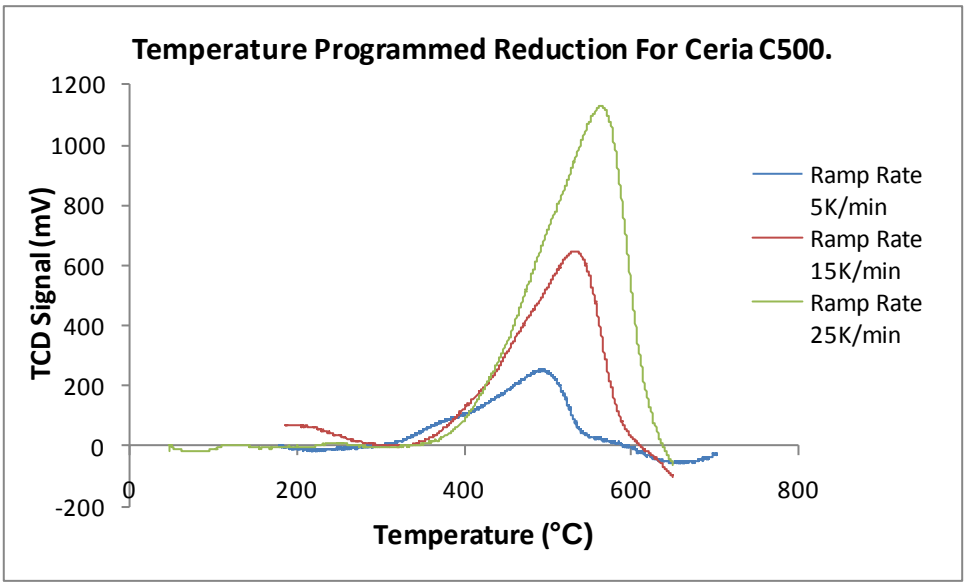

Figure 4-18. Temperature programmed reduction of ceria C500 at 3 different ramp rates.

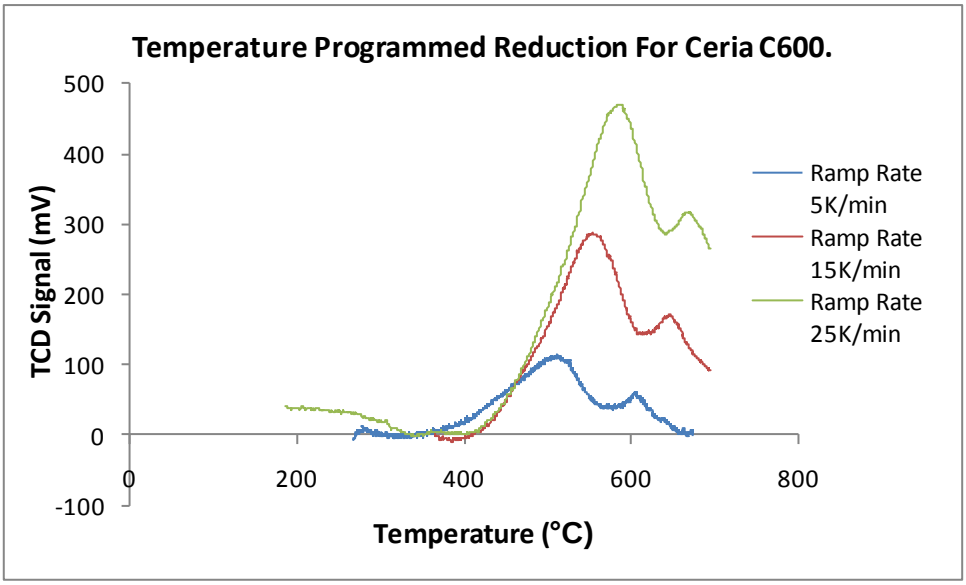

Figure 4-19. Temperature programmed reduction of ceria C600 at 3 different ramp rates.

Table 4-9. The effect of calcination temperature on the temperature at the reduction peak maximum at different temperature ramp rates.

Calcination temperature (°C)	Temperature at peak maximum on run 1 (ramp rate of 5 K/min)	Temperature at peak maximum on run 2 (ramp rate of 15 K/min)	Temperature at peak maximum on run 3 (ramp rate of 25 K/min)
400	472 °C	520 °C	541 °C
500	485 °C	537 °C	556 °C
600	500 °C	548 °C	504 °C
650	597 °C	643 °C	-

By taking the temperature of the peak maximum at each different ramp rate TPR run and using the Kissinger equation;

$$\ln\beta/T^2_{max} = \ln AR/E_A - E_A/RT_{max}$$

Equation 4-1. Kissinger equation

β = Ramp rate,

T_{max} = Temperature at peak maximum,

E_A = Activation energy,

R = Gas constant and

A = Pre-exponential factor.

A plot of $\ln(\beta/T^2_{max})$ versus $1/T_{max}$ can be performed and a straight line fitted to the data, the pre-exponential factor A and the activation energy (E_A) can be calculated from the intercept and slope respectively.

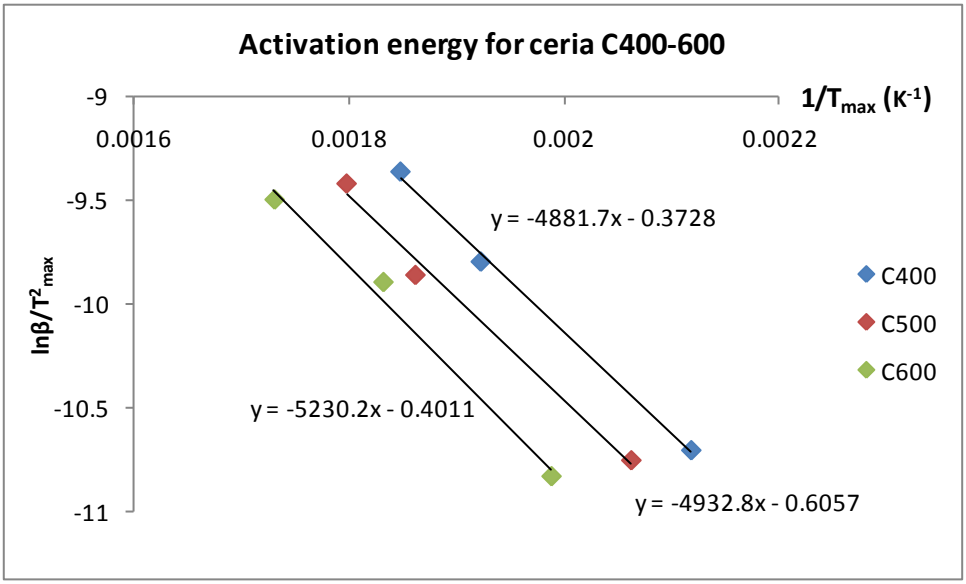

Figure 4-20. Activation energy calculation of ceria C400, C500 and C600 using the Kissinger method.

Table 4-10. Activation energy data for ceria C400-C650.

Calcination Temperature (°C)	Surface Area (m^2g^{-1})	Crystallite Size (nm)	Activation Energy ($kJ\ mol^{-1}$)
400	42	10	41
500	34	16	41
600	9	27	44
650	5	59	-

The activation energy required for surface reduction of ceria is approximately the same for samples ceria C400 - C600; this indicates that the activation energy for surface reduction is not dependent on surface area or crystallite size. As expected the number of moles of hydrogen consumed decreases with increasing calcination temperature and decreasing surface area. The activation for ceria C650 has not been calculated. This is because the increase in the ramp rate caused a shift in the temperature maximum of the surface reduction peak. In the case of the reduction of C650 at a ramp rate of 25 K/min, this caused the surface peak to merge with the peak resulting from the bulk reduction, making clear distinction between the two difficult.

4.2.10.4 Comparison by surface area

Temperature programmed reduction reactions were run on ceria C400 to C650 adjusting the weights in order to obtain the same surface area for each sample. These

experiments were done in order to determine whether surface reduction of ceria was surface area dependant.

Table 4-11. Weights of samples used for TPR same surface area runs.

Sample	Surface area (m^2g^{-1})	Weight used (g)
C400	42	0.1
C500	35	0.12
C600	9	0.5
C650	5	0.84

4.2.10.4.1 Surface reduction

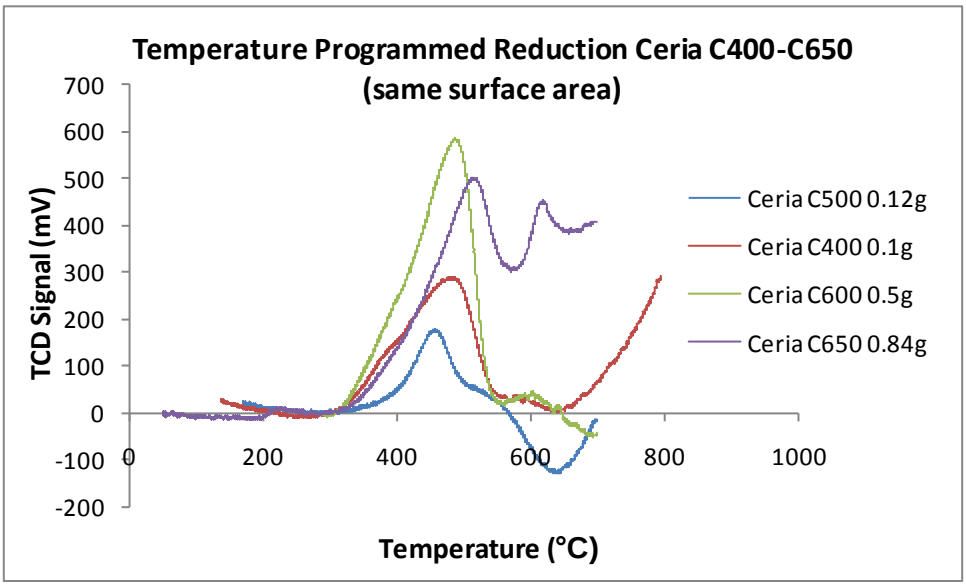

Figure 4-21. Temperature programmed reduction of ceria C400-C650 with same surface area.

Table 4-12. No. of moles of hydrogen consumed during reduction and the temperature at the peak maximums for ceria samples C400 - C650.

Sample.	No. of moles of hydrogen consumed.	Temperature at peak maximum (°C).
C400	$1.9e^{-04}$	472
C500	$7.3e^{-05}$	445
C600	$3.3e^{-04}$	479
C650	$1.2e^{-04}$	506

There is no direct trend seen between ceria samples C400 - C650 during the reduction reactions. However, the numbers of moles of hydrogen consumed during surface reduction are much closer in value when ceria C400 - C650 have the same surface area than when they have different surface areas. This suggests that when samples of the same weight but different surface areas are compared, the samples with the higher surface areas will experience a higher degree of surface reduction. This supports previous work that indicated that there is a linear relationship between hydrogen consumption in TPR experiments and the initial BET surface area of the ceria being reduced.[12]

4.2.10.5 Redox cycles

Temperature programmed reduction reactions were run on ceria samples C400 - C650 followed by a temperature programmed oxidation reaction. This was then followed by another reduction reaction.

These reactions have been performed in order to if the ceria surface is completely re-oxidised in the presence of oxygen after the surface has been reduced by hydrogen.

4.2.10.5.1 Surface reduction

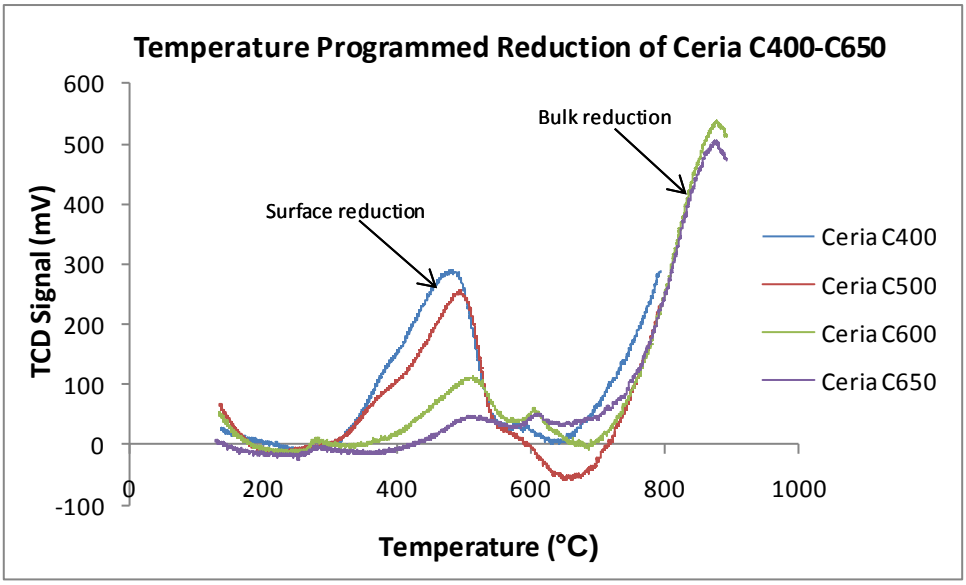

Figure 4-22. TPR of ceria C400 - C650.

Table 4-13. No. of moles of hydrogen consumed and temperature at peak maximums for ceria samples C400 - C650 after TPR.

Sample	No. of moles of hydrogen consumed.	Temperature at peak maximum (°C)
C400	$1.9e^{-04}$	472
C500	$1.6e^{-04}$	485
C600	$5.9e^{-05}$	500
C650	$1.8e^{-05}$	594

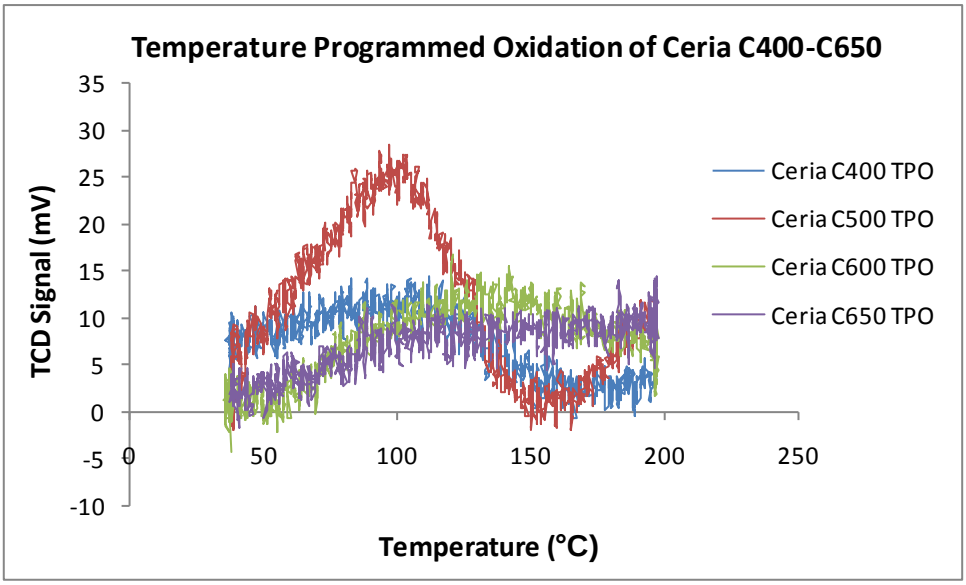

Figure 4-23. TPO of ceria C400 - C650.

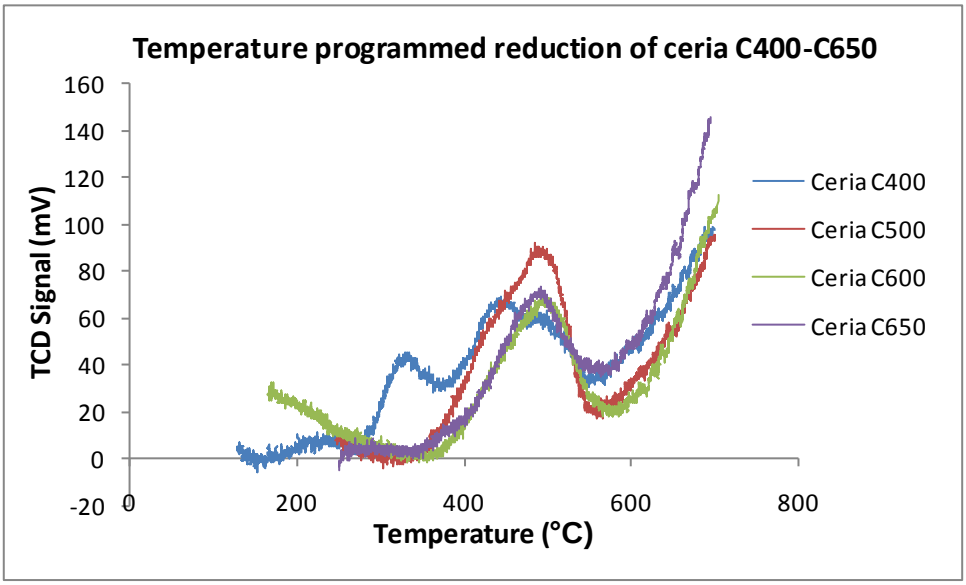

Figure 4-24 TPR of ceria C400 - C650.

Table 4-14. No. of moles of hydrogen consumed and temperature at peak maximums for ceria samples C400 - C650 after TPR-TPO-TPR.

Sample	No. of moles of hydrogen consumed.	Temperature at peak maximum (°C)
C400	$3.8e^{-05}$	443
C500	$4.3e^{-05}$	480
C600	$3.1e^{-05}$	497
C650	$2.0e^{-05}$	485

The results for the TPR-TPO-TPR cycles on ceria C400 - C650 indicate that ceria C400 to C650 are only partially re-oxidised after hydrogen reduction. Figures 4-22 to 4-24 show that allowing the temperature to rise (during the first hydrogen TPR) to a temperature where bulk reduction occurs causes a change of the surface from CeO_2 to Ce_2O_3, which is not fully re-oxidised by a 10 % oxygen in argon flow during the temperature programmed oxidation.

4.2.11 Temperature programmed reduction of powdered ceria after storage in H_2O_2, HNO_3 and H_2O.

These experiments were undertaken to determine the effect of hydrogen peroxide, nitric acid and water on the hydrogen reduction of ceria. A ceria sample was soaked in hydrogen peroxide, nitric acid and water for 48 hours and Buchner funnelled dry. Temperature programmed reduction was then performed on each sample.

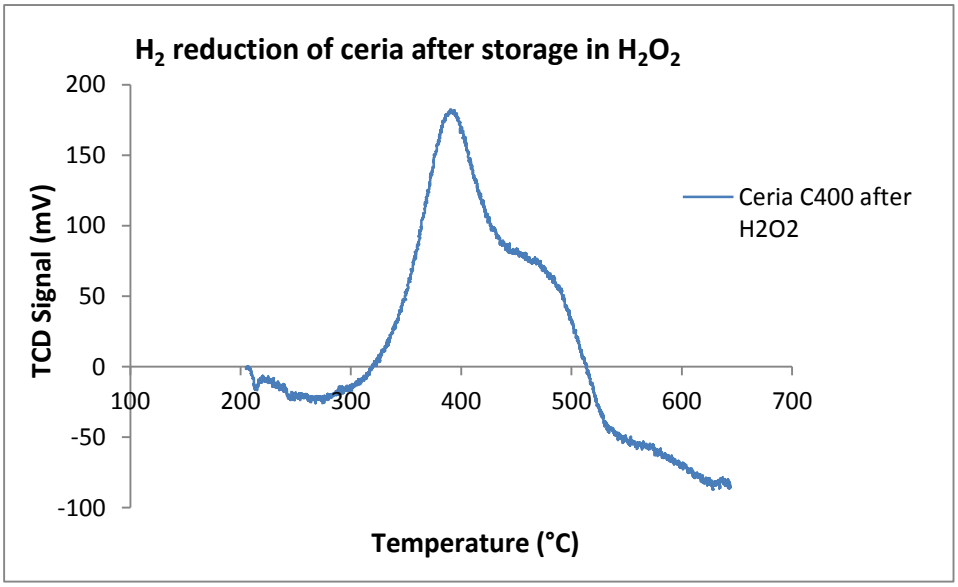

Figure 4-25. Temperature programmed reduction of ceria (surface area of 44 m^2g^{-1}) after storage in H_2O_2 for 48 hours.

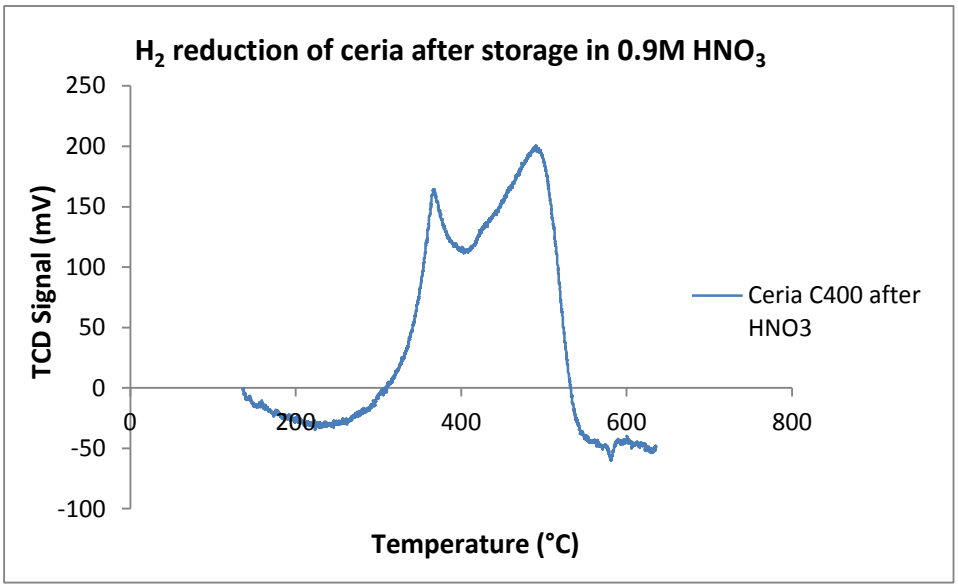

Figure 4-26. Temperature programmed reduction of ceria (surface area of 44 m^2g^{-1}) after storage in HNO_3 for 48 hours.

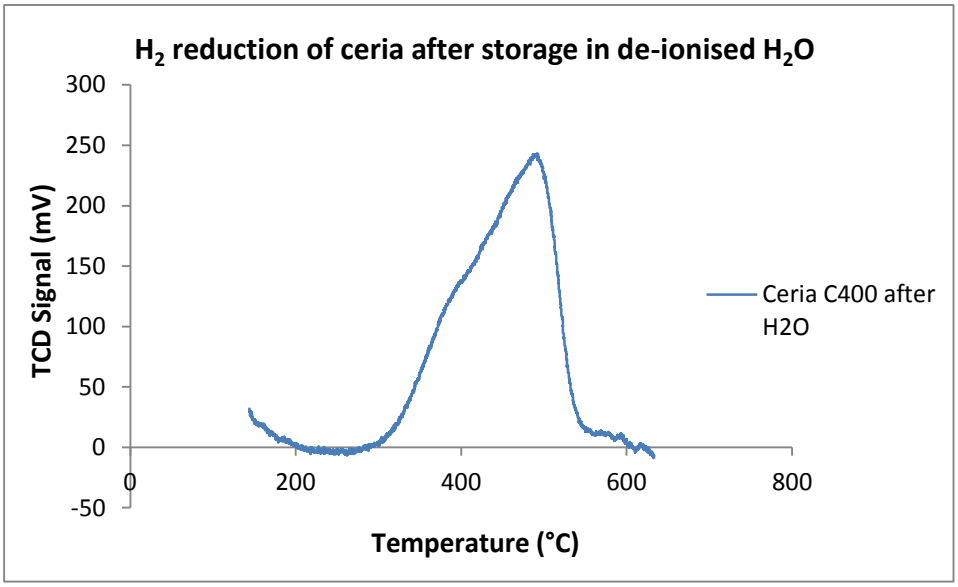

Figure 4-27. Temperature programmed reduction of ceria (surface area of 44 m^2g^{-1}) after storage in H_2O for 48 hours.

Table 4-15. No. of moles of hydrogen consumed during TPR of ceria C400 after storage in H_2O_2, HNO_3 and H_2O for 48 hours.

Storage solution	No. of moles of hydrogen consumed	Temperature at peak maximum (°C)
None	1.9×10^{-4}	470
H_2O_2	1.2×10^{-4}	383
HNO_3	1.9×10^{-4}	364 / 480
H_2O	1.6×10^{-4}	480

A colour change was seen as a result of placing ceria in H_2O_2 from yellow to light orange/gold. From table 4-15 and figure 4-25 it can be seen that the amount of hydrogen consumed is slightly lower but comparable to the amount of hydrogen consumed by ceria C400 that has not been stored in H_2O_2. However, the hydrogen peroxide treatment lowered the temperature at which maximum surface reduction took place when compared to the TPR results of ceria that had not been stored in H_2O_2.

The surface reduction profile of ceria is altered after storage in HNO_3 for 48 hours. There are two peaks observed for surface reduction. It has been reported[13] that when ceria comes into contact with HNO_3 it can react and form species such as nitrates which remain on the surface of ceria. It is believed that the first peak in figure 4-26 is as a result of a reaction between the hydrogen in gas feed and these nitrate species on the ceria surface. The second peak is resulting from hydrogen reduction of the ceria surface. The number of moles of hydrogen consumed and the temperature at the peak maximum for the surface reduction is comparable with that of the results for ceria which has not been stored in HNO_3. No change is seen in the reduction profile of ceria after storage in H_2O for 48 hours when comparing against the reduction profile for hydrogen reduction over ceria that has not been stored in H_2O for 48 hours.

4.2.12 Studying the effect of temperature on hydrogen oxidation on ceria C400, C600 and C900 in a sealed autoclave over time.

Ceria samples C400, C600 and C900 (0.1g) were sealed in a stainless steel autoclave with a gas mixture of 2 % hydrogen in synthetic air and the pressure monitored over time. These reactions were performed to determine the extent of hydrogen oxidation on ceria samples

C400, C600 and C900 as a result of temperature over time when placed in a sealed vessel. This was determined by measuring pressure change over time.

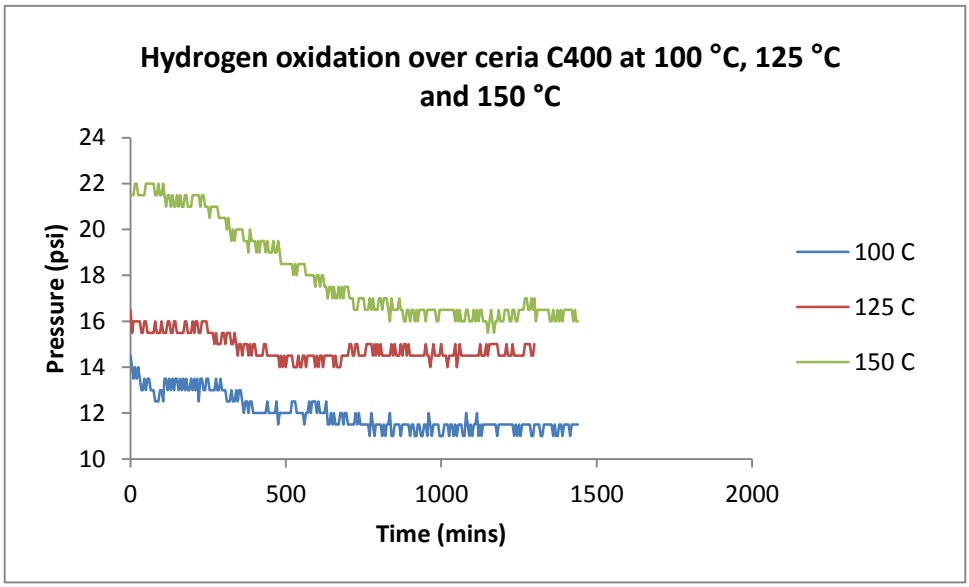

Figure 4-28. Pressure change over time resulting from oxidation of hydrogen over ceria C400 at different temperatures.

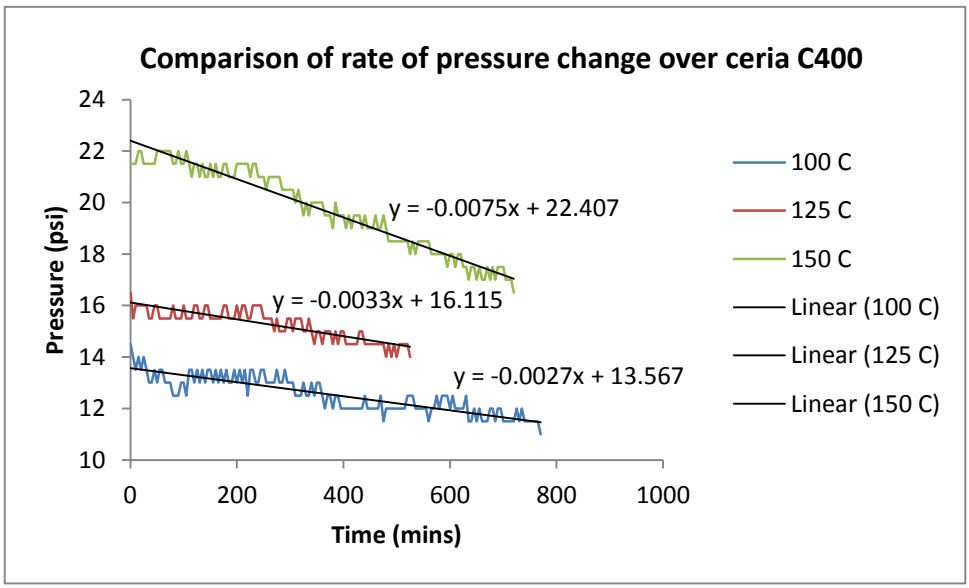

Figure 4-29. Rate of pressure change over time resulting from oxidation of hydrogen over ceria C400 at different temperatures.

Table 4-16. Hydrogen oxidation over ceria C400 by monitoring pressure change.

Temperature (°C)	Pressure change (psi)	Rate of hydrogen consumption (psi/min)
100	3	0.003
125	2.5	0.003
150	5.5	0.008

Figures 4-28 and 4-29 and table 4-16, show that there is an increase in the rate of oxidation of the hydrogen in the reactive gas mixture as a result of increasing the temperature. The amount and rate of oxidation seen at 100 °C and 125 °C is the same. A difference is seen when the temperature is raised to 150 °C, where the higher temperature increases the rate and amount of oxidation by more than double.

The same reactions were conducted on ceria C600 and ceria C900 but no pressure change was observed. The most notable difference between these samples is the surface area of each sample, with ceria C600 and C900 having lower surface areas than ceria C400. It can be suggested that hydrogen oxidation over ceria is not only dependent on temperature and pressure but the surface area of the ceria sample in question.

4.3 Conclusions

From the work in this chapter, one can conclude that the surface reduction of cerium oxide is highly dependent on the surface area of the ceria in question. This is supported by the decrease in surface reduction seen as the surface area of the ceria sample decreases, which is

shown in figure 4-22. Work by Laachir et al and others[2, 9, 12], where hydrogen reduction of cerium oxide with two different surface areas was compared support this observation

That reduction of ceria by hydrogen is characterised by two peaks in TPR analysis, the first of which is as a result of surface reduction, which begins at 300 °C for a ceria sample with a surface area of 45 m^2g^{-1}. The number of moles of hydrogen consumed during the surface reduction decreases with decreasing surface area of the ceria sample. The reduction of the bulk ceria requires temperatures in excess of 650 °C for in order to occur. Surface reduction of samples was not observed for ceria with a surface area of less than 5 m^2g^{-1} by TPR. This is likely to be a sensitivity issue with the technique in question as XPS analysis after TPR shows all the samples C400 to C900 have experienced a high degree of surface reduction. However, analysis to determine the activation energy required for surface reduction showed that the activation energy for surface reduction to occur is independent of surface area.

When a ceria sample of high enough surface area is sealed in a vessel with a reactive mixture containing H_2 and O_2 under the right temperature and pressure conditions, a thermal reaction will occur. The results in figure 4-28 to 4-29 and table 4-16 shows an increase in the rate of this thermal reaction as a result of raising the temperature of the reaction vessel. Similar work by Luis Morales[14] showed the same conclusions by sealing the same reaction mixture in a reaction vessel with PuO_2. However, the work by Morales showed a higher degree of reaction. This was indicated by a greater pressure drop than the one observed in this chapter. It was concluded in the work by Morales that the recombination of hydrogen and oxygen over PuO_2 was a thermal surface reaction rather than being a radiolytic driven reaction. The results here support this theory, using CeO_2 as a model for PuO_2.

4.4 References

1 C. Binet, A. Badri and J. C. Lavalley, *J. Phys. Chem.*, 1994, **98**, 6392.

2 A. Trovarelli, *Catalysis by Ceria and Related Materials*, 2002.

3 Y. Altaş and H. Tel, *J. Nucl. Mater.*, 2001, **298**, 316; A. Bumajdad, M. I. Zaki, J. Eastoe and L. Pasupulety, *Langmuir*, 2004, **20**, 11223.

4 L. De Almeida, S. Grandjean, N. Vigier and F. Patisson, *Eur. J. Inorg. Chem.*, 2012, 4986; M. A. Gabal, S. A. K. Elroby and A. Y. Obaid, *Powder Technol.*, 2012, **229**, 112.

5 S. A. C. Carabineiro, S. S. T. Bastos, J. J. M. Órfão, M. F. R. Pereira, J. J. Delgado and J. L. Figueiredo, *Applied Catalysis A: General*, 2010, **381**, 150.

6 J. W. Niemantsverdriet, *Spectroscopy in Catalysis*, Wiley, 2007.

7 I. Kosacki, T. Suzuki, H. U. Anderson and P. Colomban, *Solid State Ionics*, 2002, **149**, 99.

8 T. Suzuki, I. Kosacki, H. U. Anderson and P. Colomban, *Journal of the American Ceramic Society*, 2001, **84**, 2007.

9 A. Laachir, V. Perrichon, A. Badri, J. Lamotte, E. Catherine, J. C. Lavalley, J. Elfallah, L. Hilaire, F. Lenormand, E. Quemere, G. N. Sauvion and O. Touret, *Journal of the Chemical Society-Faraday Transactions*, 1991, **87**, 1601.

10 D. R. Mullins, S. H. Overbury and D. R. Huntley, *Surface Science*, 1998, **409**, 307.

11 J. Elfallah, S. Boujana, H. Dexpert, A. Kiennemann, J. Majerus, O. Touret, F. Villain and F. Lenormand, *J. Phys. Chem.*, 1994, **98**, 5522.

12 V. Perrichon, A. Laachir, G. Bergeret, R. Frety, L. Tournayan and O. Touret, *J. Chem. Soc.-Faraday Trans.*, 1994, **90**, 773.

13 J. A. Rodriguez, T. Jirsak, S. Sambasivan, D. Fischer and A. Maiti, *Journal of Chemical Physics*, 2000, **112**, 9929.

14 L. A. Morales, US Department of Energy, Los Alamos National Laboratory, 1998.

5 Chapter 5 – The reduction and oxidation of cerium (111) oxide single crystal.

5.1 Introduction

The aim of this work is to look at the thermal reactions of hydrogen and oxygen over cerium (IV) oxide, for the purpose of mimicking the thermal reactions of hydrogen and oxygen over plutonium (IV) oxide mentioned in chapter 1. In this chapter we follow these reactions over a cerium oxide (111) single crystal in ultra-high vacuum conditions.

As mentioned in chapter 1 the reduction of cerium oxide and the oxidation of hydrogen by cerium oxide follows a Mars van Krevelen type mechanism as proposed by El Fallah et al[1] and others[2, 3].

The oxygen terminated (111) index plane of cerium oxide was chosen for study as it has been shown to be the most stable surface[4]. The formation of Ce^{3+} on the surface of ceria follows the formation of oxygen vacancies. Oxygen vacancies play a key role in the surface chemistry of oxides and are the key in understanding the surface reactions of CeO_2[5]. Defects within the lattice structure of CeO_2 are the cause of its redox ability and subsequently its ability to form non-stoichiometric compositions. These defects can be caused extrinsically, i.e. created by a reaction of the solid with the surrounding atmosphere, or caused intrinsically, caused by impurities in the structure[2]. With regards to intrinsic defects, a large proportion of these defects can be formed by exposure of ceria to a reducing gaseous environment. As a result of reduction, ceria will have excess metal content when compared to its anion content, i.e. some oxygen has been removed, creating an overall positive charge. Retention of neutrality can be attributed to the donation of two electrons to the resulting oxygen vacancy site after reduction has occurred. This is done by two cerium atoms changing charge from +4 to +3[2].

In this chapter, we look at the reduction of a cerium oxide (111) single crystal under varied conditions and atmosphere by following the formation of Ce^{3+} on the surface of the ceria by x-ray photoelectron spectroscopy.

The x-ray photoelectron Ce 3d spectra of Ce_2O_3 and CeO_2 show uniquely identifiable characteristics of the presence of Ce^{3+} and Ce^{4+}.

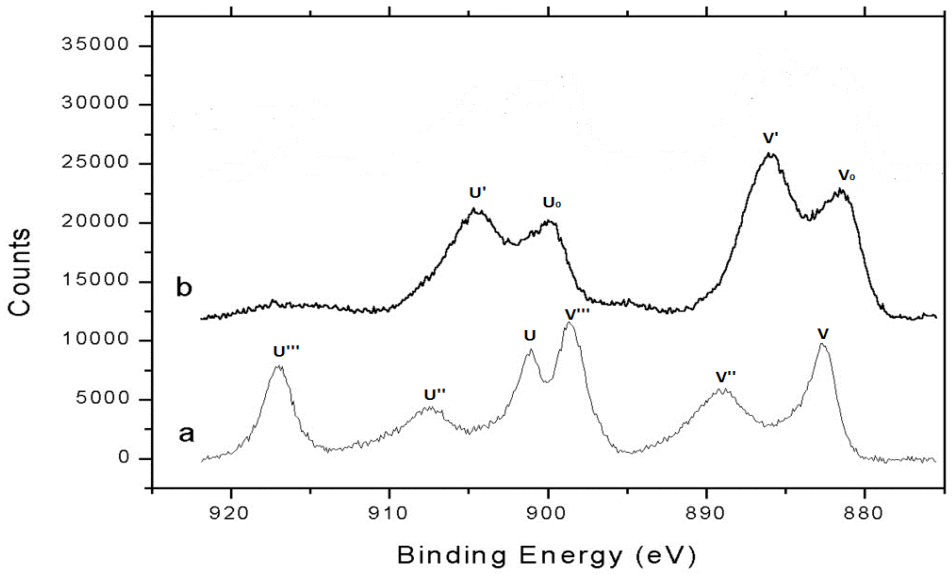

Figure 5-1. Ce 3d spectrum for cerium oxide[2]. a) assumed 100% Ce^{4+} (CeO_2), b) assumed 100% Ce^{3+} (Ce_2O_3).

Figure 5-1 shows the Ce 3d spectrum of CeO_2 and Ce_2O_3, from this it is evident that the U''' peak is a characteristic of Ce^{4+}. Without the presence of this peak, it would be assumed that the surface has no $4f^0$ states and thus the surface is completely made up of Ce^{3+} which indicates total reduction of the surface.

5.2 Results and discussion

5.2.1 The reduction of the ceria (111) single crystal under vacuum (10^{-9} Torr).

The ceria single crystal was heated in vacuum to determine if, and to what extent, reduction occurs upon heating under vacuum. The XPS spectra were taken at room temperature, then in 50 °C intervals up to 400 °C. The XPS spectra were taken coming down in temperature from 400 °C in 50 °C intervals.

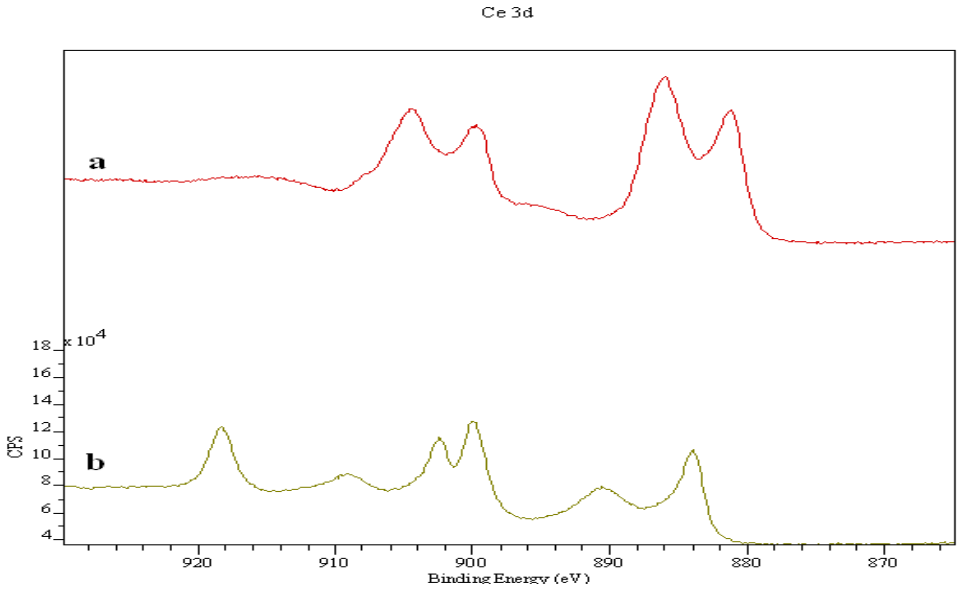

Figure 5-2. Room temperature XPS Ce 3d spectrum of a) a CeO_2 (111) single crystal reduced by argon sputtering and b) fully oxidised CeO_2 (111) single crystal.

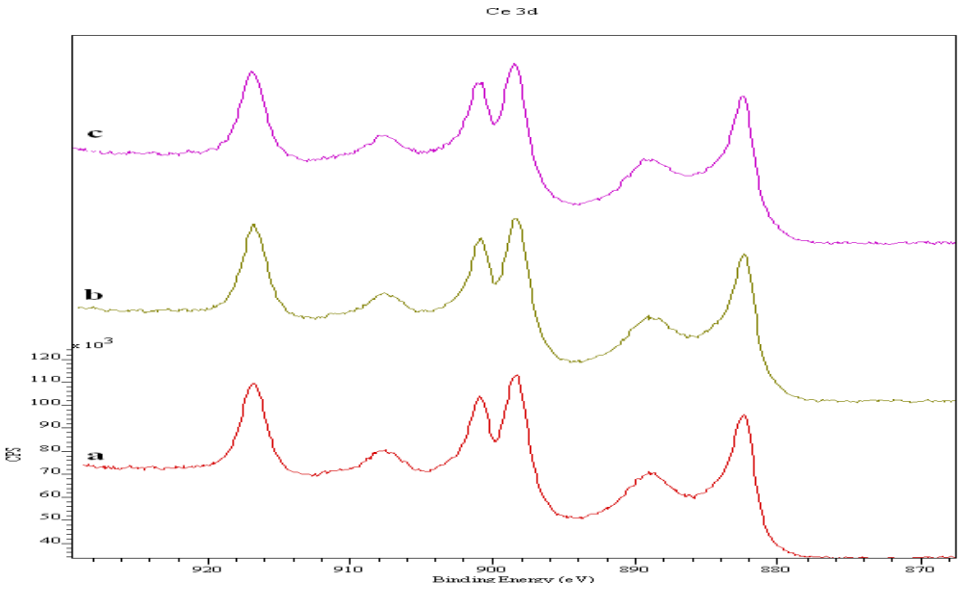

Figure 5-3. XPS Ce 3d spectrum of CeO_2 (111) single crystal heating in vacuum at a) 50 °C, b) 100 °C and c) 150 °C.

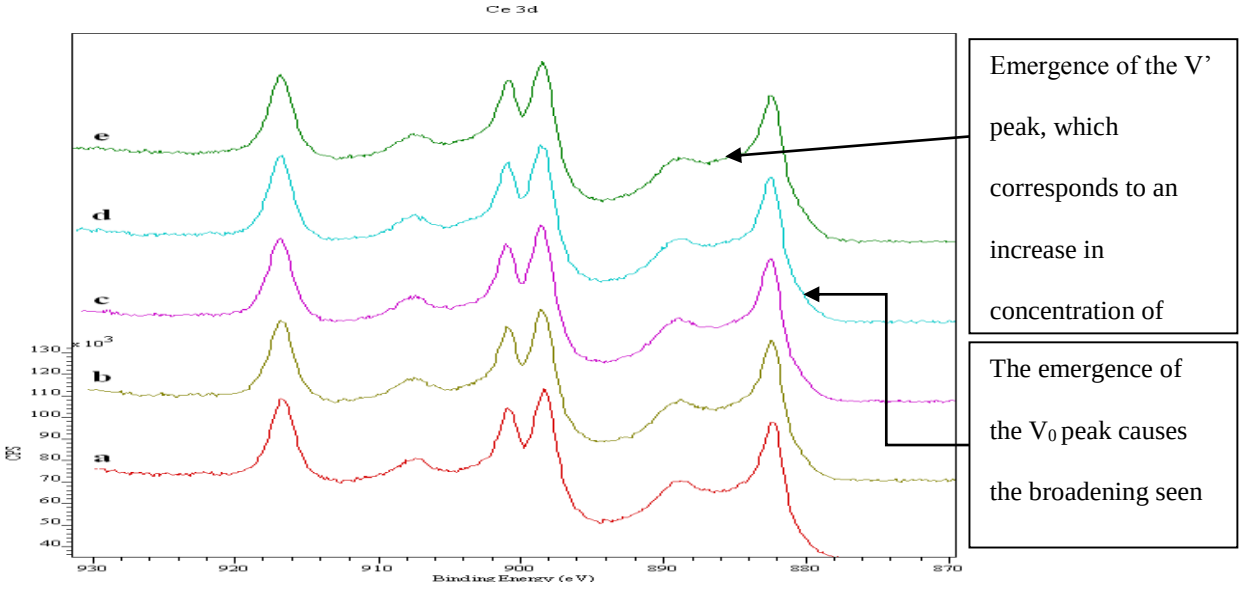

Figure 5-4. XPS Ce 3d spectrum of CeO_2 (111) single crystal heating in vacuum at a) 200 °C, b) 250 °C, c) 300 °C, d) 350 °C and e) 400 °C.

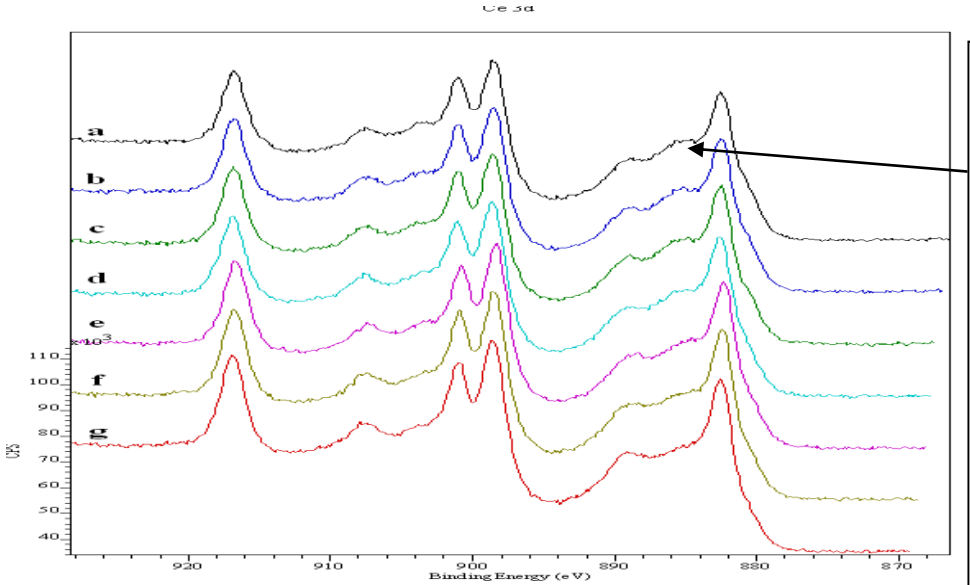

Figure 5-5. XPS Ce 3d spectrum of CeO_2 (111) single crystal cooling in vacuum at a) 50 °C, b) 100 °C, c) 150 °C, d) 200 °C, e) 250 °C, f) 300 °C and g) 350 °C.

Table 5-1. Quantitative data for XPS analysis of CeO_2 heating under vacuum.

Temperature (°C)	% Ce^{3+}	% Ce^{4+}
50	13	87
100	16	84
150	19	81
200	21	79
250	23	77
300	25	75
350	26	74
400	28	72

Table 5-2. Quantitative data for XPS analysis of CeO_2 cooling under vacuum.

Temperature (°C)	% Ce^{3+}	%Ce^{4+}
350	30	70
300	32	68
250	35	65
200	35	65
150	37	63
100	40	60
50	39	61

The Ce 3d spectrum of the CeO_2 single crystal at room temperature (figure 5-2) showed all the characteristics of a fully oxidised surface. The characteristic U''' peak to single the presence of Ce^{4+} was present and no signs of any emergence of the V', U' or V_0 peaks from the Ce_2O_3 to signal any concentration of Ce^{3+} were evident.

Quantitative data shown in table 5-1 indicates that at the start of the experiment there is a presence of Ce^{3+} on the surface of the single crystal. Up to 200 °C the CeO_2 not much change is seen in the percentage of Ce^{3+} on the surface. Table 5-1 and figure 5-4 show that at 200 °C the percentage of Ce^{3+} on the surface began to increase, this indicating the start of reduction as a result of heating under vacuum.

In figure 5-4 it can be seen that the V' peak became clearer at 250 °C. This peak is a characteristic peak of the Ce_2O_3 3d XPS spectrum. This is indicative of an increase in the

concentration of Ce^{3+} on the surface of ceria. There is an increase in the amount of reduction of the surface of the ceria as the temperature was raised to 400 °C.

The amount of reduction witnessed increased while the temperature decreased from 400 °C to 50 °C. This is shown in figure 5-5 and table 5-2. This suggests that once a specific temperature is reached and enough energy supplied reduction of ceria will begin. The results indicate that if no external oxygen is supplied, the reduction will continue until CeO_2 is completely reduced to Ce_2O_3.

5.2.2 The reduction of the ceria (111) single crystal by hydrogen (10^{-7} Torr).

The ceria single crystal was heated in a hydrogen atmosphere. This was undertaken to determine the extent of reduction upon heating and cooling in a hydrogen atmosphere. The XPS spectrum was taken at 50 °C and then at increments of 50 °C up to 400 °C and at 50 °C intervals upon cooling.

The Ce 3d spectrum of the CeO_2 single crystal at room temperature seen in figure 5-6 showed all the characteristics of a fully oxidised surface. The characteristic U''' peak to single the presence of Ce^{4+} was present and no signs of any emergence of the V', U' or V_0 peaks from the Ce_2O_3 to signal any concentration of Ce^{3+} were evident.

Up to 100 °C the CeO_2 there is no increase seen in the Ce^{3+} concentration. No presences of the peaks corresponding to Ce^{3+} were seen to emerge in figure 5-7. At 150 °C the percentage of Ce^{3+} as shown in table 5-3, starts to increase. This becomes clearer in figure 5-7 at 150 °C, as shown by the emergence of the V' peak of the Ce_2O_3 XPS Ce 3d spectrum. The extent of reduction increased as the temperature was raised to 400 °C.

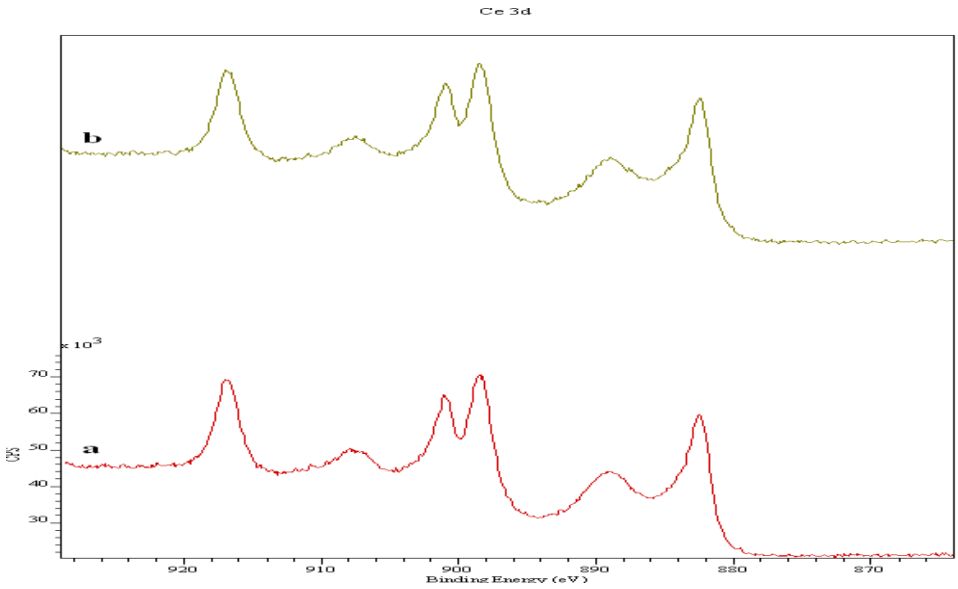

Figure 5-6. XPS Ce 3d spectrum of CeO_2 (111) single crystal heating in hydrogen at a) 50 °C and b) 100 °C.

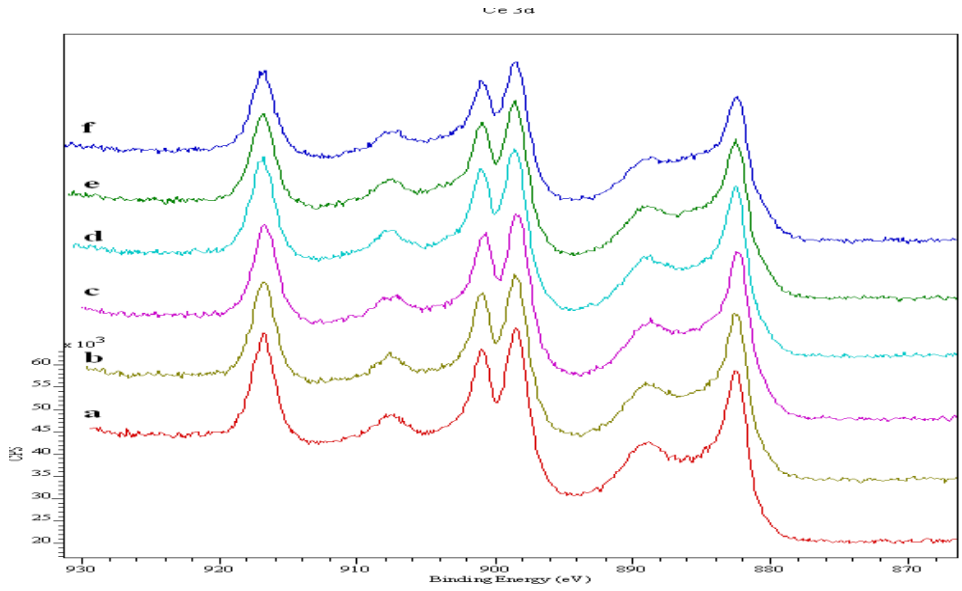

Figure 5-7. XPS Ce 3d spectrum of CeO_2 (111) single crystal heating in hydrogen at a) 150 °C, b) 200 °C, c) 250 °C, d) 300 °C, e) 350 °C and f) 400 °C.

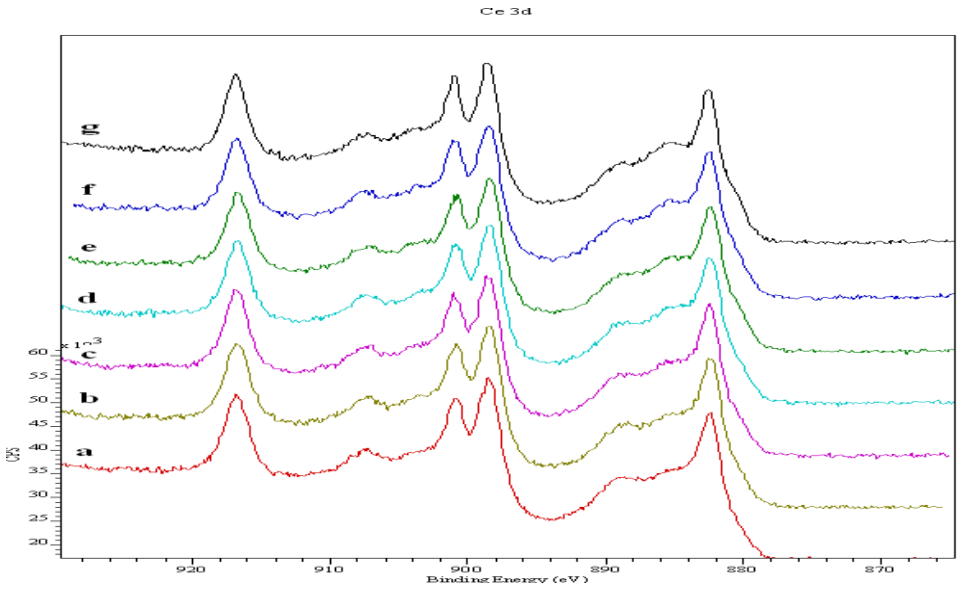

Figure 5-8. XPS Ce 3d spectrum of CeO_2 (111) single crystal cooling in hydrogen at a) 50 °C, b) 100 °C, c) 150 °C, d) 200 °C, e) 250 °C, f) 300 °C and g) 400 °C.

Table 5-3. Quantitative data for XPS analysis of CeO_2 upon heating in a hydrogen atmosphere.

Temperature (°C)	% Ce^{3+}	% Ce^{4+}
50	10	90
100	11	89
150	18	82
200	19	81
250	22	78
300	21	79
350	22	78
400	27	73

Table 5-4. Quantitative data for XPS analysis of CeO_2 upon cooling in a hydrogen atmosphere.

Temperature (°C)	% Ce^{3+}	%Ce^{4+}
350	28	72
300	30	70
250	33	67
200	32	68
150	35	65
100	38	62
50	39	61

It can be observed in figure 5-8 that the extent of reduction increased while the reaction was cooled from 400 °C to 50 °C. This suggests that once a specific temperature is reached and enough energy supplied reduction of ceria will begin. The results indicate that if no external oxygen is supplied, the reduction will continue until CeO_2 is completely reduced to Ce_2O_3.

5.2.3 The heating of the ceria (111) single crystal in a hydrogen peroxide atmosphere. (10^{-7} Torr)

The ceria single crystal was heated under a sub ambient hydrogen peroxide atmosphere. This was undertaken in order to determine the effect that hydrogen peroxide has on the reduction profile of ceria. Hydrogen peroxide has the ability to be both reducing and oxidising.

XPS spectra were taken at 100 °C increments from room temperature up to 400 °C and conversely from 400 °C to room temperature.

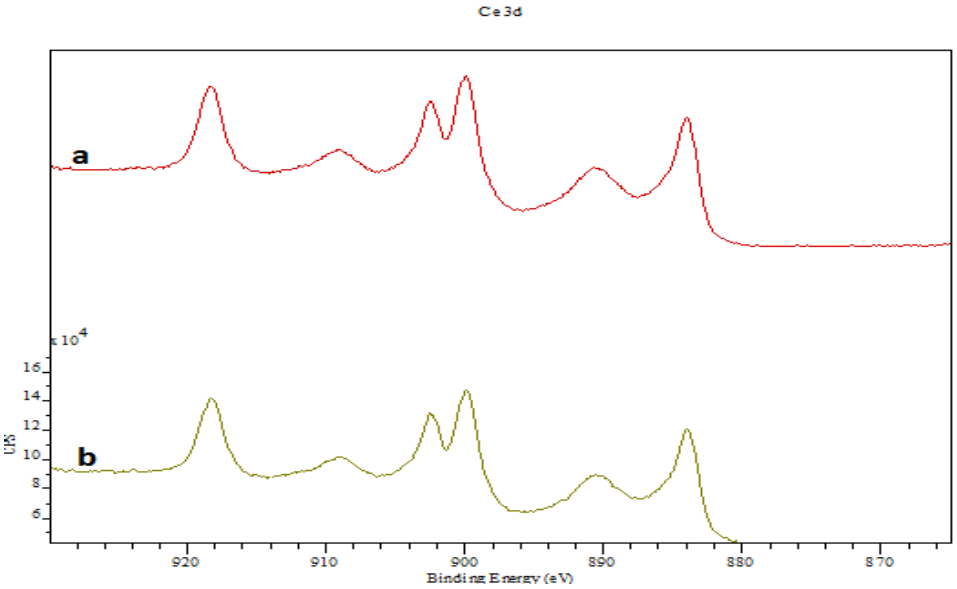

Figure 5-9. XPS Ce 3d spectrum of CeO_2 (111) single crystal in hydrogen peroxide a) Room temperature after cleaning, b) Room temperature under an hydrogen peroxide atmosphere.

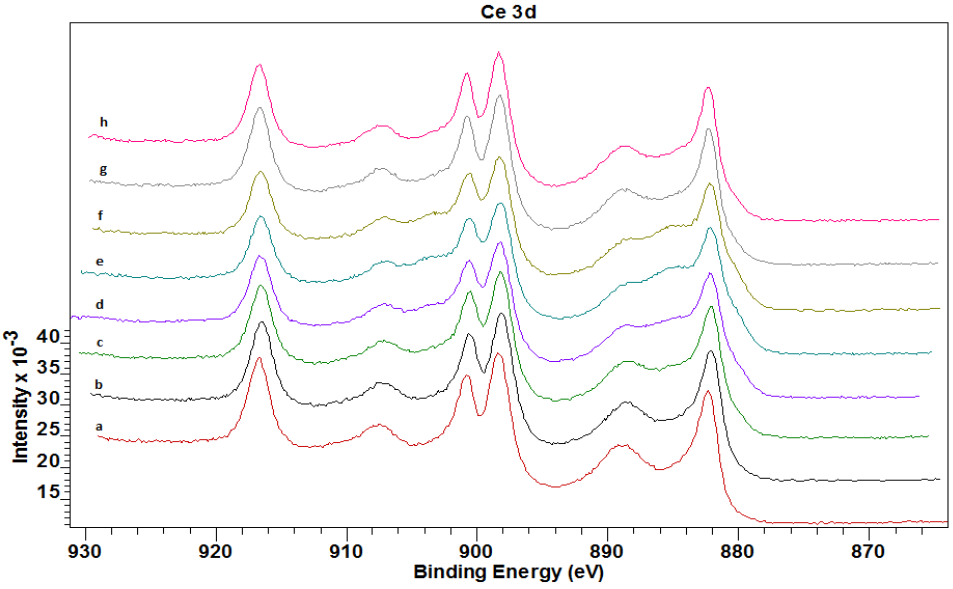

Figure 5-10. XPS Ce 3d spectrum of CeO_2 (111) single crystal heating and cooling in an hydrogen peroxide at a) room temperature b) 100 °C, c) 200 °C, d) 300 °C, e) 400 °C, f) 300 °C, g) 200 °C, and h) 100 °C.

Table 5-5. Quantitative data of Ce^{3+}/Ce^{4+} percentage concentrations upon heating and cooling in a hydrogen peroxide atmosphere.

Temperature (°C)	**% Ce^{3+}**	**% Ce^{4+}**
Room temperature	8	92
100	17	83
200	24	76
300	30	70
400	37	63
300	35	65
200	20	80
100	19	81

The Ce 3d spectrum of the CeO_2 single crystal at room temperature after the cleaning process was complete and at room temperature under a hydrogen peroxide atmosphere showed all the characteristics of a fully oxidised surface. This can be seen in figure 5-9. The characteristic U''' peak to single the presence of Ce^{4+} was present and no signs of any emergence of the V', U', U_0 or V_0 peaks from the Ce_2O_3 to signal any concentration of Ce^{3+} were evident.

Up to 200 °C, little reduction is witnessed and no peaks corresponding to Ce^{3+} were seen to emerge. Between 200 °C and 300 °C the V' peak of the Ce_2O_3 XPS Ce 3d spectrum (figure 5-10) started to become clearer. This indicates an increase in the concentration of Ce^{3+}

on the surface; this is supported by the quantitative data in table 5-5. The extent of reduction increased as the temperature was raised to 400 °C.

Figure 5-10 shows that upon cooling in a hydrogen peroxide atmosphere the concentration of Ce^{3+} decreased. This was indicated by the re-emergence of the V'' peak from the CeO_2 Ce 3d spectrum and the gradual decrease in the presence of the V' peak from the Ce_2O_3 spectrum. This is supported by the data in table 5-5 which shows a decrease in the percentage of Ce^{3+} on the surface. This signified the re-oxidation of the reduced sites on the ceria surface upon cooling.

5.2.4 Heating the reduced ceria (111) single crystal in a sub ambient oxygen atmosphere. (10^{-7} Torr)

This experiment was performed in order to identify the oxidation profile of an assumed 100 % Ce_2O_3 surface. The ceria single crystal was reduced by sputtering with argon ions (4keV, 10^{-6} Torr argon, 550 °C) for 10 min. The ceria single crystal was then heated to 400 °C under a sub ambient oxygen atmosphere. Spectra were taken at 100 °C increments.

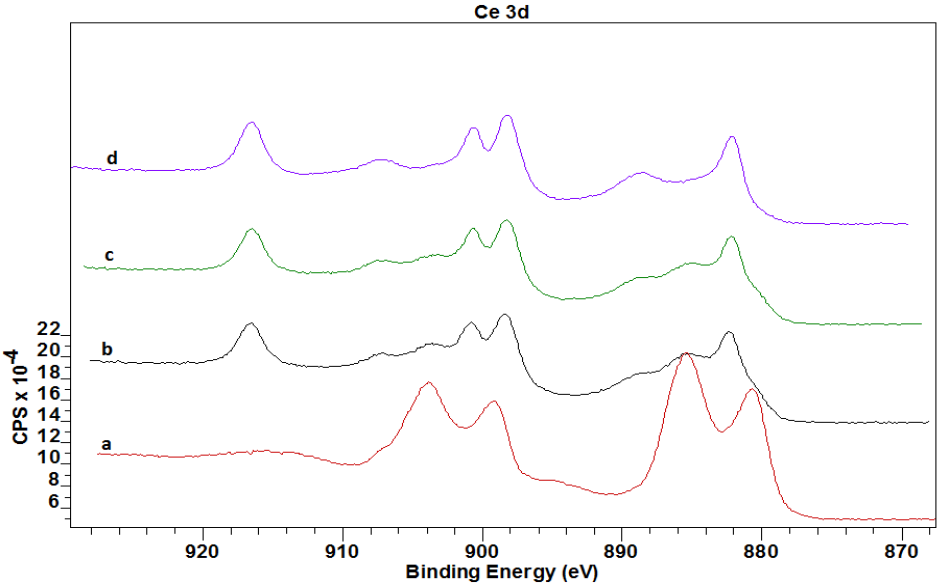

Figure 5-11. XPS Ce 3d spectra of the reduced CeO_2 (111) after a)reduction by argon sputtering, b) at room temperature in an oxygen atmosphere at c) upon heating in an oxygen atmosphere at 100 °C and d) upon heating in an oxygen atmosphere at 200 °C.

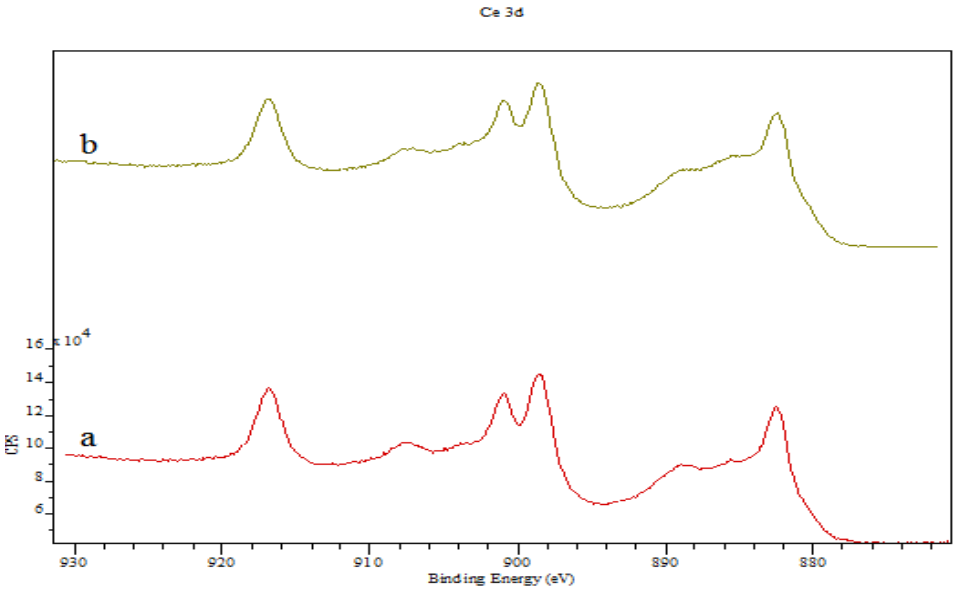

Figure 5-12. XPS Ce 3d spectra of the reduced CeO_2 (111) single crystal upon heating in an oxygen atmosphere a) 300 °C and b) 400 °C.

Table 5-6. Quantitative data of Ce^{3+}/Ce^{4+} percentage concentrations upon heating a reduced CeO_2 (111) single crystal in an oxygen atmosphere.

Temperature (°C)	% Ce^{3+}	% Ce^{4+}
Room temperature	42	58
100	42	58
200	20	80
300	30	70
400	35	65

The Ce 3d XPS spectrum (figure 5-11) of the CeO_2 single crystal after argon sputtering showed all the characteristic peaks of a Ce_2O_3 surface. None of the peaks relating to the presence of Ce^{4+} were observed. Therefore, the surface was assumed to be 100 % Ce^{3+}.

From the appearance of the U''' peak in the spectra at room temperature, presented figure 5-11 it can be concluded that the surface was significantly re-oxidised as soon as oxygen was introduced to the system at room temperature. The surface was shown to be fully re-oxidised by 200 °C.

Above 200 °C the concentration of Ce^{3+} increased, indicating that the surface was starting to reduce. This is shown in figure 5-12. This showed that at high temperatures in sub ambient atmospheres, the CeO_2 surface will experience reduction even when oxygen is present in the atmosphere.

5.2.5 Reduction of the ceria (111) single crystal under vacuum (10^{-9} Torr) at 100 °C, 150 °C and 200 °C for a period greater than 240 minutes.

The ceria single crystal was heated under vacuum at 100 °C, 150 °C and 200 °C and held at those temperatures for a period greater than 240 minutes. These experiments were undertaken to determine the extent of reduction on the ceria single crystal as a result of exposure to the vacuum at different temperatures over an extended time period. XPS spectra were taken at 45 minute intervals.

As can be seen in figures 5-13 to 5-15 and the from the quantitative data in table 5-7 a slight increase in the concentration of Ce^{3+} on the surface of CeO_2 was observed over time as a result of exposing the single crystal to vacuum at 100 °C, 150 °C and 200 °C. This is shown by an emergence of the V' peak from the Ce_2O_3 spectrum, as indicated on figures 5-13 to 5-15. There is no discernible difference between the amount of reduction seen at 100 °C, 150 °C and 200 °C when exposing the single crystal to vacuum over time. This suggests that the number of defects formed on the surface of the single crystal will be a consequence of exposing the single crystal to ultra-high vacuum conditions and will be the same at each temperature tested.

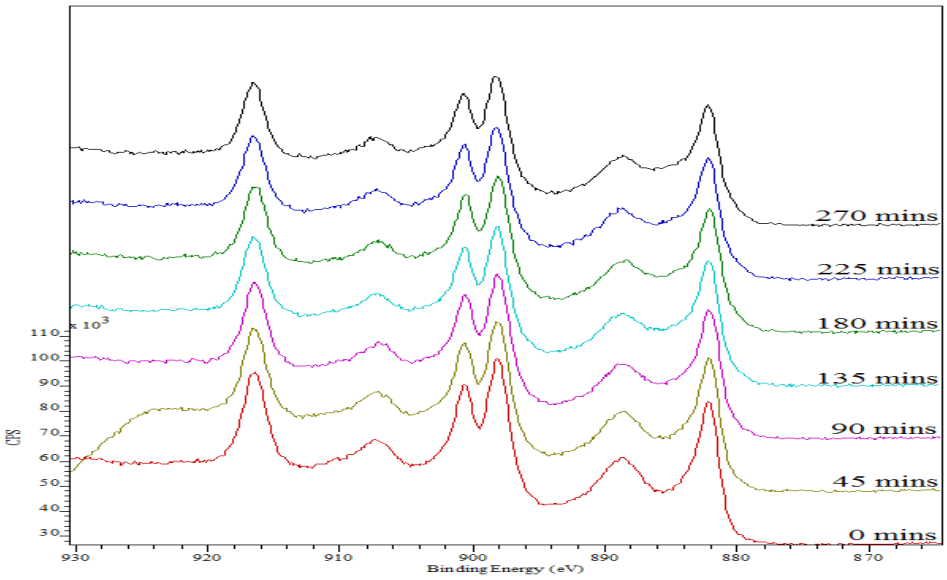

Figure 5-13. XPS Ce 3d spectra of the CeO_2 (111) single crystal at 100 °C in vacuum (10^{-9} Torr) for greater than 240 minutes.

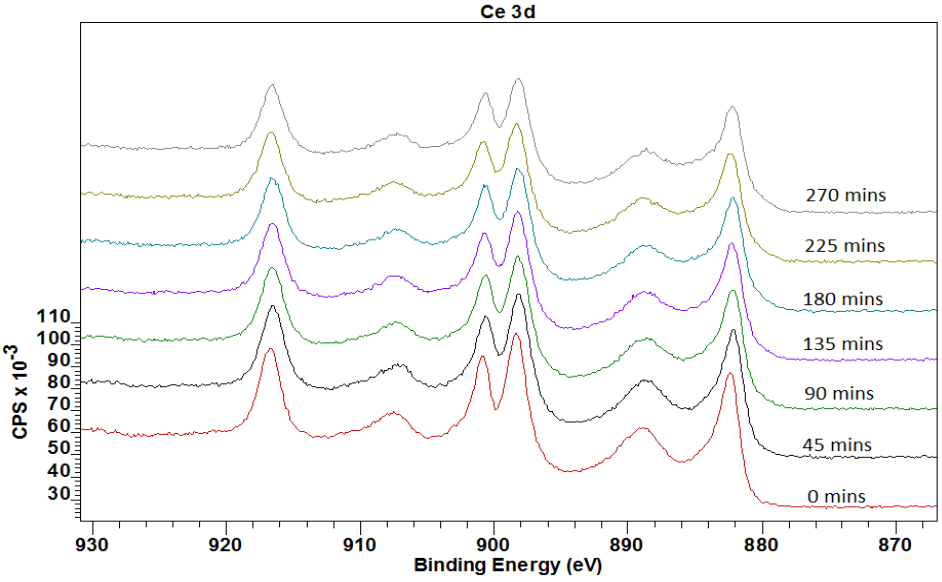

Figure 5-14. XPS Ce 3d spectra of the CeO_2 (111) single crystal at 150 °C in vacuum (10^{-9} Torr) for greater than 240 minutes.

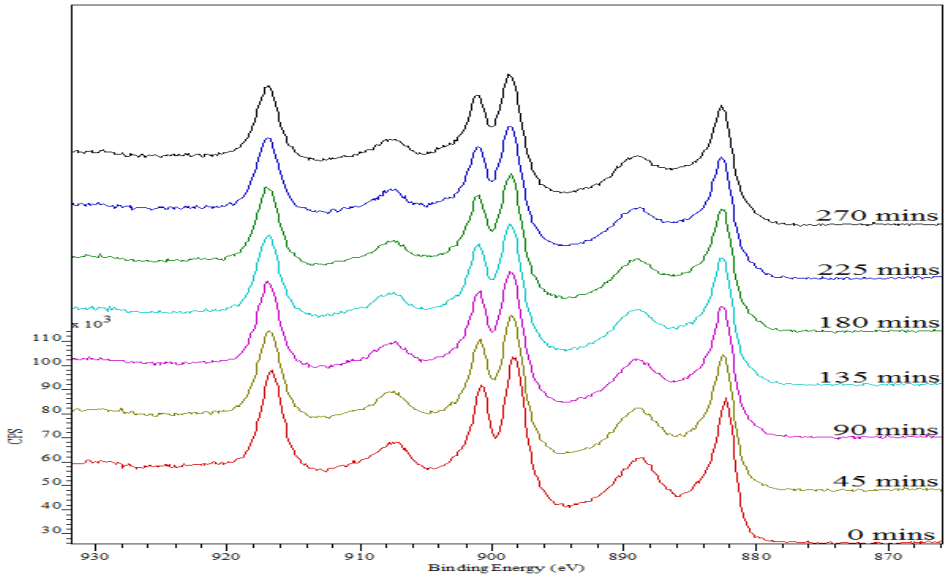

Figure 5-15. XPS Ce 3d spectra of the CeO_2 (111) single crystal at 200 °C in vacuum (10^{-9} Torr) for greater than 240 minutes.

Table 5-7. Quantitative data of Ce^{3+}/Ce^{4+} percentage concentrations upon heating under vacuum for greater than 240 minutes.

Time (Minutes)	Ce^{3+} percentage at 100 °C	Ce^{3+} percentage at 150 °C	Ce^{3+} percentage at 200 °C
0	0	0	0
45	12	9	11
90	13	13	14
135	15	12	13
180	17	15	14
225	17	12	15
270	17	16	15

5.2.6 Reduction of the ceria (111) single crystal under a hydrogen atmosphere (partial pressure of 10^{-7} Torr) at 100 °C, 150 °C, and 200 °C for a period greater than 240 minutes.

The ceria single crystal was heated under a sub ambient hydrogen atmosphere at 100 °C, 150 °C and 200 °C and held at those temperatures for a period greater than 240 minutes. These experiments were undertaken to determine the extent of reduction on the ceria single crystal as a result of exposure to a reducing atmosphere at different temperatures over an extended time period. XPS spectra were taken at 45 minute intervals.

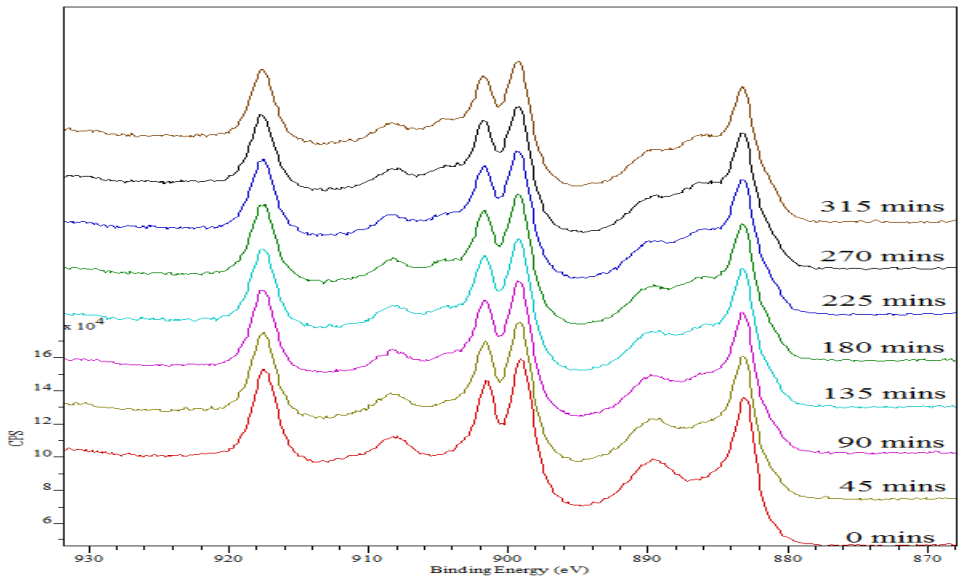

Figure 5-16. XPS Ce 3d spectra of the CeO_2 (111) single crystal at 100 °C in a hydrogen atmosphere (10^{-7} Torr) for greater than 240 minutes.

A greater extent of reduction was observed when exposing the ceria single crystal to a hydrogen atmosphere over time compared with that seen under just UHV conditions (figures 5-13 to 5-15). This is seen in figures 5-16 to 5-18. The V' peak from the Ce_2O_3 spectrum has becomes clearer in the CeO_2 spectrum. This indicated a significantly higher concentration of Ce^{3+} on the surface of the single crystal when compared to the results from the vacuum studies.

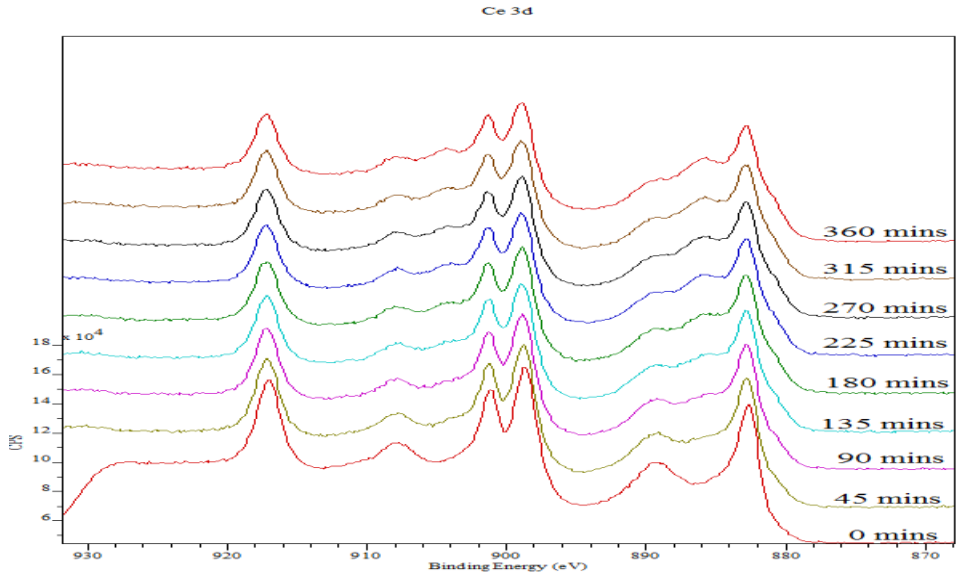

Figure 5-17. XPS Ce 3d spectra of the CeO_2 (111) single crystal at 150 °C in a hydrogen atmosphere (10^{-7} Torr) for greater than 240 minutes.

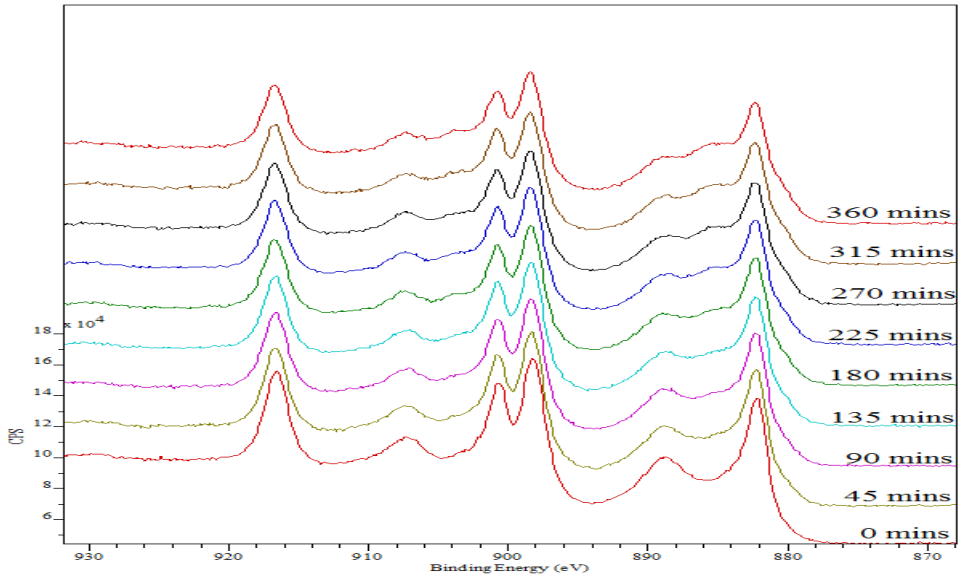

Figure 5-18. XPS Ce 3d spectra of the CeO_2 (111) single crystal at 200 °C in a hydrogen atmosphere (10^{-7} Torr) for greater than 240 minutes.

Table 5-8. Quantitative data of Ce^{3+}/Ce^{4+} percentage concentrations upon heating in a hydrogen atmopshere for greater than 240 minutes.

Time (Minutes)	Ce^{3+} percentage at 100 °C	Ce^{3+} percentage at 150 °C	Ce^{3+} percentage at 200 °C
0	13	14	14
45	22	22	22
90	27	29	23
135	30	35	24
180	31	38	30
225	32	40	31
270	35	42	33
315	34	42	34

There were no discernible differences observed between the different temperatures 100 °C and 150 °C. At 100 °C after 180 minutes, quantitative data in table 5-8 shows that the amount of Ce^{3+} on the surface has reached over 30 %, this would suggest that temperatures as low as a 100 °C are sufficient for surface reduction by a reducing atmosphere to occur. Providing enough time is allowed for the reaction to take place.

5.2.7 Reduction of the ceria (111) single crystal under an atmosphere of H_2O (partial pressure of 10^{-7} Torr) at 100 °C, 150 °C, and 200 °C for a period greater than 240 minutes.

The ceria single crystal was heated under a sub ambient H_2O atmosphere at 100 °C, 150 °C and 200 °C and held at those temperatures for a period greater than 240 minutes. These experiments were undertaken to determine the extent of reduction on the ceria single crystal as a result of exposure to a H_2O atmosphere at different temperatures over an extended time period. XPS spectra were taken at 45 minute intervals.

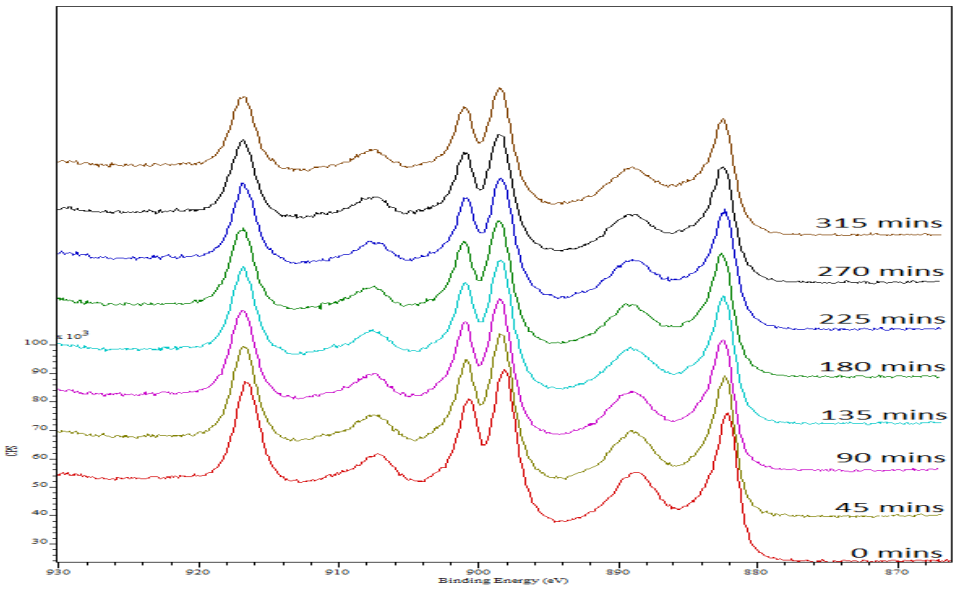

Figure 5-19. XPS Ce 3d spectra of the CeO_2 (111) single crystal at 100 °C in a H_2O atmosphere (10^{-7} Torr) for greater than 240 minutes.

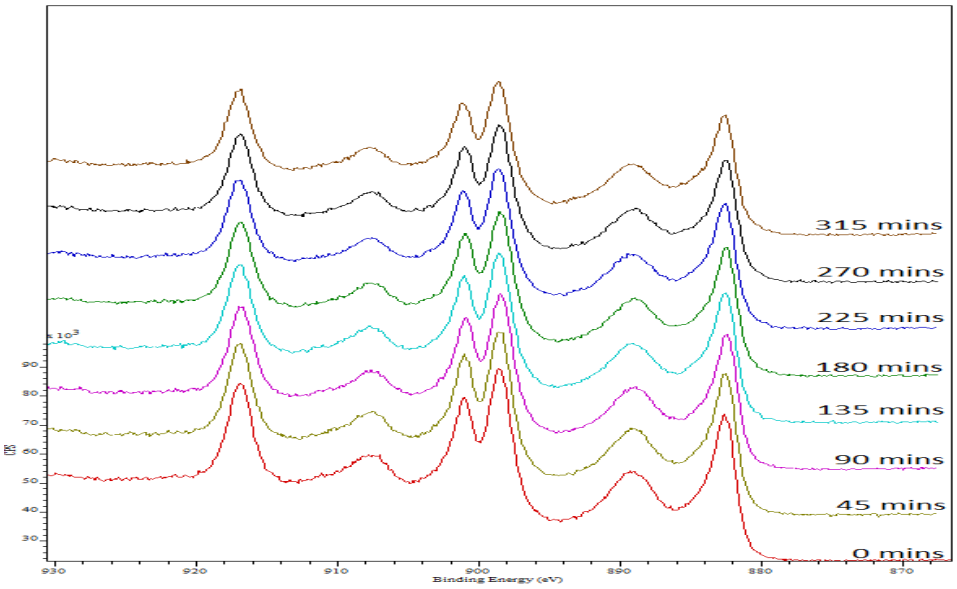

Figure 5-20. XPS Ce 3d spectra of the CeO_2 (111) single crystal at 150 °C in a H_2O atmosphere (10^{-7} Torr) for greater than 240 minutes.

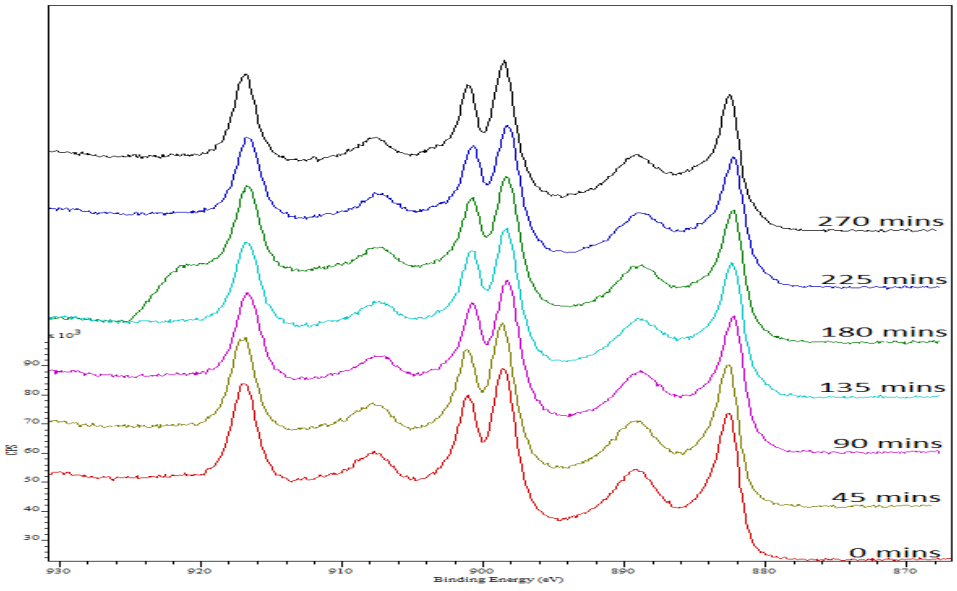

Figure 5-21. XPS Ce 3d spectra of the CeO_2 (111) single crystal at 200 °C in a H_2O atmosphere (10^{-7} Torr) for greater than 240 minutes.

Table 5-9. Quantitative data of Ce^{3+}/Ce^{4+} percentage concentrations upon heating in a H_2O atmosphere for greater than 240 minutes.

Time (Minutes)	Ce^{3+} percentage at 100 °C	Ce^{3+} percentage at 150 °C	Ce^{3+} percentage at 200 °C
0	0	0	0
45	0	0	0
90	0	0	12
135	4	0	12
180	4	0	9
225	10	7	13
270	7	8	13
315	7	7	-

A very small amount of reduction was seen when the single crystal was exposed to a H_2O atmosphere at 100 °C, 150 °C and 200 °C over time. This can be seen in figures 5-19 to 5-21 and from the data in table 5-9. When comparing the results of exposing the single crystal to a H_2O atmosphere at 200 °C results to the results produced when exposing the ceria single crystal to vacuum at 200 °C over time (figures 5-13 to 5-14 and table 5-7), it can be seen that the amount of reduction is comparable.

This would indicate that the small amount of reduction seen here is as a result of exposure of the single crystal ceria to ultra-high vacuum conditions rather than the H_2O atmosphere. Therefore, we can assume water has little to no effect on the reduction of ceria.

5.2.8 Reduction of the ceria (111) single crystal under a H_2O/H_2 atmosphere (partial pressure of 10^{-7} Torr) at 100 °C, 150 °C and 200 °C for a period greater than 240 minutes.

The ceria single crystal was heated under a sub ambient H_2O/hydrogen mixed atmosphere in a 3:1 ratio at 100 °C, 150 °C and 200 °C and held at those temperatures for a period greater than 240 minutes. These experiments were undertaken to determine the effect of water on the hydrogen reduction profile of the ceria single crystal at different temperatures over an extended time period. These reactions were run under water rich conditions. XPS spectra were taken at 45 minute intervals.

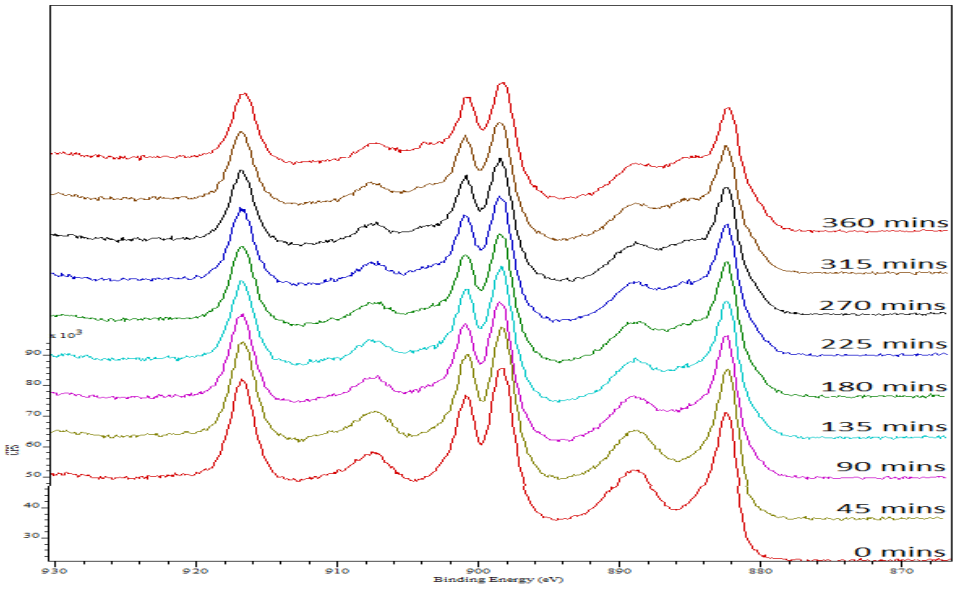

Figure 5-22. XPS Ce 3d spectra of the CeO_2 (111) single crystal at 100 °C in a H_2O/H_2 atmosphere (10^{-7} Torr) for greater than 240 minutes.

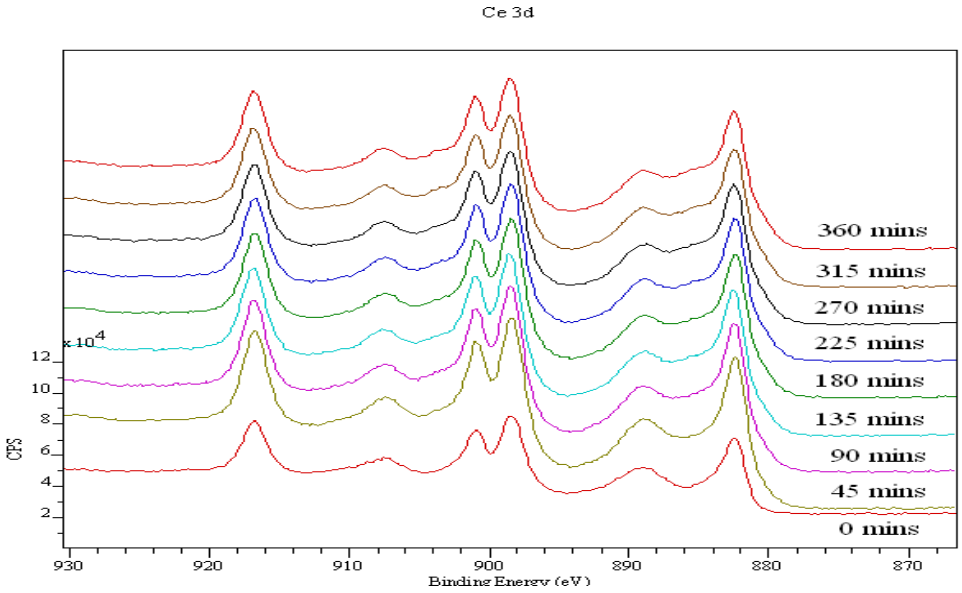

Figure 5-23. XPS Ce 3d spectra of the CeO_2 (111) single crystal at 150 °C in a H_2O/H_2 atmosphere (10^{-7} Torr) for greater than 240 minutes.

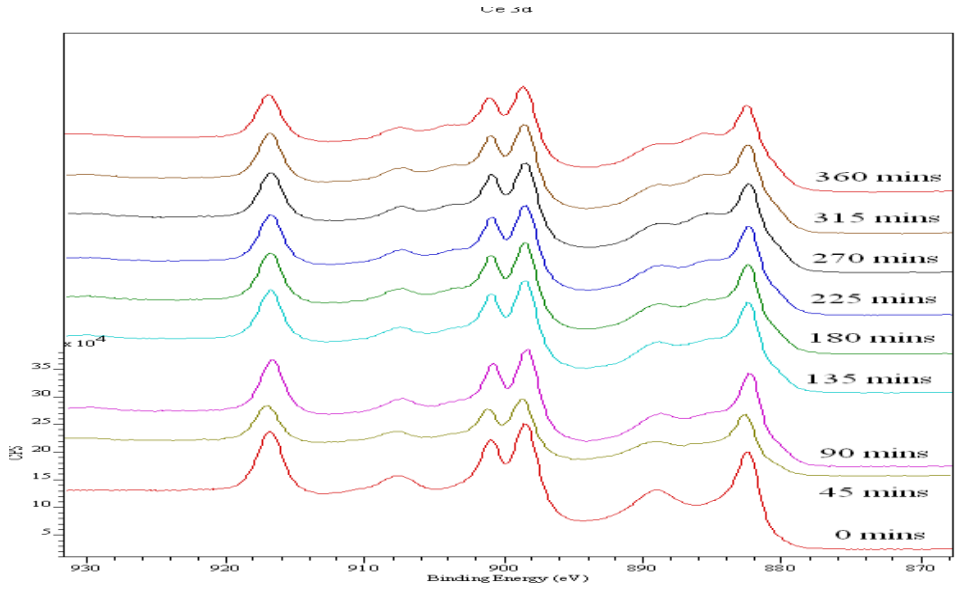

Figure 5-24. XPS Ce 3d spectra of the CeO_2 (111) single crystal at 200 °C in a H_2O/H_2 atmosphere (10^{-7} Torr) for greater than 240 minutes.

Table 5-10. Quantitative data of Ce^{3+}/Ce^{4+} percentage concentrations upon heating in a H_2O/H_2 atmosphere for greater than 240 minutes.

Time (Minutes)	Ce^{3+} percentage at 100 °C	Ce^{3+} percentage at 150 °C	Ce^{3+} percentage at 200 °C
0	0	0	11
45	16	17	25
90	23	24	28
135	25	22	29
180	25	28	31
225	29	24	31
270	30	23	36
315	29	25	36
360	26	26	35

The results shown in figures 5-22 to 5-24 and table 5-10 indicate that from exposing the ceria single crystal to a H_2O/H_2 atmosphere at 100 °C, 150 °C and 200 °C, a higher degree of reduction is witnessed when compared to the results from exposing the single crystal to a H_2O atmosphere (figures 5-19 to 5-21 and table 5-9). The results are comparable to the results when the single crystal is exposed to a H_2 atmosphere (figures 5-16 to 5-18 and table 5-8)

The H_2O/H_2 atmosphere was at a 3:1 ratio of water to hydrogen. The results suggest that having a water rich atmosphere would little to no effect on the hydrogen reduction profile of ceria.

5.3 Conclusions

It has been reported that CeO_2 can suffer from spontaneous reduction at room temperature during XPS measurements due to x-ray irradiation and ultra-high vacuum (UHV) conditions[6]. Laachir et al[7] also noted that initial concentrations of Ce^{3+} observed could correspond to reduction as a result of x-ray irradiation and UHV conditions. Therefore, the small reduction seen at the beginning of each experiment is likely to be a result of x-ray irradiation and UHV conditions.

The results in figures 5-2 to 5-8 and table 5-1 to 5-4 support previous work[2] that indicates that defects on the surface can be caused intrinsically as results of heating under vacuum and extrinsically by reaction of the surface with a hydrogen environment. It can also be seen during these experiments that reduction continues while cooling. It has been reported[8] that ceria has the ability to store oxygen under fuel lean conditions, and it can be seen here that without oxygen in the atmosphere for the ceria to store, it appears to affect the oxygen migration to the surface at room temperature. This could be as a result of cluster formation on the surface which has been reported to be favourably during the reduction of ceria[9].

It has been reported that reduction of ceria by hydrogen begins above 200 °C[10]. When comparing this to the results in figure 5-7 for the reduction of the ceria single crystal by hydrogen a difference was seen with reduction beginning at above 150 °C, and in chapter 4 we see a hydrogen oxidation occurring at temperatures as low as 150 °C, as is reported in studies of hydrogen oxidation over ceria powder in sealed autoclaves as show in figures 4-28 to 4-29.

This is also supported by the results shown in figures 5-16 to 5-18. This provides a good link between studies of powdered ceria sample and a ceria single crystal, which both show some reactivity towards hydrogen at 150 °C or above. It is to be noted that reduction is not observed in the TPR studies in chapter 4 at temperatures below 300 °C, section 4.2.10.1, however, this could be a sensitivity issue associated with the technique used.

Re-oxidation of the ceria surface appears to be favourable below 200 °C when oxygen is present in the atmosphere, results shown in figures 5-10, 5-11 and table 5-6 support this observation. This is consistent with data that has previously be reported for ceria studies, which states that re-oxidation of ceria is complete by room temperature and with only small oxygen pressure[2, 11].

It can be concluded from the results in figures 5-13 to 5-24 that the presence of water does inhibit the reduction of ceria by hydrogen. The results here would suggest that water content in plutonium storage would not inhibit the any thermal reduction reaction by hydrogen on the surface of PuO_2.

5.4 References

1 J. Elfallah, S. Boujana, H. Dexpert, A. Kiennemann, J. Majerus, O. Touret, F. Villain and F. Lenormand, *Journal of Physical Chemistry*, 1994, **98**, 5522.

2 A. Trovarelli, *Catalysis by Ceria and Related Materials*, 2002.

3 G. Ranga Rao, a. Mishra and B. G., *Bulletin of the Catalysis Society of India*, 2003, 122.

4 J. C. Conesa, *Surf. Sci.*, 1995, **339**, 337.

5 S. Gritschneder and M. Reichling, *Nanotechnology*, 2007, **18**, 6.

6 E. Paparazzo, *Surf. Sci.*, 1990, **234**, L253.

7 A. Badri, J. Lamotte, J. C. Lavalley, A. Laachir, V. Perrichon, O. Touret, G. N. Sauvion and E. Quemere, *Eur. J. Solid State Inorg. Chem.*, 1991, **28**, 445.

8 A. Trovarelli, M. Boaro, E. Rocchini, C. de Leitenburg and G. Dolcetti, *Journal of Alloys and Compounds*, 2001, **323-324**, 584.

9 J. L. Ma, F. Ye, D. R. Ou, L. L. Li and T. Mori, *Journal of Physical Chemistry C*, 2012, **116**, 25777.

10 C. Binet, A. Badri and J.-C. Lavalley, *The Journal of Physical Chemistry*, 1994, **98**, 6392; C. Binet, A. Badri and J. C. Lavalley, *Journal of Physical Chemistry*, 1994, **98**, 6392.

11 G. Munuera, A. Fernandez and A. R. Gonzalezelipe, *Catalysis and Automotive Pollution Control Ii*, 1991, **71**, 207.

6 Chapter 6 – Conclusions and future work

6.1 Conclusions

Chapter 4 shows hydrogen reduction of the surface of CeO_2 powder to begin at 300 °C and is shown to be highly dependent on the surface area of the CeO_2. This is significantly different to the results for hydrogen reduction of the CeO_2 single crystal surface presented in chapter 5. Reduction of the single crystal is seen to begin at 150 °C. However, it has been reported by Laachir et al and others[1, 2] that reduction of CeO_2 powders by hydrogen begins at 200 °C for samples of CeO_2 with higher surface areas than the samples tested in this work. It has also been shown that CeO_2 will undergo spontaneous reduction as a result of exposure to UHV conditions[3, 4]. Therefore, it can be suggested that the differences seen in the start temperatures for reduction by hydrogen could be as result of the surface area of the powder samples and the effect of UHV conditions[3, 4] on the single crystal.

Results from the powder samples in sealed autoclave vessels in chapter 4 show a reaction of the 2 % hydrogen in air mixture with CeO_2 powder at 150 °C. This provides a good link between studies of powdered CeO_2 and a CeO_2 single crystal, which both show some reactivity towards hydrogen at 150 °C or above. These results combined with the results in chapter 5 for the reduction of CeO_2 by hydrogen at 100 °C, 150 °C and 200 °C over time are comparable with the work carried out by Morales *et al.*[5] Providing evidence to support the theory that CeO_2 powders and CeO_2 (111) single crystal are a good model for studying the thermal reactions of H_2 and O_2 over PuO_2.

If we compare the results for the redox TPR studies in chapter 4 and the re-oxidation of the reduced CeO_2 it is noted that oxidation occurs more readily on the reduced surface of the single crystal than it does on the reduced powder. These results would indicate that a single

crystal is not a good model for the powder CeO_2. However, reduction of the bulk CeO_2 has occurred in the TPR studies and this will make re-oxidisation of the surface more difficult. This could be the reason for the difference observed in re-oxidation of a reduced CeO_2 surface. It should also be noted that the single crystal is only the (111) plane whereas, the powder samples will be a mixture of many planes as the XRD analysis shows.

The H_2 reduction of the CeO_2 powders and CeO_2 single crystal presented in this work support previous findings that the reduction of CeO_2 by H_2 follows a Mars van Krevelen type reaction. It is therefore suggested that the H_2 produced in water splitting by radiolysis in nuclear storage will reduce the surface of PuO_2 via a Mars van Krevelen reaction. It is shown in both chapters 4 and 5 that water does not inhibit the H_2 reduction of CeO_2. This work indicates that water present in nuclear storage will not inhibit any reaction of H_2 with the surface of PuO_2.

It should also be noted that the single crystal is only the (111) plane whereas, the powder samples will be a mixture of many planes as the XRD analysis shows.

6.2 Future work

The reduction and oxidation of CeO_2 powders under vacuum (10^{-9} Torr) and a partial pressure of hydrogen (10^{-7} Torr) by XPS.

Repeating the experiments in chapter 5 on CeO_2 powder samples would provide a direct comparison of the results between CeO_2 powder and CeO_2 (111) single crystal. It would be interesting to see how the results compare to the results presented for the single crystal. This would provide further experimental results to prove or disprove whether a CeO_2 single crystal is a good model for CeO_2 powders.

Initial UHV studies using a ceria C400 sample were tested; the results can be seen in figure 6-1.

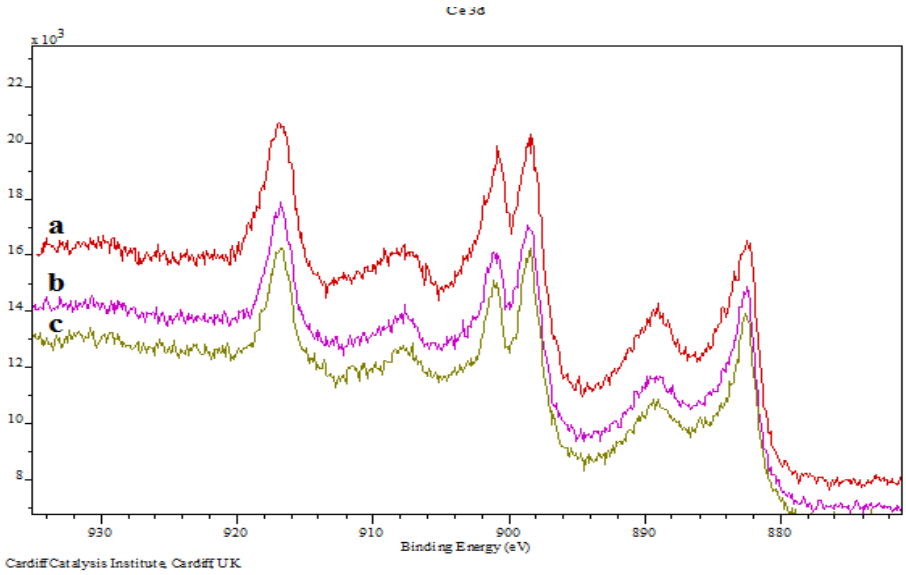

Figure 6-1.Ce 3d XPS spectra of ceria C400 powder at a) room temperature, b) 200 °C under a hydrogen atmosphere (10^{-7} Torr) and c) 450 °C under a hydrogen atmosphere (10^{-7} Torr).

As can be seen in figure 6-1 no reaction was witnessed by exposing a ceria C400 powder sample to hydrogen under UHV conditions.

Unfortunately, the initial attempts to link the powder CeO_2 and single crystal studies were unsuccessful. This could be due a number of factors, such as the reactive gas not reaching the surface of the powder sample. There wasn't sufficient time to investigate why there is no reaction witnessed in these initial studies.

The reduction of CeO_2 (111) single crystal by NO, N_2O and NH_3 at 100 °C, 150 °C and 200 °C over time studied by XPS.

It has been reported[6] that the reaction of HNO_3 with the radioactivity in nuclear storage can form species such as NO, N_2O and NH_3. It would be beneficial to monitor the reactions taking place between these compounds and the CeO_2 (111) single crystal.

The reduction of CeO_2 (111) single crystal by H_2/NO, H_2/N_2O and H_2/NH_3 at 100 °C, 150 °C and 200 °C over time studied using XPS.

It would also be beneficial to see what effect, if any, impurities such as NO, N_2O and NH_3 have on the hydrogen reduction profile of CeO_2 (111) single crystal at conditions similar to those in nuclear waste storage. These experiments would indicate whether NO, N_2O and NH_3 would inhibit or enhance the H_2 reduction of CeO_2 and PuO_2.

The reduction and oxidation of CeO_2 (100) single crystal under UHV conditions studied using XPS.

Studying the reduction of a CeO_2 (100) single crystal under UHV conditions, as result of temperature and reducing atmospheres, would provide further insight into the viability of

CeO_2 single crystal UHV conditions to model powder CeO_2 reactions. The CeO_2 (100) has been reported to be the second most reactive plane of CeO_2 after the (111) plane[7].

6.3 References

1 A. Laachir, V. Perrichon, A. Badri, J. Lamotte, E. Catherine, J. C. Lavalley, J. Elfallah, L. Hilaire, F. Lenormand, E. Quemere, G. N. Sauvion and O. Touret, *Journal of the Chemical Society-Faraday Transactions*, 1991, **87**, 1601.

2 A. Trovarelli, *Catalysis by Ceria and Related Materials*, Imperial College Press, 2002.

3 E. Paparazzo, *Surf. Sci.*, 1990, **234**, L253.

4 A. Badri, J. Lamotte, J. C. Lavalley, A. Laachir, V. Perrichon, O. Touret, G. N. Sauvion and E. Quemere, *Eur. J. Solid State Inorg. Chem.*, 1991, **28**, 445.

5 L. A. Morales, US Department of Energy, Los Alamos National Laboratory, 1998.

6 J. A. Lloyd and G. P. Eller, *Los Alamos National Laboratory*, 1998.

7 J. C. Conesa, *Surface Science*, 1995, **339**, 337.